

NASA-CR-172,455

NASA Contractor Report 172455

FOR REFERENCE

NASA-CR-172455
19850003730

NOT TO BE TAKEN FROM THIS ROOM

Extended Aeroelastic Analysis for Helicopter Rotors With Prescribed Hub Motion and Blade Appended Pendulum Vibration Absorbers

Richard L. Bielawa

UNITED TECHNOLOGIES RESEARCH CENTER
EAST HARTFORD, CT 06108

Contract NAS1-16803
December 1984

LIBRARY COPY

DEC 6 1984

LANGLEY RESEARCH CENTER
LIBRARY, NASA
HAMPTON, VIRGINIA

NASA

National Aeronautics and
Space Administration

Langley Research Center
Hampton, Virginia 23665



21

1

1 RN/NASA-CR-172455

DISPLAY 21/2/1

85N12038** ISSUE 3 PAGE 315 CATEGORY 2 RPT#: NASA-CR-172455 NAS
1.26:172455 CNT#: NAS1-16803 84/12/00 217 PAGES UNCLASSIFIED
DOCUMENT

UTTL: Extended aeroelastic analysis for helicopter rotors with prescribed hub motion and blade appended pendulum vibration absorbers

AUTH: A/BIELAWA, R. L.

CORP: United Technologies Research Center, East Hartford, Conn. AVAIL.NTIS
SAP: HC A10/MF A01

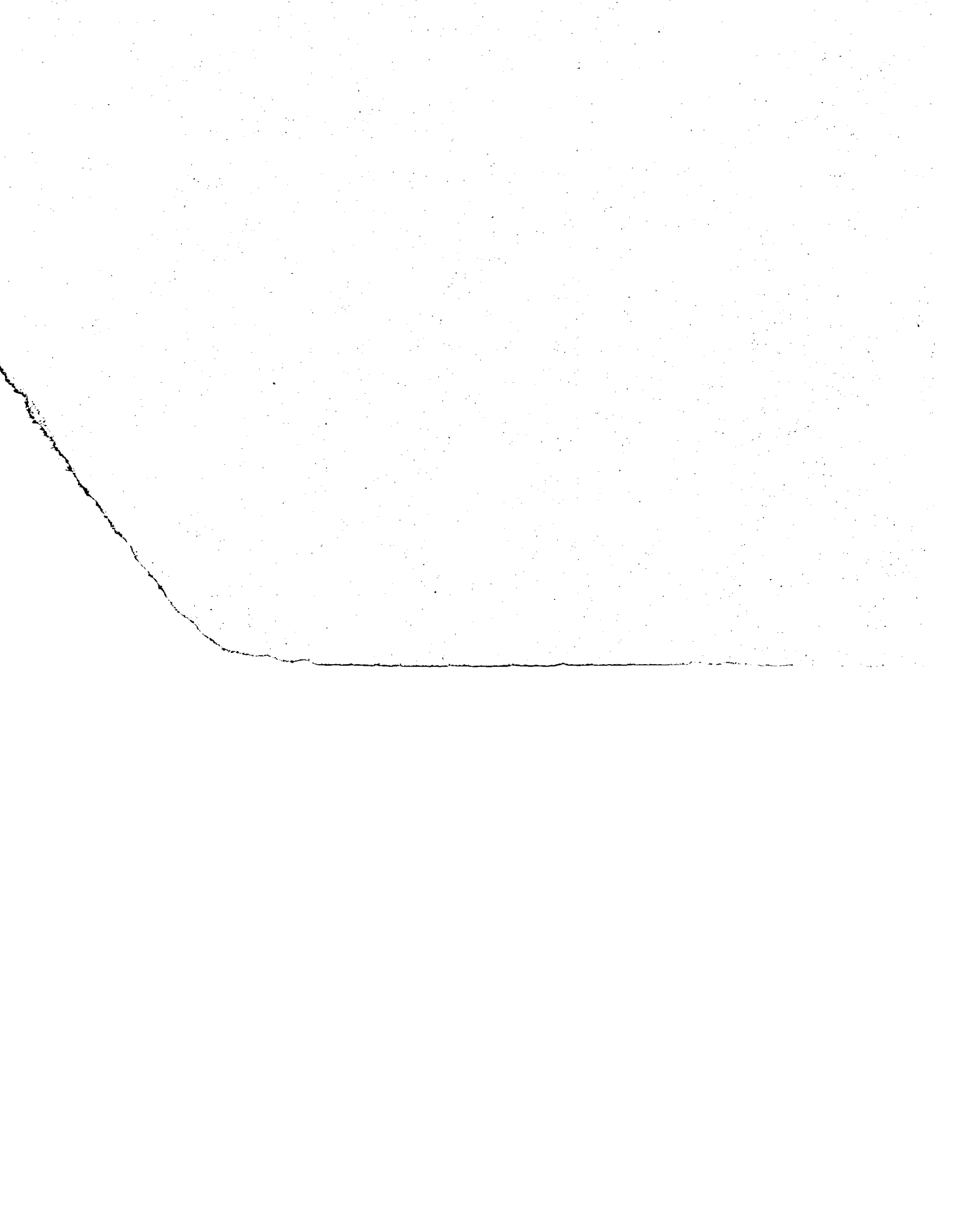
MAJS: /*AEROELASTICITY/*HUBS/*LOADS (FORCES)/*ROTARY WINGS/*ROTOR AERODYNAMICS/*
VIBRATION ISOLATORS

MINS: / MATHEMATICAL MODELS/ MECHANICAL IMPEDANCE/ MECHANICAL PROPERTIES/
UNSTEADY FLOW/ WING LOADING

ABA: E. A. K.

ABS: The mathematical development for the expanded capabilities of the G400 rotor aeroelastic analysis was examined. The G400PA expanded analysis simulates the dynamics of all conventional rotors, blade pendulum vibration absorbers, and the higher harmonic excitations resulting from prescribed vibratory hub motions and higher harmonic blade pitch control. The methodology for modeling the unsteady stalled airloads of two dimensional airfoils is discussed. Formulations for calculating the impedance matrix appropriate to the higher harmonic blade excitation are outlined. This impedance matrix, and the associated vibratory hub

ENTER:



Extended Aeroelastic Analysis for Helicopter Rotors
with Prescribed Hub Motion and Blade Appended
Pendulum Vibration Absorbers

TABLE OF CONTENTS

	<u>Page</u>
PREFACE	iii
LIST OF FIGURES AND TABLES	iv
SUMMARY	1
INTRODUCTION	2
LIST OF SYMBOLS	4
SIMULATION OF UNDERSLUNG TEETERED ROTORS	15
Basic Modeling Considerations	15
Aerodynamic and Dynamic Load Distributions	16
Implementation of Teetered Blade Root Constraint	18
Teeter Stop Moment Characteristics	20
BLADE APPENDED PENDULUM VIBRATION ABSORBERS	23
Basic Assumptions	23
Dynamic Loads	25
Equations of Motion	26
BLADE LOADS DUE TO HIGHER HARMONIC EXCITATIONS	29
Prescribed Harmonic Hub Motions	29
Higher Harmonic Blade Pitch Control	35
Impedance Matrix Calculation	36
SPANWISE VARIABLE ELASTIC AXIS OFFSET	37
Torsion Excitation for Elastic Axis as a Space Curve	37
Kinematic Representation for Structural Sweep	41
Kinematics of Radial Foreshortening	46

TABLE OF CONTENTS (Cont'd)

	<u>Page</u>
UNSTEADY STALLED AIRLOADS	49
Review of Basic Methodology	49
Prediction of Dynamic Stall Events	57
Unsteady Section Coefficients	60
GENERAL DESCRIPTION OF THE G400PA PROGRAM	63
Program Structure	63
Brief Description of Program Elements	67
PROGRAM INPUT DESCRIPTION	79
Airfoil Data	80
Loader Data Descriptions	85
Blade Modal Input Data	136
Variable Inflow Data	138
Rotor Inflow Program F389 Required Data	139
Multiple Case Runs	142
Initial Conditions	143
Input/Output File Unit Numbers	144
G400 Data File Output	145
General Information to Facilitate Operation of Program and Improve Efficiency	147
PROGRAM OUTPUT DESCRIPTION	152
Listing of Input Airfoil Data	152
Results of Uncoupled Blade Mode Calculation Processor E159	156
Listing of Remaining Input Data	169
Parameters Calculated from the Input Data	171
Results of Solution Part II - Time-History Solutions	185
Impedance Matrices	196
Results of Solution Part III - Transient Spectral Stability Analysis	199
Subsequent Cases	203
REFERENCES	205
APPENDIX I - UPDATES TO DOCUMENTATION OF BASIC G400 ANALYSIS	207

PREFACE

The mathematical formulations and resulting computer code described herein are revisions to and extensions of earlier versions of the G400PA program. These developments were provided by United Technologies Research Center (UTRC) under sponsorship of the Army Structures Laboratory/USARTL (AVSCOM), through contract NAS1-16803, "Study of Expansion of Synthesized Unsteady Airfoil Data Method".

The present G400PA analysis represents an integration and culmination of various G400 related aeroelastic analysis development programs supported over a fifteen year span by several sources. All development of the G400 analysis was conducted and/or supervised by Dr. Richard L. Bielawa, presently of Rensselaer Polytechnic Institute. Initial development was performed under United Technologies Corporate and Divisional sponsored independent research and development. Since then extensive refinements to the analysis were made under varied governmental agency sponsorship:

1. Langley Research Center of the National Aeronautics and Space Administration (NASA) and the U.S. Army Air Mobility Research and Development Laboratory, Langley Directorate as part of Contract NAS1-10960.
2. Structures Laboratory of the USRTL (AVRADCOM) under Contract NAS1-16058.
3. Lewis Research Center of NASA under Contract NAS3-22753.

This report represents documentation of all pertinent G400PA developments which incorporate: (1) state-of-the-art analysis techniques, (2) program user identified improvements, (3) an improved methodology for modeling unsteady stalled airloads of two dimensional airfoils, developed by Dr. Santu T. Gangwani at UTRC.

These technological efforts constitute a continuing contribution to the Simplified Coupled Rotor Fuselage Vibration Analysis (SIMVIB), which was funded through contract NAS1-16058.

LIST OF FIGURES AND TABLES

<u>FIGURES</u>	<u>PAGE</u>
1. Schematic of Teetered Rotor System - Kinematic Definitions and Flapping Moment Equilibrium	17
2. Generalization of Nonlinear Teeter Stop Moment vs. Teeter Angle Characteristics	21
3. Pictorial of Typical Pendular Absorber Installation	24
4. Blade Trailing Edge View of Blade/Pendular Absorber System-Kinematic Definitions and Moment Equilibrium	27
5. Schematics of the "5" and "6" Coordinate Systems	42
6. Contributions to Incremental Radial Foreshortening Due to Structural Sweep and Elastic Deformations	47
7. Dynamic Stall Modeling	50
8a. Typical Unsteady Lift Coefficient Loop Data, SC 1095 Airfoil, $M=0.3$, $\alpha_0=12.0$ deg, $\bar{\alpha}=8.0$ deg, $k=0.1$	52
8b. Typical Unsteady Pitching Moment Coefficient Loop Data, SC 1095 Airfoil, $M=0.3$, $\alpha_0=12.0$ deg, $\bar{\alpha}=8.0$ deg, $k=0.1$	53
8c. Typical Unsteady Drag Coefficient Loop Data, SC 1095 Airfoil, $M=0.3$, $\alpha_0=12.0$ deg, $\bar{\alpha}=8.0$ deg, $k=0.1$	54

<u>TABLES</u>	
I. Hierarchial Listing of G400PA Elements	64
II. Loader Data Transferred from G400 to F389	140
III. Required F389 Data not Automatically Transferred from G400	140
IV. Summary of Optional Basic Trim Combinations	151

Extended Aeroelastic Analysis for Helicopter Rotors
with Prescribed Hub Motion and Blade Appended
Pendulum Vibration Absorbers*

by

Richard L. Bielawa
Rensselaer Polytechnic Institute
Troy, New York

SUMMARY

Mathematical development is presented for the expanded capabilities of the United Technologies Research Center (UTRC) G400 Rotor Aeroelastic Analysis. The G400PA expanded analysis simulates the dynamics of all conventional rotors, blade pendulum vibration absorbers, and the higher harmonic excitations resulting from prescribed vibratory hub motions and higher harmonic blade pitch control. The analysis includes the methodology for modeling the unsteady stalled airloads of two-dimensional airfoils. Formulations are also presented for calculating the rotor impedance matrix appropriate to the higher harmonic blade excitations. This impedance matrix, and the associated vibratory hub loads, are the rotor dynamic characteristic elements for use in the Simplified Coupled Rotor/Fuselage Vibration Analysis (SIMVIB). Updates to the development of the original G400 theory, program documentation, user instructions and information are presented.

*The research effort which led to the results in this report was financially supported by the Structures Laboratory, USARTL (AVRADCOM).

INTRODUCTION

The G400PA helicopter rotor aeroelastic analysis described herein represents a generalization and extension of the original United Technologies Research Center (UTRC) G400 Rotor Aeroelastic Analysis described in Reference 1. This analysis was originally developed in response to the unique aeroelastic characteristics of the composite bearingless rotor and represented an advancement in the state-of-the-art with regard to the modeling of rotors with time-variable, nonlinear structural twist and multiple structural redundancy. Since the publication of Reference 1, the G400 analysis has evolved into a family of analyses with a completely general range of applicability in rotor type (articulated, hingeless, teetered) and vehicle application (helicopters, propellers, wind turbines).

The principal features of the G400PA analysis relative to the Reference 1 version are:

1. A capability for analyzing underslung teetered rotors.
2. The implementation of the nonlinear equations of motion for two independent blade-appended pendulum vibration absorbers.
3. Inclusion of the dynamic and aerodynamic loads due to specified harmonic accelerations in arbitrary combinations of all six components of hub motion.
4. The expansion of the blade pitch control description to include cosine and sine components of the $(b-1)$, b , and $(b+1)$ harmonics of cyclic pitch angle, (where b is the number of blades).
5. Provision for calculating impedance matrices, wherein each of the components of hub acceleration are systematically perturbed to obtain numerical partial derivatives of hub loads with respect to hub motion.
6. Extension of the blade coupling effects to include structural sweep.
7. Inclusion of an advanced methodology for modeling unsteady stalled airloads.
8. Increase in the number of blade segments from 15 to 20.
9. Improved input format by generic grouping of input data.

This report presents the technical background pertinent to the G400PA features listed. A general description of the program structure and elements is documented, along with user information to successfully run the program. A detailed description of the required input and output results is presented.

LIST OF SYMBOLS

<u>Symbol</u>	<u>Fortran Equiv.</u>	<u>Description</u>
a_{oL}	AO	Aerodynamic section static lift curve slope, deg^{-1} .
[A]	AA	Inertia coupling matrix for a single blade.
[AA]	BB11, BB12, BB22	The combined inertia coupling matrix for the degrees-of-freedom of the two blades of a teetered rotor.
A_{n_s}, B_{n_s}	HHTHET(2), HHFTHET(5)	n'th Fourier cosine and sine components, respectively, of inputted cyclic blade pitch control (higher harmonic control angles), deg.
$A_{qq}, A_{q\beta}, A_{\beta\beta}$	AA1, AA2, ALBET1, ALBET1, ALBET2, AABTTR	Submatrices comprising [A].
b	BL	Number of blades.
c	CHORD, CHORDB	Blade section chord, ft and (ND).
$c\psi, s\psi$	CPSI, SPSI	Abbreviated notation for cosine and sine of ψ , respectively.
C_A, C_w, C_α	(CADM, CARE), (CWDM, CWRE), CATE	Empirical coefficients multiplying A, α_w and α , respectively, in dynamic stalled airloads functionality, (ND).
C_{Ds}, C_{Ls}, C_{Ms}	CDS, CLS, CMS	Aerodynamic section static drag, lift and pitching moment coefficients, respectively, as used in unsteady stalled airloads modeling
C_{Du}, C_{Lu}, C_{Mu}	UNCD, UNCL, UNCM	Aerodynamic section unsteady drag, lift and pitching moment coefficients, respectively, (ND).
C_p	DMPP	Damper rate of explicit restraint of pendulum absorber about hinge, in-lb-sec/rad.
$DS1_i, DS2_i,$ $DS3_k, DS4_k,$ $DS5_j$	(same)	Integration constants used to calculate the blade internal loads immediately outboard of the flexbeam torque tube juncture, (ND).

LIST OF SYMBOLS (Cont'd)

<u>Symbol</u>	<u>Fortran Equiv.</u>	<u>Description</u>
DUEAE _k , DUEAF _i	DUEAE,DUEAF	Radial foreshortening of blade element point due to linear variations of k'th edgewise and i'th flatwise bending modes, respectively, (ND).
DUEAO	DUEAO	Radial foreshortening of blade element point due to built-in sweep.
e	ER, EOR	x ₂ coordinate of coincident flat-lag hinge or hingeless blade offset point, in.
f _i	FLIP,FLOP	Function defining fraction of pendulum absorber mass to be included in mass of i'th blade segment, (ND).
F _{x5} , F _{y5} , F _{z5}	(none)	Components of force in respective axis directions in the 5-coordinate system, lb.
h _{usℓ}	HUSL	Distance rotor/blade apex point is below teeter hinge, in.
i	(None)	Square root of -1.
[I _m]	(None)	Identify matrix of dimension m.
I _p	RINRTP	Mass moment of inertia of pendulum absorber about its flapping hinge, in-lb-sec ² .
k	(None)	Aerodynamic section reduced frequency (=ω _c /2U _N).
k _{y10} , k _{z10}	KY10,KZ10	Mass radii of gyration of blade section about axes through and perpendicular to the spanwise (x ₅) axis and in the chordwise and thicknesswise directions, respectively, in.

LIST OF SYMBOLS (Cont'd)

<u>Symbol</u>	<u>Fortran Equiv.</u>	<u>Description</u>
K_p	RKBP	Spring rate of explicit restraint of pendulum absorber about hinge, ft-lb/rad.
K_{β_1}, K_{β_2}	SPRAT1, SPRAT2	Effective spring rates defining the nonlinear elastic characteristics of teeter stops, ft-lb/rad.
l_p	XLNGP	Distance from hinge to mass center of a pendulum absorber, in.
m	(None)	Blade mass distribution, lb-sec ² /ft ² .
\bar{m}	XMASSB	Nondimensional blade mass distribution.
m_o	XMO	Reference blade mass distribution, defined by mass of the 5th blade segment, lb-sec ² /ft ² .
M	MACH	Mach number.
M_{PA}	XMBPND	Mass of pendulum absorber, lb-sec ² /ft.
$M_{x_5}, M_{y_5}, M_{z_5}$	(None)	Components of blade moment about axes in the 5-coordinate system, arising from inertia, aerodynamic and/or concentrated mechanical effects, ft-lb.
M_2	SATMOM	The saturation moment used in the nonlinear elastic characteristics of teeter stops, ft-lb.
n	N	Blade segment index.
n_I, n_O	NIP, NOP	Blade segment numbers of inner and outer segments bracketing pendulum absorber mass.
NEM, NFM, NTM	(Same)	Numbers of assumed flatwise, edgewise, and torsion natural "uncoupled" primitive modes, respectively.

LIST OF SYMBOLS (Cont'd)

<u>Symbol</u>	<u>Fortran Equiv.</u>	<u>Description</u>
P_I	(None)	Differential operator denoting differentiation with respect to time of quantities measured in the inertial frame, sec^{-1} .
$P_{x_5}, P_{y_5}, P_{z_5}$	SX5, SY5, SZ5	Section shear load distributions in directions of axes in the 5-coordinate system, lb/in.
P_1, P_2, P_3	P1, P2, P3	Empirical coefficients for C_{Lu} functionality.
q	(None)	General expression for a response variable deflection, (ND).
{ q }	Q	Vector of blade degrees-of-freedom-excluding flapping motion.
q_{v_k}	QVL(K)	Blade k'th edgewise modal response variable, (ND).
q_{w_i}	QWL(I)	Blade i'th flatwise modal response variable, (ND).
$q_{x_5}, q_{y_5}, q_{z_5}$	XM5, YM5, ZM5	Section moment load distributions about axes in the 5-coordinate system, in-lb/in.
q_{θ_j}	QTL(J)	Blade j'th torsion modal response variable, (ND).
Q_1, Q_2, \dots, Q_7	Q1, Q2, ... Q7	Empirical coefficients for C_{Lu} functionality.
r	X(N)	Blade spanwise coordinate, measured from offset, e, in x_5 direction, ft.
Δr_n	DX(N)	n'th blade spanwise segment length, ft.

LIST OF SYMBOLS (Cont'd)

<u>Symbol</u>	<u>Fortran Equiv.</u>	<u>Description</u>
R	R	Rotor radius, ft.
s	SSS	Aerodynamic time.
s _m	SSSM	Nondimensional time measured from instant of stall onset.
R ₁ , R ₂ , ... R ₈	ARE1, ARE2, ... ARE8	Empirical coefficients for C _{Du} functionality.
S _p	STCP	Amplitude of friction moment restraint of pendulum absorber about hinge, ft-lb.
S _{x5} , S _{y5} , S _{z5}	(None)	Components of concentrated shear in directions of axes in the 5-coordinate system, lb.
t	T	Time, sec.
t _{dm}	(None)	Time when dynamic stall first occurs.
[TAS]	TAS	Coordinate transformation matrix relating "5" and "6" coordinate systems, due to structural sweep, (ND).
[T ₀], [T ₁], [T ₂], [T ₅]	(None)	Coordinate system transformation matrixes relating rotating coordinate system deflection to the inertial frame.
u _e	UE	Inward radial (x ₅) foreshortening of blade element point due to combination of built-in sweep and elastic deformation, (ND).
UELSET _{kj} , UELSFT _{ij} , UELASE _{km} , UELASF _{im}	UELSET, UELSFT, UELASE, UELASF	Radial foreshortening of blade element due to nonlinear variation of edgewise, flatwise and torsion modes, (ND).

LIST OF SYMBOLS (Cont'd)

<u>Symbol</u>	<u>Fortran Equiv.</u>	<u>Description</u>
U	U	Total aerodynamic section inflow velocity, (ND).
U_N	UN	Vector sum of U_T and U_P aerodynamic section, inflow velocities, (ND).
$\Delta v, \Delta w$	(None)	Deflection correction terms due to first order twist effects, (ND).
V_x, V_y, V_z	VX,VY,VZ	Components of instantaneous lineal velocity of the nonrotating hub in the hub fixed coordinate system, ft/sec.
$\{v_5\}$	(None)	Vector of components of velocity of a point in the coned, lead-lagged, rotating coordinate system, ft/sec.
$\Delta V, \Delta W$	(None)	Deflection correction terms due to second order twist effects, (ND).
x_1, y_1, z_1	(None)	Components of the 1-coordinate system defined to be hub centered but not rotating, ft.
x_2, y_2, z_2	(None)	Components of the 2-coordinate system defined to be hub centered and rotating about the z_1 axis with rotor speed, Ω , ft.
x_3, y_3, z_3	(None)	Components of the 3-coordinate system defined to rotating with and offset from the hub.
x_4, y_4, z_4	(None)	Components of the 4-coordinate system defined to be rotating with the hub, but at a (-) lagged position.
x_5, y_5, z_5	XX5,YY5,ZZ5	Components of the 5-coordinate system, defined to be rotating with the hub, but at the blade coned and (-) lagged position, ft.
x_6, y_6, z_6	(None),YY6,ZZ6	Components of the 6-coordinate system defined to be rotating with the hub and locally aligned with x_6 tangent to the built-in elastic axis and y_6 and z_6 locally normal to the elastic axis.

LIST OF SYMBOLS (Cont'd)

<u>Symbol</u>	<u>Fortran Equiv.</u>	<u>Description</u>
X_n, Y_n	XALFW, YALFW	Time variables used to calculate α_w using a recursion formula.
$\{X_5\}$	(None)	Vector of components of displacement of a point in the coned, lead-lagged, rotating coordinate system.
y_{5EA}, z_{5EA}	Y5EAB, Z5EAB	Built-in offset distances of elastic axis from x_5 axis, in y_5 and z_5 directions, respectively, (ND).
$\Delta y_{5EA}, \Delta z_{5EA}$	Y5EABC, Z5EABC	Changes per segment (arc) length of built-in elastic axis in y_5 and z_5 directions, respectively, (ND).
y_{10}, z_{10}	(None)	Chordwise and thicknesswise position coordinate, respectively, of an arbitrary point within a blade section, in.
y_{10CG}, z_{10CG}	Y10CG, Z10CG	Chordwise and thicknesswise distances respectively of blade section mass center from the reference axis, in.
y_{10EA}, z_{10EA}	Y10EA, Z10EA	Built-in offset distances of elastic axis from x_5 axis, in edgewise and flatwise directions, respectively, (ND).
[Z]	HBIMPT	Higher harmonic impedance matrix (partial derivatives of hub loads with respect to hub acceleration and HHC angles).
α	AL, ALF, ALTAB	Section angle-of-attack, deg and rad.
$\alpha_{D\alpha}$	ALDM	Aerodynamic section dynamic stall angle-of-attack, deg.
α_E	ALTAB	Effective aerodynamic section angle-of-attack, including effects of unsteady decay parameter, deg.
α_{RE}	ALRTCH	Aerodynamic section reattachment angle-of-attack, deg.

LIST OF SYMBOLS (Cont'd)

<u>Symbol</u>	<u>Fortran Equiv.</u>	<u>Description</u>
α_{SS}	ALFSS	Aerodynamic section static stall angle-of-attack, deg.
α_{TE}	(None)	Section angle-of-attack when vortex nears the trailing edge.
α_w	ALFW	Aerodynamic section unsteady decay parameter, rad.
α_o	(None)	Mean angle-of-attack for oscillating airfoil, deg.
$\bar{\alpha}$	(None)	Angular amplitude for oscillating airfoil, deg.
$\Delta\alpha_1, \Delta\alpha_2$	DELA1, DELA2	Aerodynamic section angle-of-attack shifts to account for unsteady effects.
β	BETAT, FACPGT	Alternately, total cone angle, rad, and Prandtl-Glauert transformation factor, ($=\sqrt{1-M^2}$).
β_B	PREC, BETAB	Built-in blade precone, deg, rad. (as appropriate).
β_p	PNBET	Flapping angle of blade appended pendulum vibration absorber, rad.
β_t	BETA, BETTR	Teeter angle ($=\beta-\beta_B$), rad.
β_1	BETA1	Empirical constant, normally equals 0.18.
β_1, β_2	BETA1, BETA2	Angles defining the nonlinear elastic characteristics of teeter stops, deg.
γ_{v_k}	GV(K)	Deflection mode shape for the k'th edgewise normal mode, (ND).
γ_{w_i}	GW(I)	Deflection mode shape for the i'th flatwise normal mode, (ND).
γ_{θ_j}	GT(J)	Deflection mode shape for the j'th torsion normal mode, (ND).

LIST OF SYMBOLS (Cont'd)

<u>Symbol</u>	<u>Fortran Equiv.</u>	<u>Description</u>
$\Gamma_{y\theta j}, \Gamma_{z\theta j}$	GTNLY,GTNLZ	Nonlinear j'th torsion modal weighting function for torsion excitation due to edgewise and flatwise force loadings, respectively, (ND).
$\tilde{\Gamma}_{y\theta j}, \tilde{\Gamma}_{z\theta j}$	GTNLYP,GTNLZP	Nonlinear j'th torsion modal weighting functions for torsion excitation due to flatwise and edgewise moment loadings, respectively, (ND).
δ	DELTAT	Blade lead angle, rad.
$\delta_1, \delta_2, \delta_3, \delta_4$	DELLC1,DELLC2,DELLC3,DELLC4	Dynamic parameters used in dynamic stalled airloads functionality, (ND).
$\eta_1, \eta_2, \dots, \eta_8$	ETA1,ETA2, ..., ETA8	Empirical coefficients for C_{Mu} functionality.
θ	THE	Elastic torsion deflection angle, rad.
$\theta_{S_X}, \dots, \theta_{M_Z}$	TTHTSX, ..., TTHTMZ	Abbreviated torsion flexibility coefficients containing deflection dependency, rad/lb, rad/ft-lb.
θ_o	THO	Blade pitch angle due to input control angle, rad.
θ_{oPAH}	(None)	Built-in inclination of pendulum absorber hinge axis relative to local chord line, deg, rad (as appropriate).
Θ	TH	Total local blade pitch angle, rad.
$\Delta\theta_j$	DZZ3	Total torsion deflection of flexbeam at junction point beyond built-in value, rad.
Λ_{e5}	(None)	Structural sweep angle projection onto x_5 - y_5 plane, rad.
$\Lambda_{e5}^{(A)}$	(None)	Aerodynamic sweep angle projection onto x_5 - y_5 plane, rad.
Λ_{f5}	(None)	Structural sweep angle projection onto x_5 - z_5 plane, rad.

LIST OF SYMBOLS (Cont'd)

<u>Symbol</u>	<u>Fortran Equiv.</u>	<u>Description</u>
$\Lambda_{f_5}^{(A)}$	(None)	Aerodynamic sweep angle projection onto x_5-z_5 plane, rad.
{E}	(None)	Vector of excitations for two-bladed teetering rotor degrees-of-freedom.
Ξ_q, Ξ_β	XXI1, XXI2, XIBTTR	Component vectors of the E excitation vector relating to modal excitations and flapping excitation, respectively.
$\Delta\Xi_{TS}$	FLMSTP	The moment imparted to the teeter moment by the teeter stops.
ϕ_c	(None)	Generalized Wagner function with compressibility corrections.
ψ	PSI	Blade azimuthal (angular) position, rad.
$\omega_{w_i}, \omega_{v_k}, \omega_{\theta_j}$	FF(I), EF(K), TF(J)	(Nondimensional) uncoupled natural frequencies of i'th flatwise bending mode, k'th edgewise bending mode and j'th torsion mode, respectively, rad/sec.
$\omega_x, \omega_y, \omega_z$	WX, WY, WZ	Components of instantaneous rotational velocity of the nonrotating hub in the hub fixed coordinate system, rad/sec.
Ω	OMEGA	Rotor rotational frequency, rad/sec.

SUBSCRIPTS

() _a	Arising from aerodynamic loading.
() _B	Structurally built-in parameter, or conditions of blade immediately outboard of juncture.
() _D	Effect of dynamic origin.
() _e	Due to elastic deformation.

LIST OF SYMBOLS (Cont'd)

<u>Symbol</u>	<u>Description</u>
$()_{EA}$	Defined at the elastic axis.
$()_h$	With respect to the nonrotating hub.
$()_{HHC}$	Higher harmonic blade pitch control.
$()_I$	With respect to inertial space.
$()_J$	Conditions at flexbeam-torque tube juncture.
$()_P, ()_{PA}$	Pendulum absorber.
$()_{PAH}$	Pendulum absorber hinge.
$()_{TE}$	Defined at the blade trailing edge.
$()_{TS}$	Pertaining to teeter stops.
$()_u$	Pertaining to unsteady stalled aerodynamic effects.
$()^{(1)}, ()^{(2)}$	Pertain to first and second integrals defining the deflection correction function, respectively.
$()^{(m)}$	Pertaining to the m'th blade of a teetered rotor.
$(\bar{\quad})$	Nondimensionalization by combinations of m_0, R and/or Ω .
$(*)$	Differentiation with respect to (Ωt) .
$()'$	Differentiation with respect to (r/R) .

SIMULATION OF UNDERSLUNG TEETERED ROTORS

Basic Modeling Considerations

For articulated and hingeless rotor systems the individual rotor blades are mechanically coupled to each other only through motions of the hub. Consequently, these rotor types can be conveniently analyzed as single-bladed rotors whenever the assumption of infinite hub rigidity is involved. That is, without hub motion, the blades do not interact mechanically with each other. This is not true for teetered (two-bladed) rotors, however. Even for infinite impedance of the supporting shaft, each of the blades of a teetered rotor can impart bending loads to the other through the root load restraint. Accordingly, teetered rotors must be analyzed as a multiple (two) bladed rotor system.

The method of implementing the teetered rotor capability in the G400PA analysis was selected based upon the already inherent use of the Galerkin method of solution. The selected method actually amounts to a "modified Galerkin" approach in that the assumed uncoupled bending modes used to define the blade elastic deformations actually satisfy only the geometric boundary conditions. More specifically, the modeling is based upon the following considerations:

1. The rotor system is assumed to consist of a rigid body finite mass hub which teeters as a rigid body, and two blades which are each cantilever attached to this hub mass. Thus, the out-of-plane displacements for either blade consists of a rigid flapping part plus an elastic part based on "cantilevered" uncoupled mode shapes. For untwisted blades, this displacement distribution (for the n'th blade) assumes the following form (using the nomenclature of Reference 1):

$$z_4^{(m)}(r) = r \left[\beta_B + (-1)^{(m-1)} (\beta - \beta_B) \right] + \sum_{i=1}^{NEM} \gamma_{w_i}(r) q_{w_i}^{(m)}(t) \quad (m=1,2) \quad (1)$$

where $\gamma_{w_i}(r)$ are the uncoupled cantilevered flatwise bending mode shapes. In this formulation, each of the $q_{w_i}^{(m)}$ modal response quantities are independent degrees-of-freedom. The advantage of this formulation is that symmetric bending rotor modes, which respond typically at even harmonics, are simulated exactly, and the antisymmetric rotor modes, which respond typically at odd harmonics, can be well approximated geometrically as "pinned" modes with Equation (1).

2. The blade inplane deflections are simulated with no lead lag rotation, but with combinations of edgewise and flatwise bending as in a typical hingeless configuration.

3. The mass of the hub, to which the blades are cantilever attached, is set to zero as a limiting process. The required moment balance about the teeter hinge (in the flapping direction) is achieved by properly combining the flapping equations for the two blades together with the moment imparted to the teeter motion excitation by the teeter stops.

4. This formulation is inherently incapable of yielding correct bending moment calculations at the root region using mode deflection methods. This is because the formulation uses modes which do not satisfy the "load" boundary conditions at the root. Both the modified Galerkin formulation and the force-integration method, however, are relatively insensitive to these boundary conditions. Consequently, the bending moments and stresses obtained using force-integration, should be reasonably accurate.

The four considerations discussed above form the basis for the actual mathematical formulation discussed in the following subsections. In the first subsection, the load distributions resulting from the flapping motion of an underslung teetered blade are described. In the next subsection, the implementation of the moment equilibration across the teeter hinge is presented. Finally, in the last subsection, the details of the implementation of the teeter stop load characteristics are presented.

Aerodynamic and Dynamic Load Distributions

The analysis presented in Reference 1, and implemented in the parent G400 code, would be sufficient for formulating the teeter flap angle equation, but for the presence of the undersling distance, h_{ust} . This distance is defined as the distance of the rotor-hub apex below the teeter axis. The approach taken for defining the additional loads due to undersling is to define an incremental position vector and to then form the appropriate incremental components of inertial velocity and acceleration, as measured in the blade coordinate system. Using Equation (35) of Reference 1 as a starting point and referring to Figure 1, one can write the incremental (nondimensional) position vector as:

$$\Delta \{X_5\}_{ust} = h_{ust} \begin{Bmatrix} -\beta_B \\ 0 \\ -1 \end{Bmatrix} \quad (2)$$

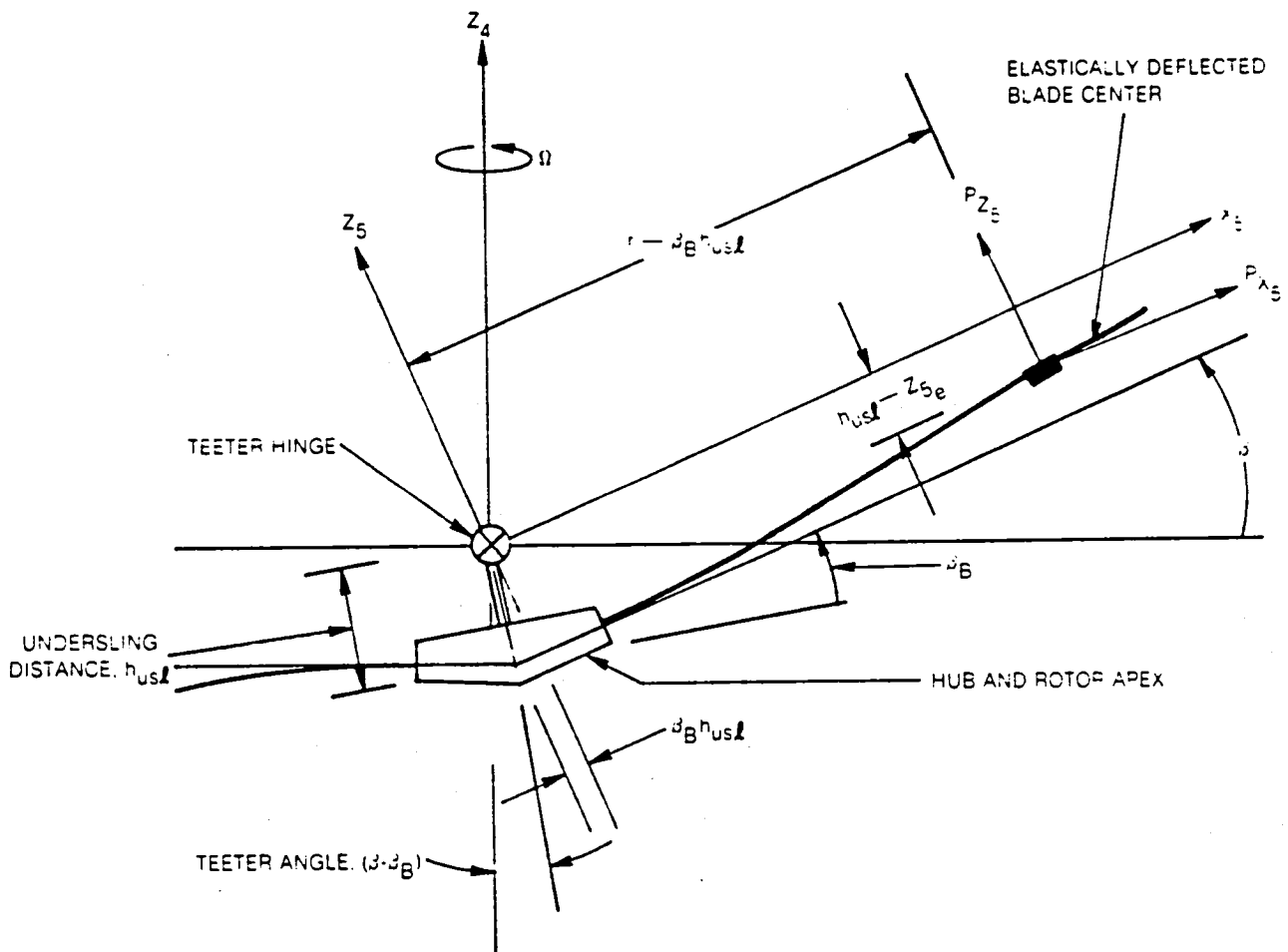


Figure 1. Schematic of Teetered Rotor System — Kinematic Definitions and Flapping Moment Equilibration

Using coordinate system transformations as described in Reference 1 and appropriate differentiation yields the following expression for incremental velocity vector:

$$\{\Delta V_5\}_{ust} = h_{ust} \begin{Bmatrix} \beta^* \\ \beta - \beta_B \\ 0 \end{Bmatrix} \quad (3)$$

This vector then modifies the definition for blade section inflow angle used for defining the quasi-static angle-of-attack, and finally the blade airload distribution. Further use of the coordinate system transformations, additional differentiation and D'Alembert's principle, yields the following vector for the incremental (inertial) dynamic load distribution:

$$\Delta \begin{Bmatrix} p_{Dy5} \\ p_{Dy5} \\ p_{Dy5} \end{Bmatrix} = -\bar{m}h_{ust} \begin{Bmatrix} \beta^{**} - (\beta - \beta_B) \\ 2\beta^* \\ -\beta[\beta^{**} - (\beta - \beta_B)] \end{Bmatrix} \quad (4)$$

Before the teetered blade root constraint can be implemented, the basic flapping equation must also be modified to account for the undersling distance. With reference to Figure 1, equilibration of the moment about the flapping hinge results in the following modified flapping equation:

$$\int_0^l [(r - h_{ust} \beta_B) p_{z5} - (z_{5e} - h_{ust}) p_{x5} - q_{y5}] dr - M_{y5} = 0 \quad (5)$$

This modified equation is to be compared with Equation (31) of Reference 1. Note that p_{x5} and p_{z5} are, respectively, the total load distributions in the x_5 - and z_5 - directions and contain the incremental loads given by Equation (4). The loads due to teeter stops are accounted for by the general moment about the flapping hinge, M_{y5} , this moment defined in greater detail in the following subsection.

Implementation of Teetered Blade Root Constraint

As implemented by the G400 analysis for a single blade (infinite impedance hub), the blade equations of motion take the following form:

$$\begin{bmatrix} A_{qq} & A_{q\beta} \\ A_{q\beta} & A_{\beta\beta} \end{bmatrix} \begin{Bmatrix} q^* \\ \beta^* \end{Bmatrix} = \begin{Bmatrix} \Xi_q(\psi) \\ \Xi_\beta(\psi) \end{Bmatrix} \quad (6)$$

In this form, the elastic mode acceleration subvector, $\{q^{**}\}$, and the flapping acceleration, β^{**} , are linearly coupled, and all remaining linear and nonlinear terms in the various equations are grouped on the right-hand side as an excitation vector. This vector is composed of a subvector for the elastic modes, $\{\Xi_q\}$, and the term for the flapping equations, $\{\Xi_\beta\}$. This form of the equations is appropriate for time-history solutions, but requires a simultaneous equations solution at each time step to decouple the accelerations.

Before two blades are mechanically constrained by the teetered blade boundary conditions, Equation (6) must be generalized to the following augmented form:

$$\begin{bmatrix} A_{qq}^{(1)} & A_{q\beta}^{(1)} & & 0 \\ A_{q\beta}^{(1)T} & A_{\beta\beta} & & \\ & & A_{qq}^{(2)} & A_{q\beta}^{(2)} \\ 0 & & A_{q\beta}^{(2)T} & A_{\beta\beta} \end{bmatrix} \begin{Bmatrix} q^{** (1)} \\ \beta^{** (1)} \\ q^{** (2)} \\ \beta^{** (2)} \end{Bmatrix} = \begin{Bmatrix} \Xi_q^{(1)} \\ \Xi_\beta^{(1)} \\ \Xi_q^{(2)} \\ \Xi_\beta^{(2)} \end{Bmatrix} \quad (7a)$$

or, in a more abbreviated form as:

$$[AA]\{Q^{**}\} = \{\Xi\} \quad (7b)$$

The teetered constraint can be conveniently implemented by first defining the following constraint relationship:

$$\{Q^{**}\} = \begin{bmatrix} 1 & & & & & \\ & 1 & & & & \\ & & 1 & & & \\ & & & 1 & & \\ & & & & 1 & \\ & & & & & 1 \end{bmatrix} \begin{Bmatrix} q^{** (1)} \\ \beta^{** (1)} \\ q^{** (2)} \\ \beta^{** (2)} \end{Bmatrix} \quad (8a)$$

$$= [T]\{\tilde{Q}^{**}\} \quad (8b)$$

The teeter constraint is applied to the equations of motion, Equation (7), with the following matrix operations:

$$[T^T][AA][T]\{\ddot{Q}^{**}\} = [T^T]\{\Xi\} + \{\Delta\Xi\}_{TS} \quad (9)$$

The partitioning of Equation (9) is as follows:

$$\begin{bmatrix} A_{qq}^{(1)} & A_{q\beta}^{(1)} & 0 \\ A_{q\beta}^{(1)T} & 2A_{\beta\beta} & -A_{q\beta}^{(2)T} \\ 0 & -A_{q\beta}^{(2)} & A_{qq}^{(2)} \end{bmatrix} \begin{Bmatrix} \ddot{q}^{** (1)} \\ \ddot{\beta}^{** (1)} \\ \ddot{q}^{** (2)} \end{Bmatrix} = \begin{Bmatrix} \Xi_q^{(1)} \\ \Xi_\beta^{(1)} - \Xi_\beta^{(2)} + \Delta\Xi_{TS} \\ \Xi_q^{(2)} \end{Bmatrix} \quad (10)$$

Equation (10) is then in the same form as Equation (6) and the same procedure must be followed to achieve a time-history solution (decoupling of the accelerations and then numerical integration). Generally, the simultaneous equations solution of Equation (10) is accompanied using partitioning methods; the details of this essentially mathematical operation are outside the scope of this report and are therefore omitted.

Teeter Stop Moment Characteristics

The moment applied to the teeter angle equation due to the teeter stops, $\Delta\Xi_{TS}$, is an essentially nonlinear function of teeter angle. This moment is characterized in the G400PA analysis by the five parameters defined graphically in Figure 2. For teeter angles between $\pm\beta_1$, the teeter stop moment is, of course, zero. When the teeter angle reaches the first limit stop angle, β_1 , the limit stop imparts an initially elastic reaction with a spring rate of K_{β_1} . Between this first limit stop angle and a saturation angle, β_2 , the reaction moment is assumed to be a generally nonlinear function of teeter angle and increases to the value of M_2 with a rate of K_{β_2} , at the saturation angle, β_2 . At teeter angles above β_2 , the reaction moment again obeys an elastic relationship. Generally, the saturation spring rate, K_{β_2} , will exceed the initial rate, K_{β_1} . However, this implementation provides sufficient latitude for modeling other nonlinear relationships. Mathematically, this implementation can be defined as follows:

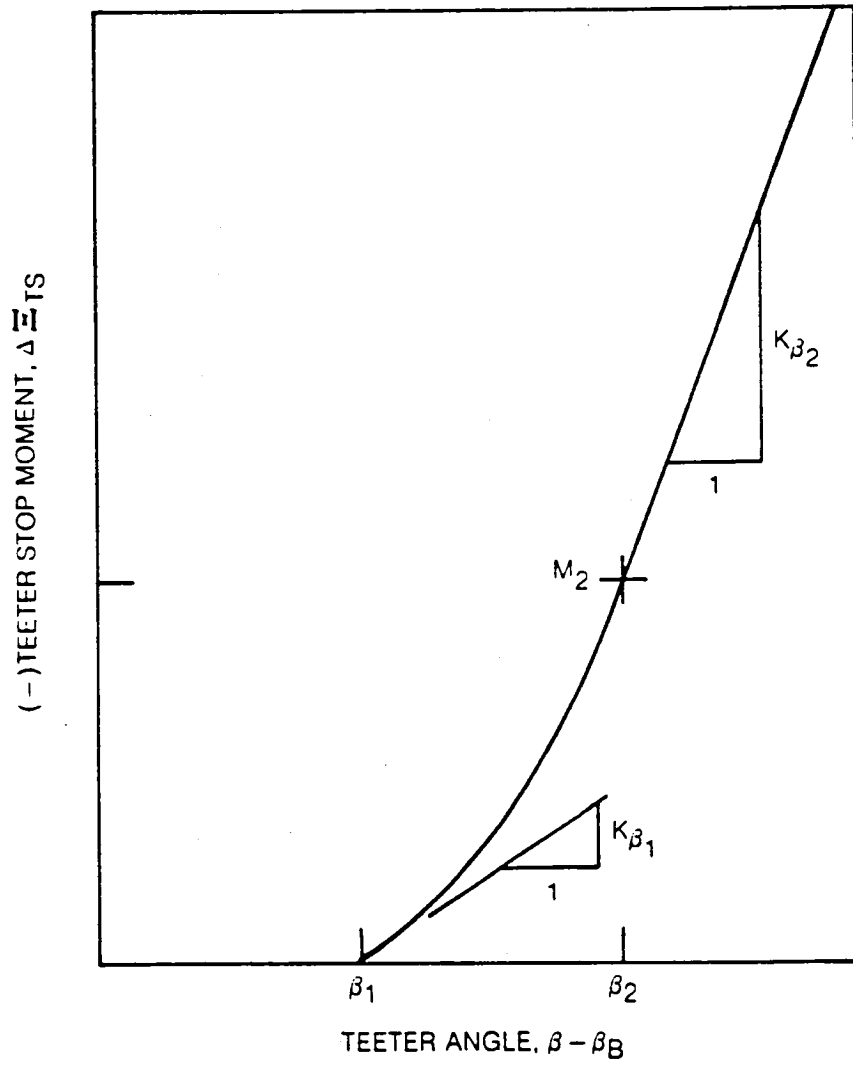


Figure 2. Generalization of Nonlinear Teeter Stop Moment vs Teeter Angle Characteristics

$$\Delta \Xi_{TS} = \left\{ \begin{array}{l} 0, |\beta| \leq \beta_1 \\ -\operatorname{sgn} \beta \left\{ \kappa_{\beta_1} \frac{(|\beta| - \beta_1)(|\beta| - \beta_2)^2}{\Delta \beta_{12}^2} \right. \\ \left. + M_2 \left[1 - \frac{2(|\beta| - \beta_2)}{\Delta \beta_{12}} \right] \left(\frac{|\beta| - \beta_1}{\Delta \beta_{12}} \right)^2 \right. \\ \left. + \kappa_{\beta_2} \frac{(|\beta| - \beta_2)}{\Delta \beta_{12}^2} (|\beta| - \beta_1)^2 \right\}, \beta_1 \leq |\beta| \leq \beta_2 \\ -\operatorname{sgn} \beta \left[\kappa_{\beta_2} (|\beta| - \beta_2) + M_2 \right], \beta_2 \leq |\beta| < \infty \end{array} \right. \quad (11)$$

BLADE APPENDED PENDULUM VIBRATION ABSORBERS

Basic Assumptions

The inclusion of blade appended pendulum absorbers in the aeromechanical description of the rotor blade requires the definition of additional equations of motion, as well as modifications to existing ones. The following list of principal assumptions forms the basis of the G400PA modeling of blade appended pendulum absorbers:

1. Provision must be made for simulating a maximum of two (2) independent pendular absorbers. State-of-the-art installations of such vibration absorbers have included up to two absorbers, each tuned to a different rotor harmonic.

2. Each pendular absorber consists of a specified hinge location, a rigid body mass (with c.g. offset and rotary inertia about that hinge), and a restraint about the hinge accruing from a rotary spring, a rotary viscous damper, and a (nonlinear) friction damper (see Figure 3).

3. The hinge location and orientation for each absorber is subject to the following constraints (again refer to Figure 3):

- a. The hinge axis must be within a blade section plane, e.g., perpendicular to the spanwise axis.
- b. The hinge axis may be both translated and inclined relative to the local chord line. This translation and inclination define the distance, $z_{10_{PAH}}$, and the angle, Θ_{OPA} , shown in Figure 3.
- c. The hinge axis may be located at any spanwise station.

4. The mass center of each absorber is nominally chordwise balanced at the blade elastic (reference) axis, (i.e., no chordwise mass offset, $y_{10_{PA}} = 0$) in the undeflected position. Note that for nonzero values of inclination angle (of the hinge axis relative to the chord line), deflections of the pendulum will produce time variable chordwise c.g., offsets.

5. To enable the analysis to make rapid parameter variations on the pendular parameters, the blade bending and torsion modes are calculated excluding the mass of the pendula. Therefore, the effect of incremental pendulum mass must be explicitly accounted for in the blade dynamic equations. This is accomplished by adding the respective pendulum masses as incremental mass distributions extended over the two blade segments which straddle that pendulum's radial location.

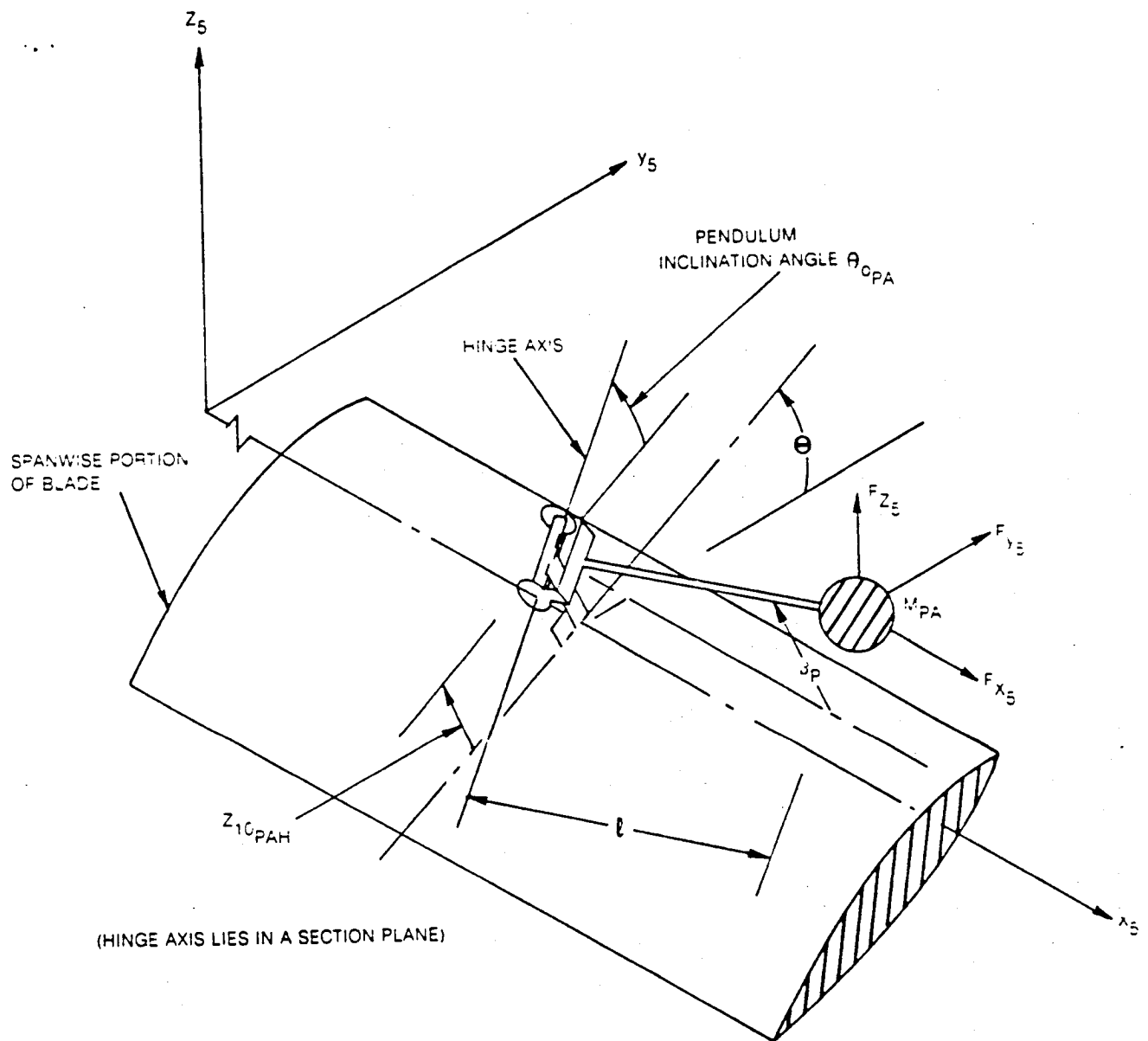


Figure 3. Pictorial of Typical Pendular Absorber Installation on Blade

6. Lastly, the pendula deflection angles are not restricted to "small" amplitudes. Thus, the realistic effects of amplitude saturation can be analyzed.

Dynamic Loads

The derivation of the dynamic loads acting on the pendulum follows the basic method described in the previous chapter wherein an incremental displacement vector is defined, and then with appropriate differentiation and coordinate transformations an inertial acceleration vector is formed. The displacement vector for a point mass hinged to an offset, inclined axis is given by:

$$\Delta \{ X_5 \}_{PA} = l \begin{Bmatrix} \cos \beta_p \\ -\sin \Theta_{PAH} \sin \beta_p \\ \cos \Theta_{PAH} \sin \beta_p \end{Bmatrix} + Z_{IO_{PAH}} \begin{Bmatrix} 0 \\ -\sin \Theta \\ \cos \Theta \end{Bmatrix} \quad (12)$$

where the total pitch angle of the hinge axis, Θ_{PAH} , is the sum of the blade pitch axis, Θ , and the built-in pitch angle relative to the blade, Θ_{OPA} . The resulting components of inertia loading are then given by the following equations:

$$\left(\Delta p_{D_{X_5}} \right)_{PA} = \frac{-M_{PA} f_i l}{m_0 \Delta r_i} \left[-\sin \beta_p \ddot{\beta}_p^* - \cos \beta_p + 2 \cos \beta_p \dot{\beta}_p^* \sin \Theta_{PAH} + (\beta + 2\theta) \sin \beta_p \cos \Theta_{PAH} \right] \quad (13a)$$

$$\begin{aligned} \left(\Delta p_{D_{Y_5}} \right)_{PA} = & \frac{-M_{PA} f_i}{m_0 \Delta r_i} \left\{ l \left[-\cos \beta_p \sin \Theta_{PAH} \ddot{\beta}_p^* - 2 \sin \beta_p \dot{\beta}_p^* \right. \right. \\ & \left. \left. + \sin \beta_p (1 + 2\delta + \beta_p^2 + \theta^2) \sin \Theta_{PAH} \right. \right. \\ & \left. \left. - (2 \cos \beta_p (\dot{\beta}_p^* \theta + \beta \dot{\beta}_p^*) + \sin \beta_p (2\beta + \theta)) \cos \Theta_{PAH} \right] \right. \\ & \left. + Z_{IO_{PAH}} \left[-2 (\dot{w}_e^* - \Delta \dot{w}^{(2)} - \Delta \dot{w}^{(2)}) - (\dot{\Theta} + 2\dot{\beta}) \cos \Theta \right. \right. \\ & \left. \left. + (1 + \dot{\Theta}^2 + 2\beta \dot{\Theta} + 2\dot{\delta}) \sin \Theta \right] \right\} \quad (13b) \end{aligned}$$

$$\begin{aligned}
\left(\Delta p_{DZ_5}\right)_{PA} &= \frac{-M_{PA} f_i}{m_o \Delta r_i} \left\{ \ell \left[\cos \beta_p \cos \Theta_{PAH} \ddot{\beta}_p^* \right. \right. \\
&\quad \left. \left. - (2 \cos \beta_p (\dot{\beta}_p^* \dot{\theta}^* + \beta \dot{\beta}_p^*) + \sin \beta_p^* \dot{\theta}^*) \sin \Theta_{PAH} - \sin \beta_p (\dot{\beta}^2 + \dot{\theta}^2 + 2 \beta \dot{\theta}^*) \cos \Theta_{PAH} \right] \right. \\
&\quad \left. + Z_{IO_{PAH}} \left[-(\dot{\Theta}^2 + 2 \beta \dot{\Theta}^* + \beta^2) \cos \Theta - \dot{\Theta}^* \sin \Theta \right] \right\} \quad (13c)
\end{aligned}$$

where the distribution function, f_i , is defined for only two of the blade spanwise segments, the centers form a straddling pair: the one closest inboard, $r(n_I)$, and the one closest outboard, $r(n_O)$, of the pendulum mass center location, r_{PA} : (see Figure 4):

$$f_i = \begin{cases} \frac{r(n_O) - r_{PA}}{r(n_O) - r(n_I)} ; i = n_I \\ \frac{r_{PA} - r(n_I)}{r(n_O) - r(n_I)} ; i = n_O \end{cases} \quad (14)$$

Equations (13) and (14) are then in a general form appropriate for inclusion in the blade dynamic equations. Note that the nominal inertia load distributions, given by Equations (41a, b, c) and (44a, b, c) of Reference 1 must also be modified since, at the two straddling radial stations, the mass distributions must be augmented by $M_{PA} f_i$.

Equations of Motion

The usual blade dynamic equations (those for modal responses, flapping and lead-lag motions) are easily modified by including the additional inertia load distributions as defined in the above subsection. The pendulum equations are formed by equilibrating the inertia moments about the hinge to the spring and damper restraints:

$$I_p \ddot{\beta}_p^* = \ell \left[\cos \beta_p F_{Z_6} - \sin \beta_p F_{X_5} \right] - K_p \beta_p - C_p \dot{\beta}_p^* - S_p \operatorname{sgn}(\dot{\beta}_p^*) \quad (15)$$

where the concentrated loads acting on a pendulum mass center, F_{X_5} and F_{Z_6} , are given by:

$$F_{X_5} = \tilde{p}_{X_5} + \Delta \tilde{p}_{X_5} \quad (16a)$$

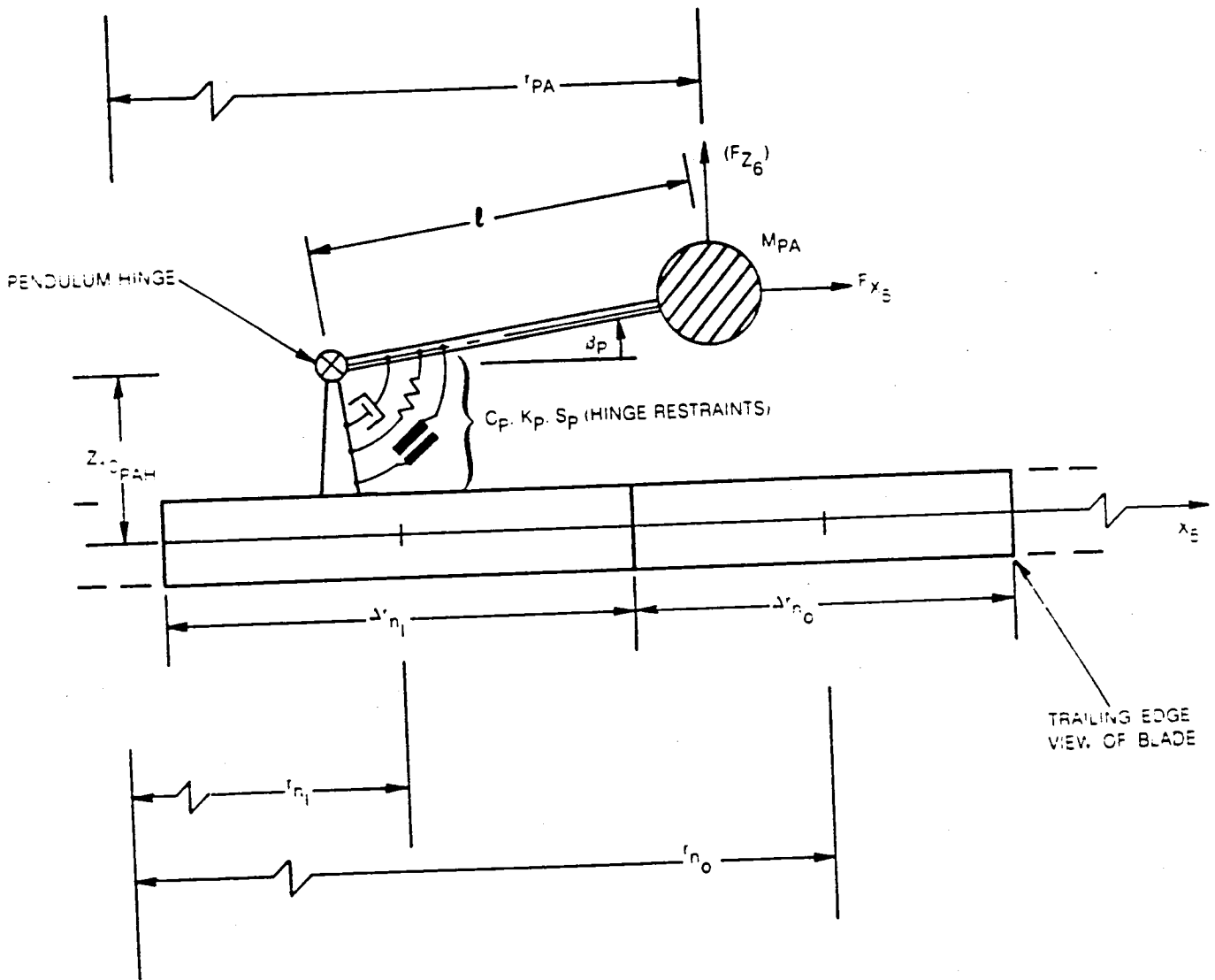


Figure 4. Blade Trailing Edge View of Blade/Pendular Absorber System — Kinematic Definitions and Moment Equilibration

$$F_{Z_6} = -\sin \Theta_{PAH} \left(\tilde{p}_{y_5} + \Delta \tilde{p}_{y_5} \right) + \cos \Theta_{PAH} \left(\tilde{p}_{z_5} + \Delta \tilde{p}_{z_5} \right) \quad (16b)$$

and where the quantities \tilde{p}_{x_5} , \tilde{p}_{y_5} , \tilde{p}_{z_5} are components of the usual blade inertia loadings for the straddling segments modified by the following multiplication:

$$\tilde{p}_{PA} = \sum_{i=n_I}^{n_0} \frac{M_{PA} f_i}{m_0 \Delta r_i \bar{m}} p(r_i) \quad (17)$$

The quantities, $(\Delta \tilde{p}_{x_5}$, $\Delta \tilde{p}_{y_5}$ and $\Delta \tilde{p}_{z_5}$ are formed from Equations (13a, b and c), respectively, but with the factor $(f_i/m_0 \Delta r_i)$ set equal to unity, and all the $\ddot{\beta}_P^*$ dependent terms deleted. All such $\ddot{\beta}_P^*$ terms are instead grouped into the single inertia-acceleration term on the left-hand side of Equation (15). Note that I_p is the effective rotary inertia of the pendulum about the hinge. The above development is the same for either pendulum and subscripting to denote pendulum index was omitted for clarity.

BLADE LOADS DUE TO HIGHER HARMONIC EXCITATIONS

As originally formulated, the G400 aeroelastic analysis simulated a wide spectrum of "higher harmonic" blade loads. The term "higher harmonic" is used herein to denote frequency content in the range of blade number (b) x rotor rotation frequency (Ω), and above. Indeed, because of the multi-harmonic nature of the local dynamic pressure of helicopter blade section in forward flight, higher harmonic airloads ensue even from the usual collective and simple harmonic cyclic blade pitch angles. Another explicit source of higher harmonic airloads is the considerable harmonic variability of the inflow velocities induced in the rotor plane by the vortex structure of the rotor itself. Reference (3) presents an in-depth description of this theory and its interactive implementation with the G400 analyses.

Two further sources of higher harmonic excitation are considered herein. The first, prescribed harmonic motion of the hub, is required to evaluate the characteristics of the rotor coupling with the airframe. This coupling is accomplished in the Simplified Coupled Rotor/Airframe Vibration Analysis (SIMVIB) using the rotor impedance matrices computed in the G400PA code. The details of this calculation are described in a subsection below. The second source of higher harmonic excitation considered, higher harmonic pitch control, is included to provide an important analytic capability for application to a timely area of helicopter vibration of research and development. Technical developments of each of these sources of higher harmonic excitation are presented in the subsections which follow.

Prescribed Harmonic Hub Motions

The required impedance matrix is the collection of partial derivatives of the six components of hub vibratory loads (3 shears and 3 moments) with respect to each of the six components of hub vibratory acceleration (3 translations and 3 rotations). This calculation is generally implemented by first achieving harmonic responses with selective perturbations in each of the components of acceleration and then forming numerical partial derivatives of the hub loads. The actual hub loads are calculated using the force-integration method (see Reference 4) together with the total resulting inertia, gravity and aerodynamic blade load distributions. The details of this calculation do not represent new technology and, consequently, are omitted herein.

Of more importance are the calculations of the incremental airloads and dynamic loads due to harmonic hub motion. For this purpose, the components of inertia velocity and acceleration, in the blade coordinate system are required. Generally, the hub degrees-of-freedom are defined in the nonrotating

(with rotor speed, Ω) body-fixed axis system; therefore, the basic degrees-of-freedom are the instantaneous velocity components along (or about) coordinate axes fixed to the "nonrotating", but generally moving hub. Because of this definition of basic hub degrees-of-freedom, the actual deflections (translations and rotations) are subject to the order of integration and the appropriate Euler angles must be suitably defined and integrated in this context. Furthermore, recourse must be made to the Theorem of Coriolis (Reference 5) to obtain the correct differentiation with respect to time as measured in an inertial space. The material to follow outlines the approach for making these differentiations and obtaining their components in the blade coordinate system. Much intermediate calculation is omitted for clarity, and the final results include the previously considered effects of undersling (teetered rotor feature) and thickness noise mass center offsets (pendulum absorber feature).

Consider the vector sum for a point mass at a blade section:

$$\bar{X}_I = \bar{X}_O + \bar{X}_1 + \bar{X}_2 \quad (18)$$

where X_I is the position vector with respect to inertial space. X_O is the position vector of the nonrotating (with respect to Ω) hub:

$$\{X_O\} = [T_O] \{X_h\} \quad (19)$$

$[T_O]$ is the coordinate transformation due to hub orientation motion and $\{X_h\}$ is the position vector of the hub in the hub fixed system. Consistent with the definition of the hub centered coordinate system, $[T_O]$ and $\{X_h\}$ can be considered to be unity and null, respectively, at any instant in time, but have finite time derivatives. $\{X_1\}$ is the position vector of the offset/blade root point:

$$\{X_1\} = [T_O][T_1]\{e\} \quad (20)$$

where $[T_1]$ is the coordinate system transformation due to rotor rotation, and $\{e\}$ is the position vector from the hub center to the blade root point. $\{X_2\}$ is the position vector due to blade element displacement within the blade coordinate system:

$$\{X_2\} = [T_O][T_1][T_2]\{X_5\} \quad (21)$$

where $[T_2]$ is the coordinate transformation due to flapping and lead-lag about a common point, and $[X_5]$ is the position vector of the point mass within the blade "5" coordinate system. Specific definitions for the coordinate transformations and position vectors are as follows:

$$[T_0^*] = \begin{bmatrix} 0 & -\omega_z & \omega_y \\ \omega_z & 0 & -\omega_x \\ -\omega_y & \omega_x & 0 \end{bmatrix} \quad (22a)$$

$$[T_1] = \begin{bmatrix} c\psi & -s\psi & 0 \\ s\psi & c\psi & 0 \\ 0 & 0 & 1 \end{bmatrix} \quad (22b)$$

$$[T_2] = \begin{bmatrix} 1 & -\delta & -\beta \\ \delta & 1 & 0 \\ \beta & 0 & 1 \end{bmatrix} \quad (22c)$$

$$\{e\} = \begin{Bmatrix} \bar{e} + \bar{h}_{ust}(\beta - \beta_B) \\ 0 \\ -\bar{h}_{ust} \end{Bmatrix} \quad (22d)$$

$$\{X_5\} = \begin{Bmatrix} \bar{r} + \epsilon_x \\ \bar{y}_{10} c\Theta - \bar{z}_{10} s\Theta + \epsilon_y \\ \bar{y}_{10} s\Theta + \bar{z}_{10} c\Theta + \epsilon_z \end{Bmatrix} \quad (22e)$$

where ϵ_x , ϵ_y and ϵ_z are the elastic deflections in the x_5 , y_5 and z_5 directions, respectively, and are functions of the modal responses, structured twist, etc. Furthermore, for convenience, a matrix $[T_5]$ is defined which transforms from the nonrotating blade root to the blade "5" coordinate system:

$$[T_5] = [T_1][T_2] \quad (23)$$

Other operations on the T_5 matrix which are useful:

$$[T_5]^{-1} = \begin{bmatrix} 1 & \delta & \beta \\ -\delta & 1 & 0 \\ -\beta & 0 & 1 \end{bmatrix} \begin{bmatrix} c\psi & s\psi & 0 \\ -s\psi & c\psi & 0 \\ 0 & 0 & 1 \end{bmatrix} \quad (24)$$

$$[T_5^*] = \begin{bmatrix} -[(1+\delta^*)s\psi + \delta c\psi] & -(1+\delta^*)c\psi + \delta s\psi & [\beta s\psi - \beta^* c\psi] \\ [(1+\delta^*)c\psi - \delta s\psi] & -[(1+\delta^*)s\psi + \delta c\psi] & -[\beta c\psi + \beta^* s\psi] \\ \beta^* & 0 & 0 \end{bmatrix} \quad (25)$$

The total inertial velocity vector, is defined using the Theorem of Coriolis and is given in matrix form as follows:

$$\begin{aligned} p_I \{X_I\} = & [T_0] \{X_h^*\} + \left[[T_0^*][T_1] + [T_0][T_1^*] \right] \{e\} \\ & + [T_0][T_1] \{\dot{e}\} + \left[[T_0^*][T_5] + [T_0][T_5^*] \right] \{X_5\} + [T_0][T_5] \{X_5^*\} \end{aligned} \quad (26)$$

where the operator p_I denotes differentiation with respect to time, as measured in the inertial coordinate frame.

The terms underlined are deleted because they do not contribute to hub motion. Note that in this formulation, the actual hub deflections (translations and rotations) are taken as zero at any instant in time.

Transformation into components in the "5" coordinate system is accomplished by premultiplication by $[T_5]^{-1}$, and retention of only those terms relating to hub motion and/or undersling results in the following:

$$\begin{aligned} \{\Delta V_5\} = & [T_5]^{-1} \{X_5^*\} \\ = & \begin{Bmatrix} V_x(c\psi - \delta s\psi) + V_y(s\psi + \delta c\psi) + \beta V_z \\ -V_x(s\psi + \delta c\psi) + V_y(c\psi - \delta s\psi) \\ -\beta(V_x c\psi + V_y s\psi) + V_z \end{Bmatrix} + \bar{e} \begin{Bmatrix} \omega_z \delta \\ \omega_z \\ -\omega_y c\psi + \omega_x s\psi \end{Bmatrix} \\ & + \bar{h}_{usl} \begin{Bmatrix} \omega_x s\psi - \omega_y c\psi \\ \omega_y s\psi + \omega_x c\psi + (\beta - \beta_B)\omega_z \\ 0 \end{Bmatrix} + \bar{r} \begin{Bmatrix} 0 \\ \omega_z - \beta(\omega_y s\psi + \omega_x c\psi) \\ -\omega_y(c\psi - \delta s\psi) + \omega_x(s\psi + \delta c\psi) \end{Bmatrix} \\ & + (\bar{y}_{10} c\Theta - \bar{z}_{10} s\Theta) \begin{Bmatrix} -\omega_z + \beta(\omega_x c\psi + \omega_y s\psi) \\ 0 \\ \omega_x c\psi + \omega_y s\psi \end{Bmatrix} + (\bar{y}_{10} s\Theta + \bar{z}_{10} c\Theta) \begin{Bmatrix} \omega_y c\psi - \omega_x s\psi \\ -(\omega_y s\psi + \omega_x c\psi) \\ 0 \end{Bmatrix} \end{aligned} \quad (27)$$

Equation (27) then gives the components of incremental velocity at the local blade section with which the tangential and normal components of air velocity, U_T and U_p , respectively, can be appropriately modified. The total blade section inflow angle, $\phi (= \tan^{-1} (U_p/U_T))$, is then formed in the usual manner and included in the section angle-of-attack. In this manner, the effects of prescribed hub motion are included in the airload distribution.

The inertia (dynamic) load distributions require the second time derivative with respect to inertial space. The Theorem of Coriolis is now applied to the velocity vector, Equation (26), rather than the displacement vector:

$$\begin{aligned}
 \rho_I \{ \rho_I X_I \} &= [T_0] \{ \dot{X}_h^* \} + [\dot{T}_0] \{ \dot{X}_h \} \\
 &+ 2 \left[\begin{array}{l} \underline{[\dot{T}_0][T_1]} + \underline{[T_0][\dot{T}_1]} \end{array} \right] \{ \dot{e} \} + \underline{[T_0][T_5]} \{ \dot{X}_5^* \} \\
 &+ \left[\begin{array}{l} \underline{[\dot{T}_0^*][T_1]} + 2 \underline{[\dot{T}_0][\dot{T}_1]} + \underline{[T_0][\dot{T}_1^*]} \end{array} \right] \{ e \} + \underline{[T_0][T_1]} \{ \dot{e}^* \} \\
 &+ 2 \left[\begin{array}{l} \underline{[\dot{T}_0][T_5]} + \underline{[T_0][\dot{T}_5]} \end{array} \right] \{ \dot{X}_5 \} \\
 &+ \left[\begin{array}{l} \underline{[\dot{T}_0^*][T_5]} + 2 \underline{[\dot{T}_0][\dot{T}_5]} + \underline{[T_0][\dot{T}_5^*]} \end{array} \right] \{ X_5 \}
 \end{aligned} \tag{28}$$

The underlined terms are deleted because they do not contain contributions accruing from hub motion. After the indicated operations have been performed, the following expressions for incremental components of inertia load distribution are obtained:

$$\begin{aligned}
\Delta \begin{Bmatrix} p_{D_{x_5}} \\ p_{D_{y_5}} \\ p_{D_{z_5}} \end{Bmatrix} &= -\bar{m} \left\{ \begin{aligned} &\beta(\dot{V}_z - \omega_y V_x + \omega_x V_y) + (\dot{V}_x - \omega_z V_y + \omega_y V_z) c(\psi + \delta) + (\dot{V}_y + \omega_z V_x - \omega_x V_z) s(\psi + \delta) \\ &(\dot{V}_y + \omega_z V_x - \omega_x V_z) c(\psi + \delta) - (\dot{V}_x - \omega_z V_y + \omega_y V_z) s(\psi + \delta) \\ &\dot{V}_z - \omega_y V_x + \omega_x V_y - \beta[(\dot{V}_x - \omega_z V_y + \omega_y V_z) c\psi + (\dot{V}_y + \omega_z V_x - \omega_x V_z) s\psi] \end{aligned} \right\} \\
&+ (\bar{r} + \bar{e}) \left\{ \begin{aligned} &-2[\omega_x - \beta(\omega_x c\psi + \omega_y s\psi)] \\ &\dot{\omega}_z - \beta(\dot{\omega}_x c\psi + \dot{\omega}_y s\psi) \\ &2\beta\omega_z - (\dot{\omega}_y - 2\omega_x) c(\psi + \delta) + (\dot{\omega}_x + 2\omega_y) s(\psi + \delta) \end{aligned} \right\} \\
&+ \bar{e} \left\{ \begin{aligned} &\dot{\omega}_z \delta - \beta(\dot{\omega}_y c\psi - \dot{\omega}_x s\psi) \\ &2\omega_z \delta + \beta(\dot{\omega}_x c\psi + \dot{\omega}_y s\psi) \\ &-\delta[(\dot{\omega}_x + 2\omega_y) c\psi + (\dot{\omega}_y - 2\omega_x) s\psi] \end{aligned} \right\} \\
&+ (\bar{y}_{10} c\Theta) - \bar{z}_{10} s\Theta \left\{ \begin{aligned} &-\dot{\omega}_z + [\beta\dot{\omega}_x + 2(\beta + \bar{\theta}_0)\omega_y] c\psi + [\beta\dot{\omega}_y - 2(\beta + \bar{\theta}_0)\omega_x] s\psi \\ &2[-\omega_z - \bar{\theta}_0(\omega_x c\psi + \omega_y s\psi)] \\ &\beta\dot{\omega}_z + (\dot{\omega}_x + 2\omega_y) c\psi + (\dot{\omega}_y - 2\omega_x) s\psi \end{aligned} \right\} \quad (29) \\
&+ \bar{n}_{ust} \left\{ \begin{aligned} &\dot{\omega}_x s\psi - \dot{\omega}_y c\psi - 2(\beta - \beta_B)\omega_z \\ &(\beta - \beta_B)\dot{\omega}_z + \dot{\omega}_x c\psi + \dot{\omega}_y s\psi \\ &\beta_B(\dot{\omega}_y c\psi - \dot{\omega}_x s\psi) + 2(\beta - \beta_B)(\omega_y s\psi + \omega_x c\psi) \end{aligned} \right\} \\
&+ (\bar{y}_{10} s\Theta + \bar{z}_{10} c\Theta) \left\{ \begin{aligned} &2(\beta + \theta_0)\omega_z + \dot{\omega}_y c(\psi + \delta) - \dot{\omega}_x s(\psi + \delta) \\ &-\beta\dot{\omega}_z - \omega_x c(\psi + \delta) - \dot{\omega}_y s(\psi + \delta) \\ &-2(\beta + \theta_0)(\omega_x c\psi + \omega_y s\psi) \end{aligned} \right\} \Bigg\}
\end{aligned}$$

In both Equations (27) and (28) the expressions for hub velocity and acceleration are completely general. For present purposes, these components of velocity and acceleration are to be prescribed as simple (but higher) harmonic functions:

$$\begin{Bmatrix} v_j \\ \omega_j \end{Bmatrix} = \begin{Bmatrix} v_{jnc} \\ \omega_{jnc} \end{Bmatrix} c(n\psi) + \begin{Bmatrix} v_{jns} \\ \omega_{jns} \end{Bmatrix} s(n\psi) \quad (30)$$

where $j = x, y, \text{ or } z$, and where n is equal to a prescribed multiple of the number of blades. To minimize the computational requirements for calculating these trigonometric functions, the following identities are utilized:

$\frac{n}{1}$	$\frac{c(n\psi)}{c\psi}$	$\frac{s(n\psi)}{s\psi}$	
2	$1 - 2(s\psi)^2$	$2(s\psi)(c\psi)$	
3	$4(c\psi)^3 - 3(c\psi)$	$3(s\psi) - 4(s\psi)^3$	
≥ 4	$2c(n-1)\psi c\psi - c(n-2)\psi$	$2s(n-1)\psi c\psi - s(n-2)\psi$	(31)

Higher Harmonic Blade Pitch Control

The implementation of higher harmonic pitch control (HHC) in the G400PA analysis is a relatively straightforward task. For this type of higher harmonic excitation, the incremental blade pitch angle is assumed to be of the following form:

$$\begin{aligned} \Delta\theta_{\text{HHC}} = & -A_{n-1_s} c(b-1)\psi - B_{n-1_s} s(b-1)\psi \\ & -A_{n_s} c(b\psi) - B_{n_s} s(b\psi) \\ & -A_{n+1_s} c(b+1)\psi - B_{n+1_s} s(b+1)\psi \end{aligned} \quad (32)$$

The amplitudes in this partial Fourier series are generally prescribed, or are perturbed in order to obtain the partial derivative matrix of hub loads with respect to HHC pitch amplitudes. The incremental pitch control angle given by Equation (32) is then used to define the blade airloads and to complete the calculations for θ_o , $\dot{\theta}_o$ and $\ddot{\theta}_o^*$ used in forming the blade inertia load distributions.

Impedance Matrix Calculation

The impedance matrix is defined as the array of partial derivatives of components of hub loads with respect to components of higher harmonic excitation variables.

$$[Z] = \begin{bmatrix} \frac{\partial(x_{c_i}, x_{s_i})}{\partial(q_{c_j}, q_{s_j})} \end{bmatrix} \begin{matrix} | \leq i \leq 6 \\ | \leq j \leq 9 \end{matrix} \quad (33)$$

These X_{c_i} and X_{s_i} terms are, respectively, the cosine and sine components of each of the six components of hub load, X_T , and similarly, q_{c_j} and q_{s_j} are, respectively, the cosine and sine components of the higher harmonic excitation variables, q_j . Specifically, these consist of each of the six components of hub vibratory amplitude (cosine and sine) and three higher harmonic control pitch amplitudes (cosine and sine). The calculations for these derivatives are accomplished numerically by first obtaining responses which are converged to periodicity without, and then, with perturbations in each of the higher harmonic excitation variables, q_j :

$$\frac{\partial x_i}{\partial q_j} \approx \frac{x_i(q_j + \Delta q_j) - x_i(q_j)}{\Delta q_j} \quad (34)$$

In practice, the perturbation amplitudes are selected to achieve calculations of the partial derivatives which approach limit values. Due to round-off characteristics of the computer and the inability to achieve exactly converged responses, there is generally a practical limit to how small the various Δq_j values can be. Some care and experimentation are therefore warranted in the selection of the Δq_j perturbation levels.

SPANWISE VARIABLE ELASTIC AXIS OFFSET

Originally, the G400 technology assumed the elastic axis to define a space-curve as a result of combined flatwise and edgewise bending. For this case, the blade curvature is directly proportional to the elastic modal degrees-of-freedom. This situation simplified the structural modeling especially with regard to the nonlinear torsion excitation which resulted from a combination of flatwise and edgewise bending. For built-in variable elastic offset (structural sweep), the accurate definition of sweep in terms of its curvature becomes impractical. An approximation to the blade kinematics resulting from "small sweep" could be obtained by just considering the structural sweep to consist of "pre-bends" in the elastic axis, however this procedure becomes suspect at moderate to large structural sweep. In the case of the kinematics of radial foreshortening, the absence of elastic axis offset can be shown to be a quadratically nonlinear function of bending deformations. The presence of elastic axis offset, however, introduces linear terms in the bending deformations.

Torsion Excitation for Elastic Axis as a Space Curve

As given in Reference 1, the torsion differential equation (35) is comprised of elastic stiffening terms, combinations of distributed moments, and nonlinear torsion loads. These torsion loads are due to distributed forces acting on moment arms provided by curvature in the elastic axis.

$$\underbrace{\left[GJ\theta_e' + \Theta_A^2 T + \frac{1}{2} EB_1(\Theta^2 - \theta_B^2)\theta' - EB_2\theta_B'v_e'' \right]'}_{\text{elastic stiffening}} \quad \textcircled{I}$$

$$= \underbrace{\left[-q_{x_5} - y_5' q_{y_5} - z_5' q_{z_5} \right]}_{\text{moment loadings}} \quad \textcircled{II} \quad (35)$$

$$+ \left\{ y_5'' \int_r^1 \left[z_5' \int_{r_1}^1 p_{x_5}(r_2) dr_2 - \int_{r_1}^1 p_{z_5}(r_2) dr_2 + q_{y_5}(r_1) \right] dr_1 \right. \\ \left. - z_5'' \int_r^1 \left[y_5' \int_{r_1}^1 p_{x_5}(r_2) dr_2 - \int_{r_1}^1 p_{y_5}(r_2) dr_2 - q_{z_5}(r_1) \right] dr_1 \right\} \quad \textcircled{III}$$

curvatures
functions of force loadings

In Reference 1, the curvatures used in the (nonlinear) third portion of the torsion equation were assumed to arise entirely from the elastic bending deflections, v_e'' and w_e'' . It can be shown that the nonlinear excitation term in Equation (35) can be reduced to the familiar difference of bending stiffness shown in equation (36):

$$\{\dots\}_{\text{III}} = \left[(EI_z - EI_y) v_e'' w_e'' - (e_A T + EB_2 (\theta_B' + \frac{1}{2} \theta_e') \theta_e') w_e'' \right] \quad (36)$$

Though this method for including the effect is simple, several difficulties exist in implementing it. First, the implementation of equation (36) is based on a "mode deflection" formulation. Studies on the characteristics of "mode deflection" (References 4 and 6) have established that convergence to accurate representations of internal bending moment is often not assured with a small number of modes. This accuracy problem is then compounded by the fact that the two components of this nonlinear excitation are subtractive as is evidenced by the differencing of the section bending stiffnesses shown above.

The second difficulty with using the δEI method relates to the assumed space-curve character of the elastic axis. Torsion deflections are contribute to inplane and out-of-plane deflections in the presence of bending. Thus, an analogous nonlinear excitation effect exists in both the flatwise and edgewise bending equations. In the framework of the G400 analysis, these nonlinear excitations in the bending equations are most practically implemented using a "force integration" approach. Consequently, the combination of using a ΔEI mode deflection method in the torsion equation and a force integration method in the bending equations results in a (coupled) modal mass matrix, which is generally nonsymmetric. A nonsymmetric mass matrix is not intrinsically a weakness for isolated rotor simulation and has been successfully used for years in that mode. However, the potential exists for spurious divergent response conditions caused by an inertia matrix becoming nonpositive-definite.

Finally, the third difficulty is in including the built-in curvature due to structural sweep. Equation (36) requires curvature information which is not generally available for the built-in geometry.

Because of these difficulties, the conventional ΔEI approach of Equation (36) was abandoned in favor of a "force integration" approach. Accordingly, the Galerkin approach is applied to the nonlinear excitation term and integration by parts is used to achieve an intermediary step needed to eliminate the explicit curvature terms:

$$\begin{aligned}
 \int_0^1 \gamma_{\theta_j} \{ \dots \}_{\text{III}} dr &= \int_0^1 \left\{ -p_{z_5} \int_0^{\bar{r}} \int_0^{\bar{r}_1} \gamma_{\theta_j} y_5'' dr_2 dr_1 \right. \\
 &+ p_{y_5} \int_0^{\bar{r}} \int_0^{\bar{r}_1} \gamma_{\theta_j} z_5'' dr_2 dr_1 + (z_5' T + q_{y_5}) \int_0^{\bar{r}} \gamma_{\theta_j} y_5'' dr_1 \\
 &\left. - (y_5' T - q_{z_5}) \int_0^{\bar{r}} \gamma_{\theta_j} z_5'' dr_1 \right\} d\bar{r}
 \end{aligned} \tag{37}$$

Since this term represents the nonlinear effects, it is reasonable to use a zeroth order approximation to the curvature terms wherein the structural sweep is assumed to be "small". With this assumption, all the integrals in Equation (37) can be evaluated using the deflection correction functions defined in the previous subsections. Thus, Equation (37) becomes:

$$\begin{aligned}
 \int_0^1 \gamma_{\theta_j} \{ \dots \}_{\text{III}} dr &= \int_0^1 \left\{ \Gamma_{y_{\theta_j}} [p_{y_5} \cos \Theta + p_{z_5} \sin \Theta] \right. \\
 &- \Gamma_{z_{\theta_j}} [p_{z_5} \cos \Theta - p_{y_5} \sin \Theta] \\
 &+ \tilde{\Gamma}_{z_{\theta_j}}^x [T(w_e' - \Delta w^{(2)'} - \Delta w^{(2)'}) + q_{y_5} \cos \Theta + q_{z_5} \sin \Theta] \\
 &\left. - \tilde{\Gamma}_{y_{\theta_j}}^x [T(v_e' + \Delta v^{(2)'} - \Delta v^{(2)'}) - q_{z_5} \cos \Theta + q_{y_5} \sin \Theta] \right\} dr
 \end{aligned} \tag{38}$$

where:

$$\Gamma_{y_{\theta_j}} = \gamma_{\theta_j} (w_e + z_{10EA} - \Delta w - \Delta W) - (\Delta v_{\theta_j} - \Delta v_{\theta_j}') \tag{39a}$$

$$\Gamma_{z_{\theta_j}} = \gamma_{\theta_j} (v_e + y_{10EA} + \Delta v - \Delta V) - (\Delta w_{\theta_j} + \Delta w_{\theta_j}') \tag{39b}$$

$$\tilde{\Gamma}_{y\theta_j} = \gamma_{\theta_j} (w_e' + z'_{10EA} - \Delta w^{(2)'} - \Delta W^{(2)'}) - (\Delta v_{\theta_j}^{(2)'} - \Delta V_{\theta_j}^{(2)'}) \quad (39c)$$

$$\tilde{\Gamma}_{z\theta_j} = \gamma_{\theta_j} (v_e' + y'_{10EA} + \Delta v^{(2)'} - \Delta V^{(2)'}) - (\Delta w_{\theta_j}^{(2)'} + \Delta W_{\theta_j}^{(2)'}) \quad (39d)$$

and where Δv_{θ_j} , ΔV_{θ_j} , Δw_{θ_j} and ΔW_{θ_j} are the torsion mode dependent portions of the deflection correction functions arising from built-in elastic offset (Δv_{EA_j} , ... etc.) as well as elastic bending effects ($\Delta v_{e_{ij}}$, q_{w_i} , ... etc.). Equation (38) represents the required form of the "force integration" implementation of the nonlinear torsion excitation term. The final torsion equation can then be written as:

$$\begin{aligned} \int_0^l \gamma_{\theta_j}' [GJ\theta_e' + \dots]' dr = \int_0^l \{ & \gamma_{\theta_j} q_{x_5} - \Gamma_{y\theta_j} [p_{y_5} \cos \Theta + p_{z_5} \sin \Theta] \\ & + \Gamma_{z\theta_j} [p_{z_5} \cos \Theta - p_{y_5} \sin \Theta] \\ & - \tilde{\Gamma}_{z\theta_j} [\tau(w_e' + \dots + q_{z_5} \sin \Theta)] \\ & + \tilde{\Gamma}_{y\theta_j} [\tau(v_e' + \dots + q_{y_5} \cos \Theta)] \} dr \end{aligned} \quad (40)$$

To conclude this subsection, three observations can be made of the force integration formulation:

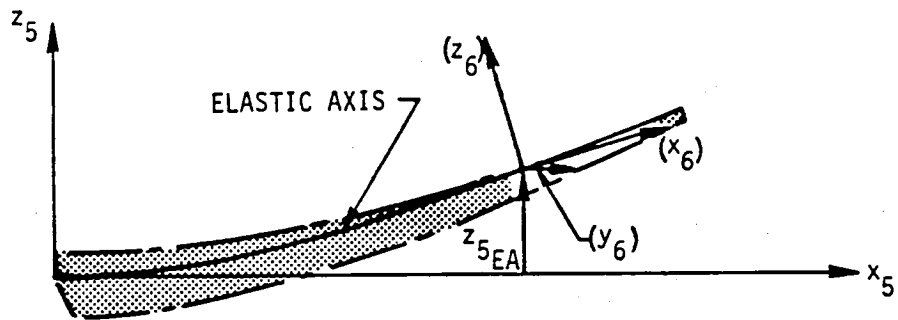
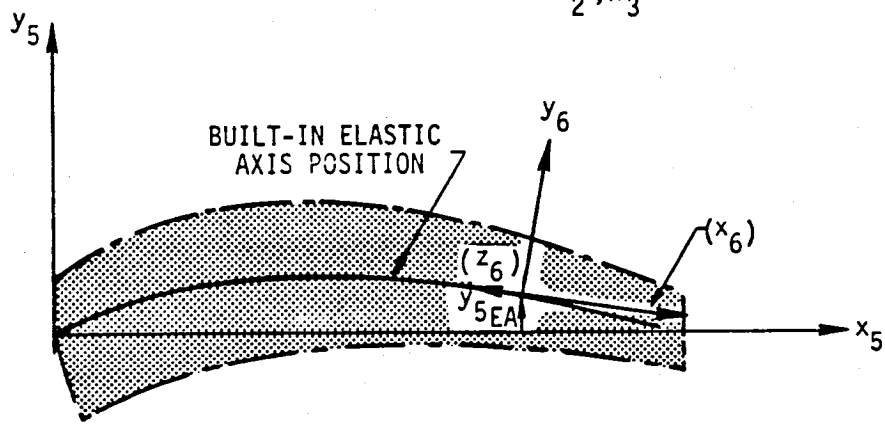
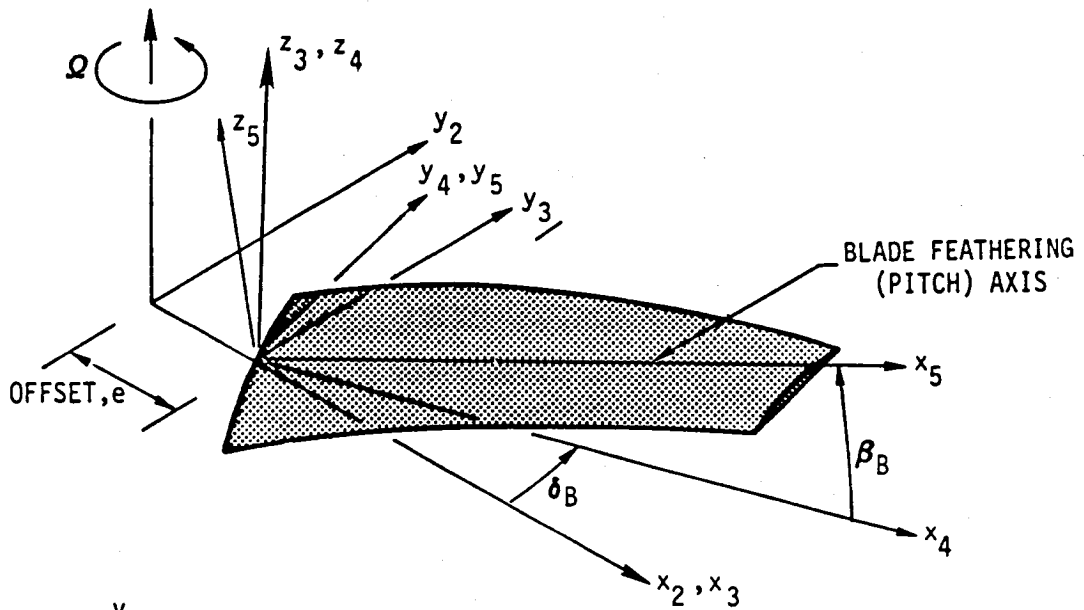
1. Equations (39) all reduce to zero, for zero structural sweep, and zero elastic deflection, as would be expected from the behavior of Equation (36).

2. In Equation (38), the terms multiplying the nonlinear torsion weighting functions ($\Gamma y_{\theta}^j, \dots$) are actually the force and moment loadings defined for the linear excitations of the bending equations. The nonlinear torsion weighting functions, Equations (39), thus serve in effect, as the virtual deflection functions arising from torsion deflections appropriate to the bending generalized loads.
3. The validity of the force integration approach is enhanced by the fact that the resulting terms in the torsion equation, which represent rows of the inertia matrix (reflecting the integration of inertia forces), produce complete mass matrix symmetry, and consequently insure positive-definiteness.

Kinematic Representation for Structural Sweep

The approach for modeling structural sweep is to use simple well-established concepts for bending and torsion of straight beams. Blade elastic bending is defined by conventional beam bending differential equations where the independent spanwise variable is taken to be the arc length along the elastic axis. Furthermore, these bending differential equations are defined locally using the loadings normal to the built-in elastic axis. Within this context, explicit elastic bending-torsion coupling due to structural sweep is omitted in favor of implicit coupling due to inertial, aerodynamic and gravitational loadings taken with appropriate sweep related kinematics. In modeling structural sweep, the kinematics of the blade element mass centers and aerodynamic centers are defined as explicit functions of the blade modal response variables. This subsection addresses this major task, from which the formulations of inertial aerodynamic and gravity loads follow in a straightforward manner. These subsequent formulations for loadings are thus omitted herein for clarity.

Structural sweep is defined generally by including both inplane and out-of-plane offsets of the built-in elastic axis, $y_{5_{EA}}$ and $z_{5_{EA}}$, respectively (see Figure 5). The basic approach of the structural sweep related reformulations consists of: (1) defining a coordinate system rotation transformation from the "5" pitch axis system to the swept "6" system (which is locally attached to the elastic axis), and (2) defining the deflections in the "5" system as functions of the built-in structural sweep and the elastic bending and torsion motions, which are measured in the "6" system. For consistency with previous formulations this approach must also account for the presence of structural twist. The procedure formulated for including these two structural elements (sweep and twist) is summarized in the material which follows; the reader is directed to Reference 7 for a more detailed description.



(): INDICATES PROJECTIONS

Figure 5. Schematics of the "5" and "6" Coordinate Systems

The general modeling of the blade y_5 and z_5 kinematics due to combined structural twist and sweep is accomplished in the following steps:

1. The elastic axis of the "equivalent beam", described in the previous subsection, is "distorted" back to the original planform defined by the built-in structural sweep and segment arc length distributions (but without pitch or twist). This step defines the position of the elastic axis space curve. This positioning requires the x_5 , y_5 and z_5 offset distances of the centers of the segments, as well as projections onto the x_5 - y_5 and x_5 - z_5 planes of the swept elastic axis line segments. These projections define the sweep angle distributions Λ_{e5} and Λ_{f5} .
2. As shown in Figure 5, the orientations of the elastic axis line segments define the local "6" coordinate system. The x_6 is defined parallel to the axis of the elastic axis line segment; y_6 is defined parallel to the x_5 - y_5 plane, (+) in leading edge direction; z_6 is orthogonal to x_6 and y_6 , (+) in the normally positive thrusting motion. It should be stressed that the result of step 1 is to produce, in addition to the inplane and out-of-plane offsets (Δy_5 and Δz_5) of the elastic axis from the (reference) x_5 pitch axis, a radial foreshortening (Δx_5) due to the constancy of the total arc length of the elastic axis. This Δx_5 foreshortening is given by the negative of u_e , as developed in the next subsection.
3. The segments of the blade configuration resulting from steps 1 and 2, are then pitched and twisted about their respective elastic axis line segments (x_6 axis). The pitch and twist angles for each segment are defined relative to the y_6 axis.
4. The blade is elastically deflected in torsion ($\theta_e = \sum_j \gamma_{\theta_j} q_{\theta_j}$) about the built-in space curve elastic axis as defined by $y_{10_{EA}}$ and $z_{10_{EA}}$ to define a first set of "small" incremental y_5 and z_5 deflections.
5. The blade is elastically deflected in flatwise and edgewise bending (w and v , respectively in the presence of the torsion deflection) to define a second set of small incremental deflections. This second set of incremental deflections is measured in the "6" coordinate system and is governed by the basic G400 deflection correction transformations defined in Reference 1.
6. The second set of small incremental "6" coordinate system deflections defined in step 5 is transformed to the "5" coordinate system using an Euler angle transformation derived from sweep angle projections, Λ_{e5} and Λ_{f5} , as discussed in above step 1.

7. The results of steps, 1, 4 and 6 are then combined to define the total y_5 and z_5 position vector components.

First, the sweep angle projection distributions are defined using the built-in elastic axis line segment changes per segment length. The (invariant) segment arc lengths Δr , together with changes to the projection angles caused by elastic torsion deflection are:

$$\Lambda_{e_5} = \sin^{-1} \left\{ -\frac{\Delta y_{5EA}}{\Delta r} - \left[(\Delta v_{EA_j}^{(2)'} - \Delta v_{EA_j}^{(2)'}) \cos \Theta + (\Delta w_{EA_j}^{(2)'} + \Delta w_{EA_j}^{(2)'}) \sin \Theta \right] q_{\theta_j} \right\} \quad (41)$$

$$\Lambda_{f_5} = \sin^{-1} \left\{ \frac{\Delta z_{5EA}}{\Delta r} + \left[-(\Delta w_{EA_j}^{(2)'} + \Delta w_{EA_j}^{(2)'}) \cos \Theta + (\Delta v_{EA_j}^{(2)'} - \Delta v_{EA_j}^{(2)'}) \sin \Theta \right] q_{\theta_j} \right\} \quad (42)$$

where Δy_{5EA} and Δz_{5EA} are the built-in elastic axis offset changes per segment length. The corresponding quantities, defined in the chordwise and edgewise directions, y_{10EA} , z_{10EA} , Δy_{10EA} and Δz_{10EA} , are derived using trigonometric resolution with the "5" coordinate system quantities, and the local built-in pitch angle distribution, as appropriate.

The coordinate system transformation relating the ("5") pitch axis coordinate system with the ("6") swept coordinate system makes use of the sweep angle projections given in Equations (41) and (42):

$$\{\Delta x_6\} = [TAS] \{\Delta x_5\} \quad (43)$$

$$\{\Delta x_5\} = [TAS^{-1}] \{\Delta x_6\} = [TAS^T] \{\Delta x_6\} \quad (44)$$

where:

$$[TAS] = \begin{bmatrix} \frac{\cos \Lambda_{e_5} \cos \Lambda_{f_5}}{\chi} & \frac{-\sin \Lambda_{e_5} \cos \Lambda_{f_5}}{\chi} & \frac{\cos \Lambda_{e_5} \sin \Lambda_{f_5}}{\chi} \\ \sin \Lambda_{e_5} & \cos \Lambda_{e_5} & 0 \\ \frac{-\cos^2 \Lambda_{e_5} \sin \Lambda_{f_5}}{\chi} & \frac{\sin \Lambda_{e_5} \cos \Lambda_{e_5} \sin \Lambda_{f_5}}{\chi} & \frac{\cos \Lambda_{f_5}}{\chi} \end{bmatrix} \quad (45)$$

and where

$$\chi = \sqrt{\cos^2 \Lambda_{f5} + \sin^2 \Lambda_{f5} \cos^2 \Lambda_{e5}} \quad (46)$$

This development is combined to yield the required expressions for inplane and out-of-plane displacement:

$$\begin{aligned} \begin{Bmatrix} y_5 \\ z_5 \end{Bmatrix} &= \begin{Bmatrix} y_{10EA} \cos \Theta - z_{10EA} \sin \Theta \\ y_{10EA} \sin \Theta + z_{10EA} \cos \Theta \end{Bmatrix} \\ &+ \sum_{j=1}^{NTM} \left\{ \begin{array}{l} (\Delta v_{EA_j} - \Delta V_{EA_j}) \cos \Theta + (\Delta w_{EA_j} + \Delta W_{EA_j}) \sin \Theta \\ (\Delta v_{EA_j} - \Delta V_{EA_j}) \sin \Theta - (\Delta w_{EA_j} + \Delta W_{EA_j}) \cos \Theta \end{array} \right\} q_{\theta_j} \\ &+ [E] [TAS^{-1}] \begin{Bmatrix} 0 \\ (v_e + \Delta v - \Delta V) \cos \Theta - (w_e - \Delta w - \Delta W) \sin \Theta \\ (v_e + \Delta v - \Delta V) \sin \Theta + (w_e - \Delta w - \Delta W) \cos \Theta \end{Bmatrix} \end{aligned} \quad (47)$$

where:

$$[E] = \begin{bmatrix} 0 & 1 & 0 \\ 0 & 0 & 1 \end{bmatrix} \quad (48)$$

and where v_e , w_e , Δv , Δw , ΔV , ΔW are linear and nonlinear combinations of q_{w_i} , q_{v_k} , and q_{θ_j} , as per the original G400 structural twist formulations (1).

The addition of structural sweep is accomplished, while retaining the structural twist formulation. The formulation, given by Equation (47), together with that for radial foreshortening, extends the kinematic modeling to applications with large structural sweep and moderate structural twist. Note that these formulations are generally quite nonlinear in the elastic modal response variables q_{w_i} , q_{v_k} and q_{θ_j} .

Kinematics of Radial Foreshortening

The original G400 development (ref. 1) invoked various principal assumptions to advance the art of modeling nonlinear structural twist. The radial foreshortening of a mass element due to elastic bending, u_e , was kept simple and assumed to be limited to that accruing from flatwise bending only. The foreshortening was represented by a quadratic function in flatwise bending only:

$$u_e = \frac{1}{2} \sum_{i,m} \left[\int_0^r \gamma'_{w_i} \gamma'_{w_m} dr_i \right] q_{w_i} q_{w_m} \quad (49)$$

In the reformulated G400 technology (Reference 7), this restrictive assumption was relaxed. The two basic assumptions which were retained, expanded upon, and utilized as an alternative basis are as follows:

1. The elastic torsion axis is defined to be the spanwise locus of shear centers of the two-dimensional blade (beam) sections taken perpendicular to this spanwise locus. This definition treats the elastic axis as an abstract section property, in contrast with what would be measured in a bench test of an actual curved beam. The built-in structural sweep (elastic axis offset), together with the elastic bending deflections, define an elastic axis which is generally a space-curve about which the local torsion deflection must take place.
2. The arc length of the elastic axis is invariant for each blade segment. Radial foreshortening accrue entirely from the kinematics of bending and distributed torsion along the space-curve elastic axis.
3. Local radial foreshortening is defined relative to the total extended arc length of the elastic axis. A hypothetical beam formed by the straightening out of the arc length of the elastic axis and the elimination of all pitch and twist is herein defined to be the "equivalent beam".

As shown in figure 6, contributions to radial foreshortening consist of (a) the built-in in structural sweep, i.e. that which restores the equivalent beam to the original swept planform (b) first order (linear) functions of bending, arising from built-in structural sweep, (c) second order (nonlinear) functions of bending each with elastic torsion arising from built-in structural sweep, and (d) second order functions each of both flatwise and edgewise bending.

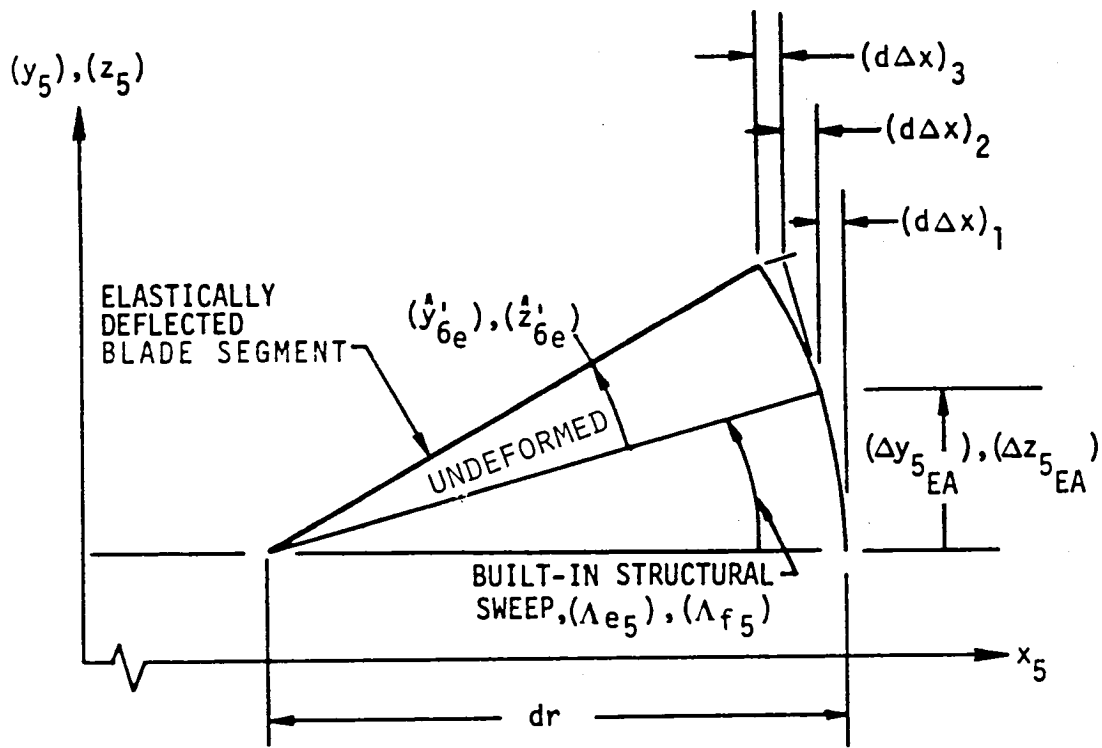


Figure 6. Contributions to Incremental Radial Foreshortening Due to Structural Sweep and Elastic Deformations

Each of these contributions can be modeled in a straightforward manner, and in lieu of the detailed development given in Reference 5, are simply stated as follows:

$$(d\Delta x)_1 = dr - dx = dr - \sqrt{dr^2 - \Delta y_{5EA}^2 - \Delta z_{5EA}^2} \quad (50)$$

$$= \left[1 - \sqrt{1 - (\Delta y_{10EA} / \Delta r)^2 - (\Delta z_{10EA} / \Delta r)^2} \right] dr$$

$$(d\Delta x)_2 = \left[\sin \Lambda_{f_5} \cos \Lambda_{e_5} \hat{z}_{6e}' - \sin \Lambda_{e_5} \cos \Lambda_{f_5} \hat{y}_{6e}' \right] dr \quad (51)$$

$$(d\Delta x)_3 = \cos \Lambda_{e_{50}} \cos \Lambda_{f_{50}} \left[1 - \sqrt{1 - v_e'^2 - w_e'^2} \right] dr \quad (52)$$

$$\cong \cos \Lambda_{e_{50}} \cos \Lambda_{f_{50}} \cdot \frac{1}{2} (v_e'^2 + w_e'^2) dr$$

where Δy_{10EA} and Δz_{10EA} are, respectively, the built-in changes per segment length of the chordwise and flatwise distances of the elastic axis from the reference, x_5 , axis, and Λ_{e_5} and Λ_{f_5} are, respectively, the structural sweep angle projections onto the x_5 - y_5 and x_5 - z_5 reference planes.

The total elastic radial foreshortening at the center of the n th segment is then determined by the following integral:

$$u_{en} = \int_0^{r_n} \left[(d\Delta x)_1 + (d\Delta x)_2 + (d\Delta x)_3 \right] \quad (53)$$

UNSTEADY STALLED AIRLOADS

A detailed analysis of dynamic stall experiments has led to a set of relatively compact analytical expressions (Reference 8) called synthesized unsteady airfoil data. These expressions accurately describe, in the time-domain, the unsteady aerodynamic characteristics of stalled airfoils, the unsteady airloads are modeled using, as the primary dynamic descriptions, the instantaneous angle-of-attack, α , the nondimensional angle of attack rate, M , and the unsteady decay parameter, α_w . This methodology represents a significant improvement over that which was used in the prior version of G400PA (Reference 9). The implementation of this new methodology in the extended G400PA utilizes unsteady data obtained for the NACA 0012 and SC1095 airfoils.

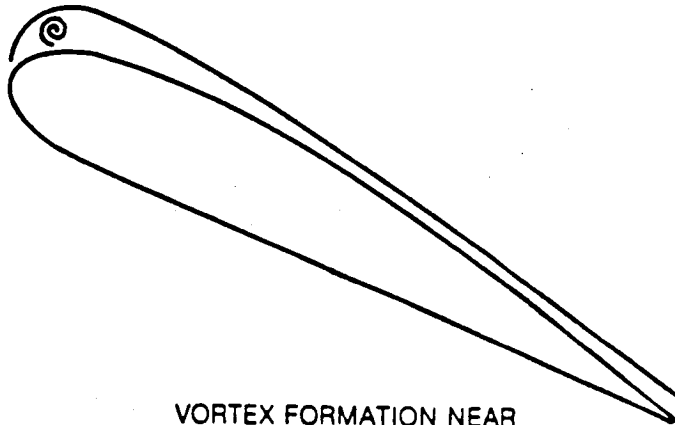
Since the inclusion of this new methodology forms an important element of the extended G400PA analysis, a presentation of highlights of this methodology is warranted in the interest of convenience and completeness. The remainder of this section constitutes an abridged reproduction of material authored by Gangwani (Reference 7 and 8). The reader is referred to these references for a more thorough exposition.

Review of Basic Methodology (Reproduced from Reference 7)

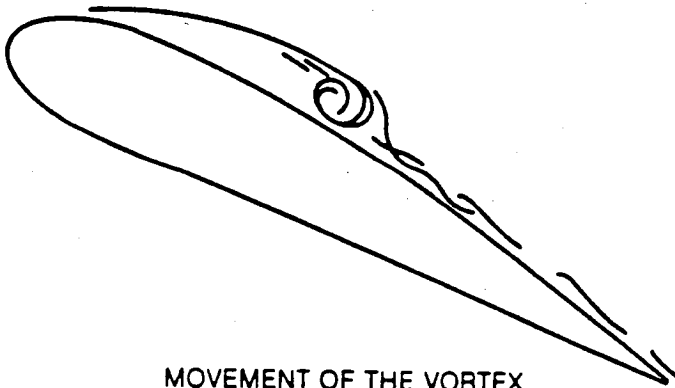
Dynamic Stall Model

The analytical model of dynamic stall, includes the main physical features of the dynamic stall phenomenon as observed in oscillating airfoil tests.

When an airfoil experiences an unsteady increase in angle-of-attack beyond the static stall angle, a vortex starts to grow near the leading edge region. As the angle continues to increase, the vortex detaches from the leading edge and is convected downstream near the surface, as shown schematically in Figure 7. The suction associated with the vortex normally causes an initial increase in lift. The magnitude of the increase depends on the strength of the vortex and its distance from the surface. The streamwise movement of the vortex depends on the airfoil shape and the pitch rate. The relative distance between the vortex and the airfoil varies according to the kinematics of the airfoil, such as the pitch rate and the instantaneous angle-of-attack. As the vortex leaves the trailing edge, a peak negative pitching moment is obtained. The airfoil then remains stalled until the angle-of-attack drops sufficiently so that reattachment of the flow can occur. The present method incorporates all of these events. For example, the strength of the vortex is made a function of the angle when the vortex leaves the leading edge (moment stall angle). The higher the moment stall angle, the higher the strength of the vortex.



VORTEX FORMATION NEAR
LEADING EDGE



MOVEMENT OF THE VORTEX
OVER THE AIRFOIL

Figure 7. Dynamic Stall Modeling

(REPRODUCED FROM REF. (7))

Parameters Influencing Dynamic Stall

The unsteady lift, drag, and pitching moment coefficients of the airfoils obtained from the two-dimensional oscillating airfoil tests show a large degree of hysteresis when plotted as functions of angle-of-attack. This is particularly true, when the reduced frequency and the maximum angle-of-attack are sufficiently high. Figures 8a, 8b, and 8c show an example of typical loop data obtained from the oscillating airfoil test. The amount of hysteresis and the shape of the loops vary in a highly nonlinear fashion with parameters such as amplitude, mean angle, and reduced frequency.

The results of the oscillation airfoil tests indicate that the dynamic characteristics of an airfoil depend on the following parameters: (1) airfoil shape and sweep; (2) Mach number; (3) Reynolds number; (4) reduced frequency, k ; (5) oscillation amplitude, $\bar{\alpha}$; and (6) mean angle-of-attack, α .

Both the static and dynamic characteristics of the airfoil are affected. Since most rotor aeroelastic analyses employ time-history solution techniques for computation of the aerodynamic loading acting on the rotor blades, frequency domain parameters such as reduced frequency or amplitude, are inappropriate to use. Moreover, for arbitrary motion it is difficult to describe the reduced frequency, the amplitude of oscillation, or the mean angle-of-attack of a rotor blade section in a precise manner. As a result, an alternative set of dynamic parameters, which are appropriate for the time domain simulations, is defined. The parameters replacing k , $\bar{\alpha}$, and α_0 in the present method are: (4) the instantaneous angle-of-attack, α ; (5) the nondimensional pitch rate, A ; and (6) the unsteady decay parameter, α_w . The α_w accounts for the time history effects of the change in α , and is based upon the Wagner function.

For the sinusoidally oscillating airfoil, the α , A , and α_w parameters can be easily expressed in terms of the reduced frequency, the amplitude, and the mean angle-of-attack. Also, they can be easily evaluated for rotor blade sections in a stepwise manner and are very convenient to use for the prediction of the onset of dynamic stall and for the determination of the unsteady airloads. Thus, the present method determines, through the synthesization process, the effect of these selected parameters (α , A , α_w) on the dynamic stall characteristics of the airfoils by utilizing the data from the oscillating airfoil tests. The synthesization process involves curve-fitting the test loop data to the prescribed analytical expressions in order to determine the unknown parameters or coefficients embedded in the analytical expressions. The analytical expressions are obtained mostly by mathematical or empirical means. In general, they represent simple quantitative approximations to the various observed physical features of the dynamic stall phenomenon.

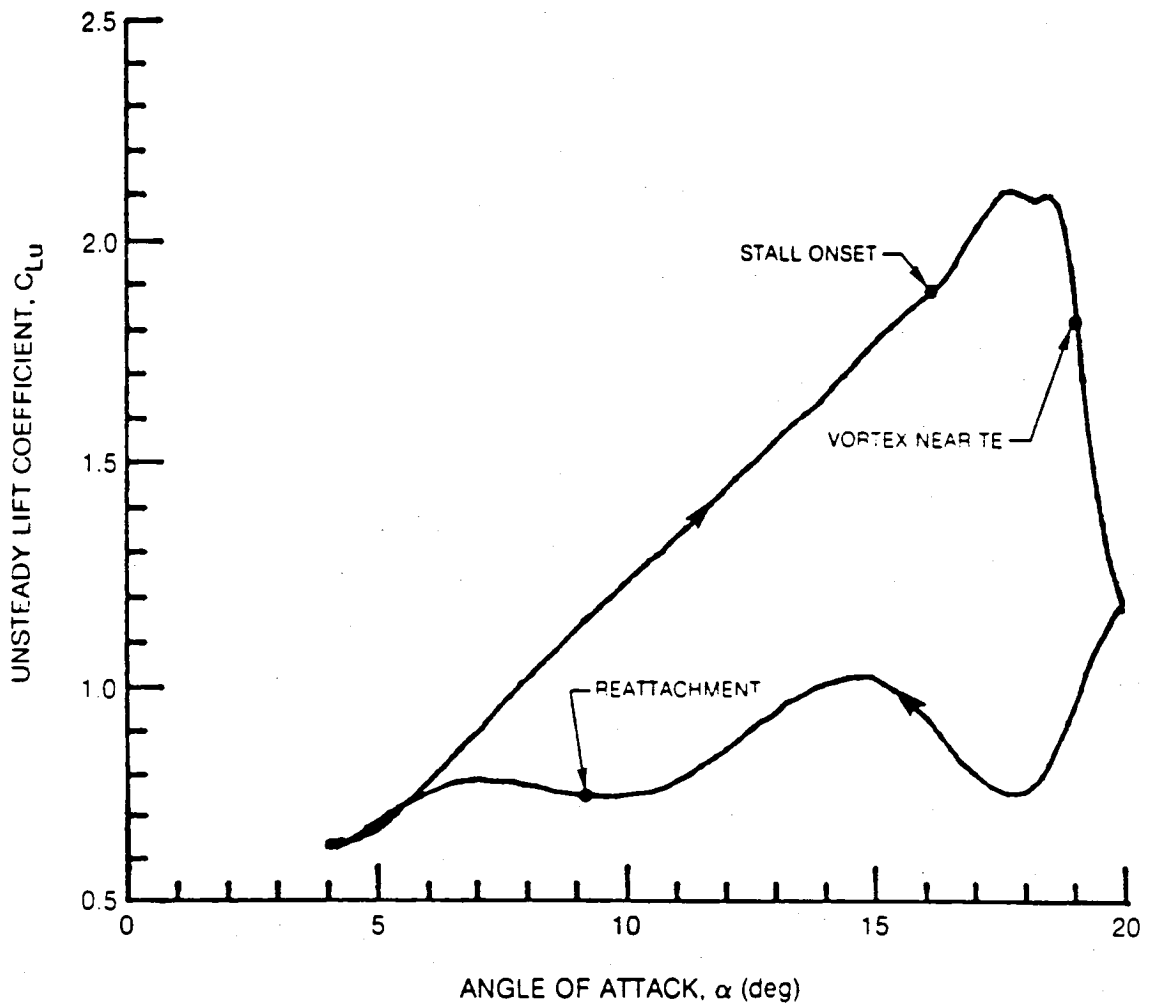


Figure 8a. Typical Unsteady Lift Coefficient Loop Data, SC 1095 Airfoil, $M = 0.3$, $\alpha_0 = 12.0$ deg, $\bar{\alpha} = 8.0$ deg, $k = 0.1$

(REPRODUCED FROM REF. (7))

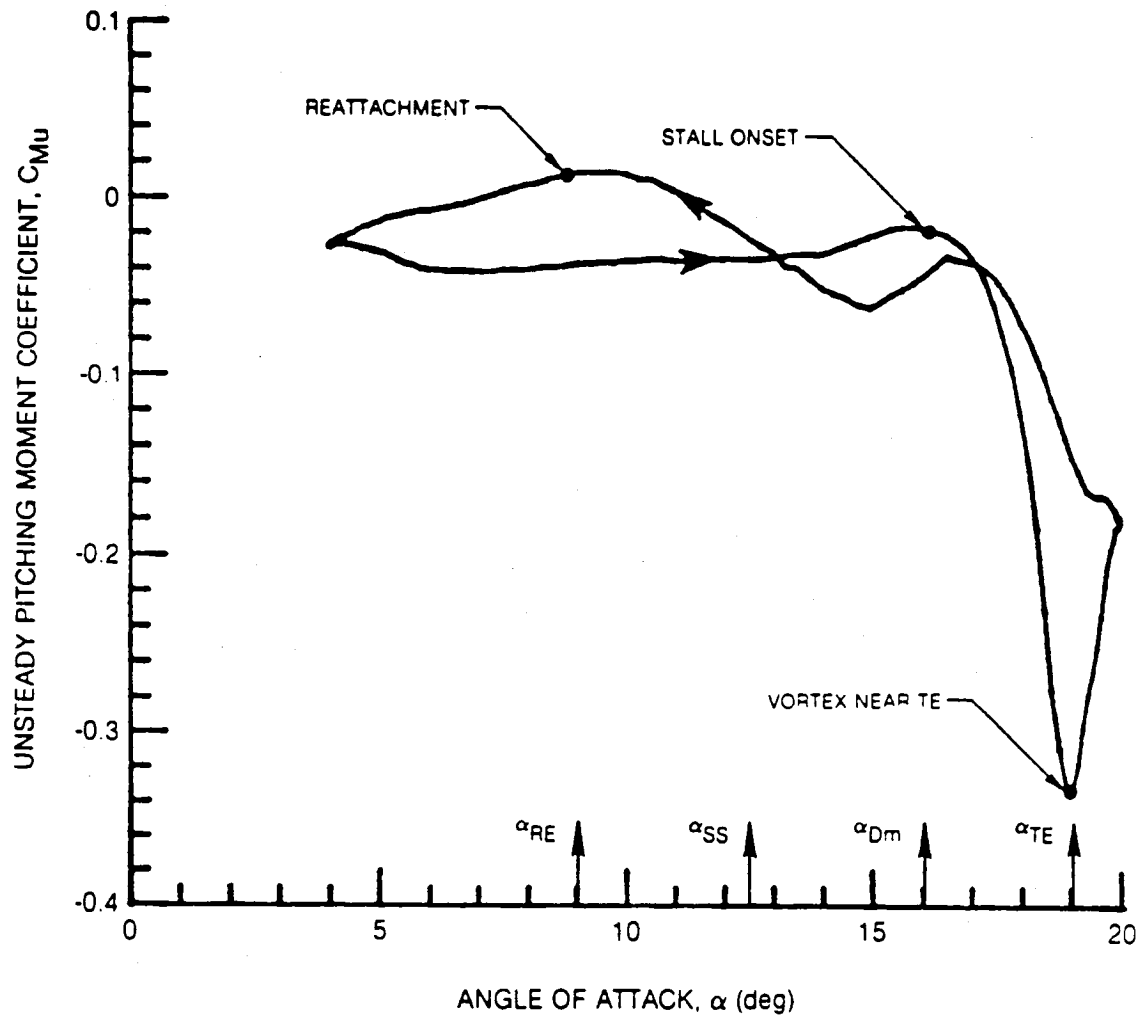


Figure 8b. Typical Unsteady Pitching Moment Loop Data, SC 1095 Airfoil, $M = 0.3$, $\alpha_0 = 12.0$ deg, $\bar{\alpha} = 8.0$ deg, $k = 0.1$

(REPRODUCED FROM REF. (7))

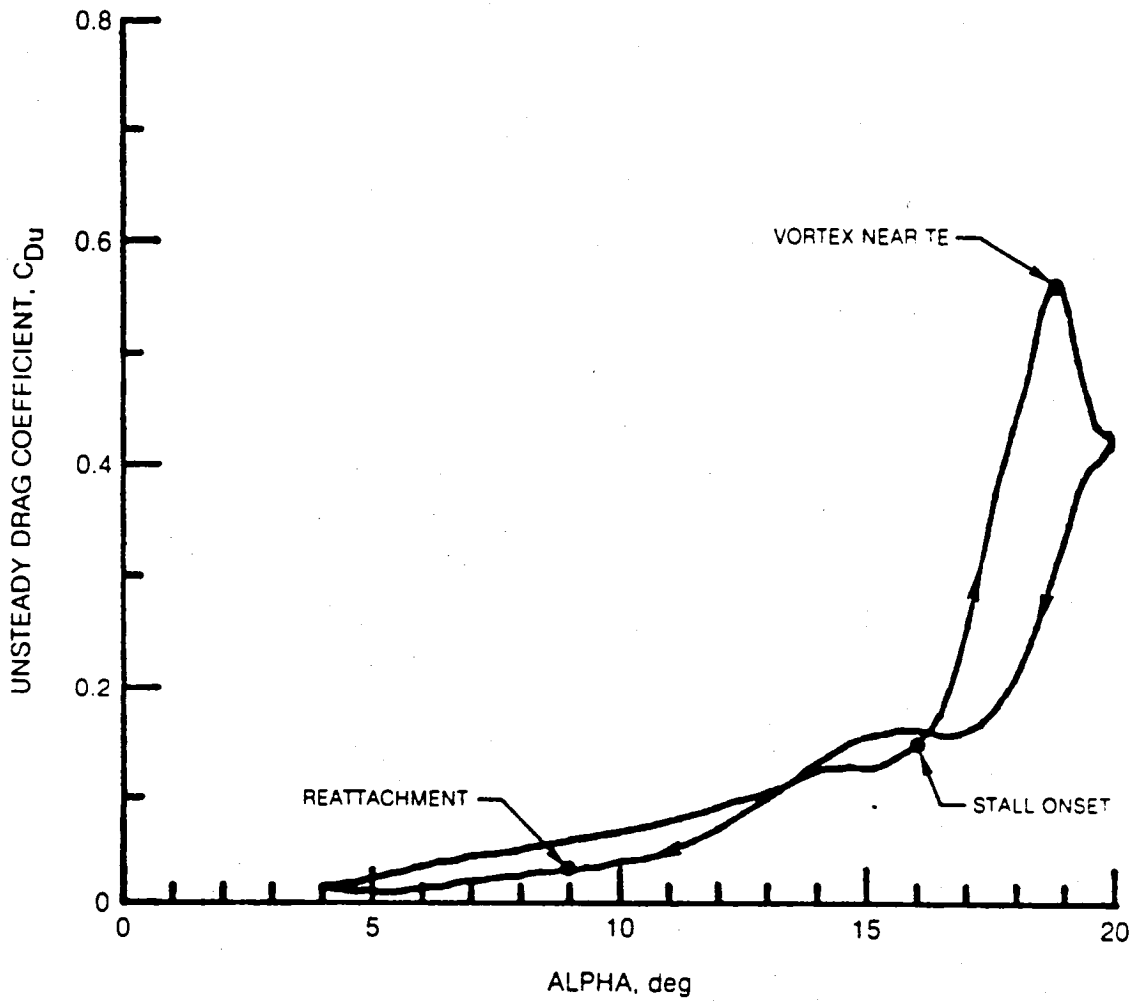


Figure 8c. Typical Unsteady Drag Coefficient Loop Data, SC 1095 Airfoil, $M = 0.3$, $\alpha_0 = 12.0$ deg, $\bar{\alpha} = 8.0$ deg, $k = 0.1$

(REPRODUCED FROM REF. (7))

Definition of the Unsteady Decay Parameter, α_w

For a two-dimensional airfoil going through an arbitrary change in angle-of-attack, one can describe an instantaneous effective angle-of-attack, α_E , by using Duhamel's integral (Reference 4) as given below:

$$\alpha_E(s) = \alpha(0) \phi_c(s, M) + \int_0^s \frac{d\alpha}{d\sigma} \beta \phi_c(s - \sigma, M) d\sigma \quad (54)$$

where $\alpha(0)$ corresponds to the initial angle-of-attack, M represents Mach number, $\phi_c(s, M)$ is the response to step change in α (a compressibility corrected form of the Wagner function), and s is the nondimensional time as given by:

$$s = \frac{2}{c} \int_0^t U dt_1 \quad (55)$$

The unsteady decay parameter, α_w , to be used extensively in the present method, is defined as follows:

$$\alpha_w = \alpha(s) - \alpha_E(s) \quad (56)$$

The α_w parameter physically represents the difference between the instantaneous angle, α and the effective angle, α_E , and therefore accounts for the time-history effects of the change in α . This physical description of α_w is valid for attached flow conditions only. In the present method, the α_w parameter is most useful for predicting the onset of dynamic stall, and for convenience, it is also used to describe approximately the unsteady coefficients after the stall.

The effects of compressibility are incorporated in the definitions of α_w by the use of the general or compressible Wagner function (see also Reference 11) obtained from the following approximate relationship

$$\phi_c(s, M) = \left[1.0 - 0.165 e^{-0.0455 s (1-M^2)} - 0.335 e^{-0.3 s (1-M^2)} \right] / \sqrt{1-M^2} \quad (57)$$

Computation of Dynamic Parameters

For the sinusoidally oscillating airfoil, where the motion of the airfoil is completely known, the parameters α , A , and α_w can be obtained analytically as given below:

$$\alpha = \bar{\alpha} \sin ks \quad (58)$$

$$A = k\bar{\alpha} \cos ks \quad (59)$$

$$\alpha_w = \gamma_1(k, M) k\bar{\alpha} \cos ks + \gamma_2(k, M) \bar{\alpha} \sin ks \quad (60)$$

where k , s , and M represent reduced frequency, nondimensional time, and Mach number, respectively. The γ_1 and γ_2 functions are described by:

$$\gamma_1(k, M) = \frac{0.165(1-M^2)(0.0455)}{k^2 + (1-M^2)^2(0.0455)^2} + \frac{0.335(1-M)(0.3)}{k^2 + (1-M^2)^2(0.3)^2} \quad (61)$$

$$\gamma_2(k, M) = \frac{0.165k^2}{k^2 + (1-M^2)^2(0.0455)^2} + \frac{0.335k^2}{k^2 + (1-M^2)^2(0.3)^2} \quad (62)$$

In contrast to the closed form evaluations obtainable for sinusoidal motion, numerical evaluations of these three section dynamic parameters must be obtained for arbitrary motion in the time domain. This is accomplished in a stepwise manner using the recursive relationships (eqs. 63, 64, 65) at time step n :

$$\alpha_n = \theta_n + \phi_n \quad (63)$$

$$A_n = \left[\frac{\partial \theta_n}{\partial \psi} + \frac{\partial \phi_n}{\partial \psi} \right] \frac{\Delta \psi}{(\Delta s)_n} \quad (64)$$

$$(\alpha_w)_n = X_n + Y_n \quad (65)$$

where:

$$x_n = x_{n-1} e^{-0.0455(1-m^2)(\Delta s)_n + 0.165(\alpha_n - \alpha_{n-1})} \quad (66)$$

$$y_n = y_{n-1} e^{-0.3(1-m^2)(\Delta s)_n + 0.335(\alpha_n - \alpha_{n-1})} \quad (67)$$

$$(\Delta s)_n = \frac{2U_n}{\Omega c} (\Delta \psi) \quad (68)$$

Here, $\Delta \psi$ is azimuthal stepsize, Ω is rotor speed, c is chord length, and U_n is streamwise velocity.

The instantaneous angle-of-attack, α_n , is described in the section normal to the midchord, θ_n and ϕ_n are the pitch angle and inflow angle, respectively. The numerical calculation of the nondimensional angle-of-attack rate, A , poses special problems. The nondimensional time derivative of pitch angle in Equation (64), $\partial \theta_n / \partial \psi$, may be computed analytically from the known control angle and elastic torsion response rates, whereas the time derivative of ϕ must be computed using some form of numerical differentiation. The nominal method is a backward difference scheme. However, in some applications, this method was found to give violent numerical instabilities and an alternative method was required. The alternate method selected is based on the assumption of a predominantly oscillatory response at some user selected frequency, $\bar{\omega}$, which typically would be taken as the dominant blade torsion natural frequency. These two numerical results are given below:

$$\frac{\partial \phi_n}{\partial \psi} = \begin{cases} \frac{1}{\Delta \psi} (1.5 \phi_n - 2 \phi_{n-1} + .5 \phi_{n-2}); & \bar{\omega} = 0 \\ \frac{\bar{\omega} \cos \bar{\omega} \Delta \psi}{\sin \bar{\omega} \Delta \psi} (\cos \bar{\omega} \Delta \psi \cdot \phi_n - \phi_{n-1}); & \bar{\omega} > 0 \end{cases} \quad (69)$$

Prediction of Dynamic Stall Events (Reproduced from Reference 7)

In the present method it is considered important to accurately predict three major events associated with dynamic stall. These events, as shown in Figure 8b, are the stall onset, the vortex at the trailing edge, and the reattachment.

Onset of Stall

Because the dynamic stall airloads acting on an airfoil are highly influenced by the leading edge vortex, an accurate prediction of the instant

the vortex breaks away from the leading edge (moment stall point) becomes very important. The occurrence of moment stall depends on factors such as Mach number, the airfoil shape and the pitch rate.

Under the conventional quasi-static theory formulation, the stall is assumed to occur when the effective angle-of-attack reaches the static stall angle,

$$\alpha_{Em} = \alpha_{ss} \quad (70)$$

In general, α_{ss} is assumed to vary with the airfoil shape, Mach number and Reynolds number. To some extent, the value of α_{ss} also depends on the criterion followed for stall.

Under the present formulation, the relationship represented by Equation (70) is extended to include dynamic stall effects. An assumption is made that at the dynamic stall point, in general, the effective angle of attack, α_{Em} , is not only a function of α_{ss} , but also depends on the pitch rate at stall, A_m , and the instantaneous angle-of-attack at stall, α_{Dm} , (Equation (71))

$$\alpha_{Em} = F(\alpha_{ss}, A_m, \alpha_{Dm}) \quad (71)$$

The actual functionality F depends on the type of stall and on the criterion followed for stall. It is assumed that F varies with airfoil shape, mach number, and Reynolds number, and can be established empirically. Linearization of the relationship of Equation (71) with respect to parameters A_m and α_{Dm} around quasi-steady conditions, $\alpha_{ss}(1+\epsilon)$, leads to the following simple expression for α_{Dm} , the angle at which dynamic moment stall first occurs:

$$\alpha_{Dm} = (1 + \epsilon + C_{Am} A_m + C_{wm} \alpha_{wm}) \alpha_{ss} \quad (72)$$

Here, α_{wm} represents the value of the parameter, α_w , at the point of moment stall. Thus, instead of the function F , one can determine empirically the coefficients ϵ , C_{Am} , and C_{wm} for various Mach numbers, Reynolds numbers, and airfoils. In Equation (72), the last two terms represent the delay in dynamic stall when compared with quasi-static stall. One available method (Reference 13) represents this delay in stall by a constant time delay. However, Equation (72) is a much more general relationship which predicts the onset of dynamic stall quite accurately for airfoils experiencing unsteady motion.

Vortex at Trailing Edge

Normally, after the occurrence of moment stall, there is a significant increase in negative pitching moment due to the travel of the stall vortex. The maximum negative pitching moment occurs when the vortex is near the trailing edge of the airfoil. For the case shown in Figure 8b the instant when the vortex leaves the trailing edge is marked by 'TE'. Preliminary results have led to empirical relationship Equation (73) for predicting the instant the vortex leaves the airfoil:

$$s_{mt} = 1.0 / (C_{At} A_{pm} + C_{\alpha t} \alpha_{pm}) \quad (73)$$

Where s_{mt} is the total nondimensional time for the vortex to travel from the leading edge to the trailing edge. The coefficients C_{A_t} and C_{α_t} vary with Mach number, airfoil shape, sweep, and Reynolds number.

Reattachment

The instant the reattachment of the flow occurs is shown in Figure 8b. Normally, for low Mach numbers ($M < 0.4$) the reattachment occurs at an angle α_{RE} which is less than the static stall angle α_{ss} . At higher Mach numbers, where the static stall may be induced by shocks, the reattachment angle α_{RE} can be higher than the static stall angle, α_{ss} . In the present formulation, a general expression for α_{RE} is assumed by (eq. 74):

$$\alpha_{RE} = (1 - \epsilon + C_{AR} A_{Dm} + C_{WR} \alpha_{WM}) \alpha_{ss} \quad (74)$$

In general, for a given airfoil, the values of C_{AR} and C_{WR} , as used in Equation (74) for reattachment, are quite different from C_{Am} and C_{Wm} used for stall onset. However, the value of the parameter ϵ is the same in both of these equations.

Unsteady Section Coefficients (Reproduced from Reference 7)

Unsteady Lift Coefficient

The unsteady lift coefficient, C_{Lu} , of an airfoil in the time domain under the present synthesization is described by Equations (75) through (82).

$$C_{Lu} = C_{Ls}(\alpha - \Delta\alpha_1 - \Delta\alpha_2) + a_{oL}\Delta\alpha_1 + \Delta C_{L1} + \Delta C_{L2} \quad (75)$$

$$\Delta\alpha_1 = (P_1 A + P_2 \alpha_w + P_3) a_{ss} \quad (76)$$

$$\Delta\alpha_2 = \delta_2 a_{ss} \quad (77)$$

$$\Delta C_{L1} = Q_1 A + Q_2 \alpha_w + Q_3 (\alpha / a_{ss}) + Q_4 (\alpha / a_{ss})^2 \quad (78)$$

$$\Delta C_{L2} = Q_5 \delta_1 + Q_6 \Delta\alpha_2 + Q_7 (a_{Dm})^2 \left[\frac{1 - e^{-(\beta_1 s_m)^3}}{(\beta_1 s_m)^2} \right] \quad (79)$$

$$s_m = \frac{2U(t - t_{dm})}{C} \quad (80)$$

$$\delta_1 = \begin{cases} 0 & \alpha \leq \alpha_{ss} \\ (\alpha / a_{ss} - 1) & \alpha_{ss} \leq \alpha \leq \alpha_{Dm} \\ (a_{Dm} / a_{ss} - 1) [1.0 - (s_m / s_{mt})^2] & 0 \leq s_m \leq s_{mt} \\ 0 & s_m > s_{mt} \end{cases} \quad (81)$$

$$\delta_2 = \begin{cases} 0 & \alpha \leq \alpha_{ss} \\ (\alpha / a_{ss} - 1) & \alpha_{ss} \leq \alpha \leq \alpha_{Dm} \\ (a_{Dm} / a_{ss} - 1) & 0 \leq s_m \leq s_{mt} \\ (a_{Dm} / a_{ss} - 1) \frac{\alpha - \alpha_{RE}}{\alpha_{TE} - \alpha_{RE}} & \alpha_{RE} \leq \alpha \leq \alpha_{TE} \\ 0 & \alpha \leq \alpha_{RE} \end{cases} \quad (82)$$

The synthesized unsteady lift coefficient (Equation (75)) has been expressed as a sum of static C_{Ls} at some shifted angle $(\alpha - \Delta\alpha_1 - \Delta\alpha_2)$ plus an incremental lift coefficient $(\Delta C_{L1} + \Delta C_{L2})$. The shift in angle is given by Equations (76) and (77) and the incremental lift coefficient by Equations (78) and (79). (The quantity a_{oL} in Equation (75) is the conventional static lift curve slope). The $\Delta\alpha_1$ shift in angle (Equation (76)) is present even when no

stall occurs, and the $\Delta\alpha_2$ shift in angle (Equation 77)) is mainly associated with the occurrence of dynamic stall and subsequent reattachment. Similarly, the ΔC_{L1} (Equation 78)) represents essentially the unsteady effects over static C_{LS} for dynamically unstalled airfoils, and ΔC_{L2} (Equation 79)) represents the effects associated with the dynamic stall events such as vortex formation and reattachment. In fact, the last term in Equation (79) represents explicitly the suction effects of the leading edge vortex and equals zero when no vortex exists.

Thus, Equation (75) is a general expression for unsteady C_L even when no dynamic stall occurs. For unstalled cases, the magnitudes of $\Delta\alpha_2$ and ΔC_{L2} are essentially zero.

The β_1 parameter in Equation (79) is an empirically determined constant and is nominally equal to 0.18. The quantity s_m , as described by Equation (80), represents the nondimensional time measured from the instant of the occurrence of dynamic moment stall. The unknown parameters P_1 through P_3 and Q_1 through Q_7 are determined empirically by means of a least-squares curve-fitting of Equation (75) with the test data. It should be noted that most of the terms in Equation (75) are linear in parameters α , A , and α_w .

Unsteady Moment Coefficient

The unsteady pitching moment coefficient, C_{Mu} , has been formulated using relationships similar to those for C_{Lu} and is described below:

$$C_{Mu} = C_{Ms}(\alpha - \Delta\alpha_2) + a_{Om} \Delta\alpha_2 + \Delta C_M \quad (83)$$

$$\Delta C_M = \eta_1 A + \eta_2 \alpha_w + \eta_3 (\alpha / \alpha_{ss}) + \eta_4 |\alpha_w| + \eta_5 \delta_1 + \eta_6 \Delta\alpha_2 + \eta_7 a_{Dm} A_{Dm} s_m \quad (84)$$

Here a_{Om} represents the static pitching moment slope at zero angle-of-attack and it normally equals zero. The last term in Equation (84) represents the vortex effects. For unstalled airfoils, the last three terms in Equation (84) are zero. The unknown parameters η_1 through η_7 once more are determined by the least-square curve-fitting of Equation (83) to the test data.

Unsteady Drag Coefficient

The unsteady drag coefficient, C_{Du} , appears to vary with the dynamic parameters in the same way as C_{Mu} and is described as follows:

$$C_{Du} = C_{Ds}(\alpha - \Delta\alpha_2) + \Delta C_D \quad (85)$$

$$\begin{aligned} \Delta C_D = & R_1 A + R_2 \alpha_w + R_3(\alpha/\alpha_{ss}) + R_4 |\alpha_w| \\ & + R_5 \delta_3 + R_6 \delta_4 + R_7 \Delta\alpha_2 + R_8 \alpha_{Dm} A_{Dm} s_m \end{aligned} \quad (86)$$

where:

$$\delta_3 = \begin{cases} 0 & \alpha \leq \alpha_{ss} \\ (\alpha/\alpha_{ss} - 1) & \alpha_{ss} \leq \alpha \leq \alpha_{Dm} \\ (\alpha_{Dm}/\alpha_{ss} - 1) [1. - (s_m/s_{mt})^{.25}] & 0 \leq s_m \leq s_{mt} \\ 0 & s_m > s_{mt} \end{cases} \quad (87)$$

$$\delta_4 = \begin{cases} 0 & \alpha \leq \alpha_{ss} \\ (\alpha/\alpha_{ss} - 1)^2 & \alpha_{ss} \leq \alpha \leq \alpha_{Dm} \\ (\alpha_{Dm}/\alpha_{ss} - 1)^2 [1. - (s_m/s_{mt})^{.25}] & 0 \leq s_m \leq s_{mt} \\ 0 & s_m > s_{mt} \end{cases} \quad (88)$$

The last term in Equation (86) represents the effects of the stall vortex on the unsteady drag. For unstalled conditions, the last four terms in Equation (86) are essentially equal to zero. Once more, the unknown parameters R_1 through R_8 are computed using the linear least-squares curve-fitting of Equation (86) to the unsteady drag test data.

GENERAL DESCRIPTION OF THE G400PA PROGRAM

Program Structure

The G400PA program is structured with an initial routine (MAIN), appropriate modular levels and a collection of utility subroutines and/or functions. The subroutine calling structure is presented in Table I. The hierarchical structure is alternately indicated using indentations with indicating symbols and/or nested parentheses. The subroutines are in alphabetical order within any given hierarchical level and not with respect to calling order.

TABLE I

HIERARCHIAL LISTING OF G400PA ELEMENTS

● G400PG

■ E159

- ▲ BMFIT
- ▲ ELAST
- ▲ INVERT
- ▲ NFMS
 - ◆ BMEVAL
 - ◆ BMFIT
 - ◆ EIGENE (INVERT, SIMUL)

- ▲ PCHDAT
- ▲ PCHMOD
- ▲ TMSS

- LOADER
- MODEIN
- MOTION

▲ ENDCON

- ◆ F389SU
 - ▼ BLIN5
 - ▼ INTERP
 - ▼ LNAERO
 - ▼ SHLDM
 - ▼ STALN

- ◆ RESETQ
- ◆ SETVAL

- ▲ HUBSUM
- ▲ INISH

- ◆ ADMCOF
- ◆ DPCHEK
- ◆ SETVAL
- ◆ PABSSU (ADMCOF)

▲ MAJITR

- ◆ AERPRF (ALFCOR(HEYSDL(HEYSK)))
- ◆ BLADEL
 - ▼ FACT12
 - ▼ HBINRT
 - ▼ RDNANL
 - ▼ RSPNSS (QQPSET,HHCANG)
 - ▼ SETUP
 - ▼ SPANS

▼ SPANS (cont'd.)

- ◆ ALFDOT
- ◆ ALWCOM
- ◆ BLIN5
- ◆ DEFLEX
- ◆ EULER
- ◆ HYSDMP
- ◆ PHIDOT
- ◆ SHLDM
- ◆ UNSTCF (BLOCK DATA (UNDATC))

- COEFF3 (ULSTAL)
- SYNTH3

- ▼ BLIN5
- ▼ GETCDS (INTERP)
- ▼ GETCLS (INTERP)
- ▼ GETCMS (INTERP)
- ▼ SHLDM

- ◆ CROUTS
- ◆ NUTRIM (GJR)
- ◆ QSTHRM (HARM)
- ◆ RESETQ
- ◆ TABLE
- ◆ TEETR
- ◆ TMARCH
- ▼ ADAMS
- ▼ EXTRAP
- ▼ QPPCAL
- ▼ QPPTST
- ▼ STRSSS (EULER)

■ NIAM

- ▲ BNDGIT (GJR, QUADFT)
- ▲ DEFCOR
- ▲ DFYZEA
- ▲ DYNMAT
- ◆ DEFLEX
- ◆ RSPNSS (QQPSET, HHCANG)
- ◆ TCOUPL
- ▲ MYKSTD (GJR)
- ▲ PTFLLG
- ▲ RSPNSS (QQPSET, HHCANG)
- ▲ SPNWIZ
- ▲ SPRINT
- ▲ TRFLX1
- ▲ TWOF

- PRNT
- RESETG
- RESETQ
- WAKUCZ

- WAKUCZ (cont'd)
 - ▲ DISCRT
 - ▲ FFTGEN
 - ◆ LFCT (NPRM)
 - ◆ REVERS (SBSCR)
 - ◆ SCTAB
 - ◆ SUBS (SBSCR)
 - ▲ LINFIT
 - ▲ MAXIMZ (DISCRT)
 - ▲ MODULS
 - ▲ SEARCH

Brief Description of Program Elements

ADAMS

This function implements an algorithm for time integration of any of the time dependent variables.

ADMCOF

This subroutine evaluates the coefficients required for the time integration algorithm

AERPRF

This subrouting completes the calculations for and outputs the summary of aerodynamic performance quantities

ALFCOR

This subroutine calculates the corrected rotor angle-of-attack due to the proximity of a ground plane or wind tunnel walls using the theory of Reference 14.

ALFDOT

This subroutine calculates the aerodynamic A parameter using backward differencing on the inflow angle and direct knowledge of the time derivative of pitch.

ALWCOM

This subroutine calculated the unsteady decay parameter α_w required for the unsteady stalled and generalized Wagner function airloads methodologies.

BLADEL

This subroutine provides the computational loop over number of blades in forming the blade response equations. The upper limit on this loop is (1,2) depending on whether the rotor is of (unteetered, teetered) type.

BLIN5

This subroutine does a tri-variant table look up of the airfoil section coefficients. The three variables are angle-of-attack, Mach number and spanwise station.

BLOCK DATA (UNDATC)

This data element contains the empirically derived coefficients required by subroutines COEFF3, SYNTH3, UNSTCF and others for using the UTRC unsteady stalled airloads methodology (Reference 8).

BMEVAL

This subroutine evaluates the bending mode shape and its derivatives at spanwise locations other than where they are calculated in the E159 eigensolution.

BMFIT

This subroutine performs a functional (polynomial) fit of the bending mode shape for use in subroutine BMEVAL for evaluating bending mode shapes at nonstandard spanwise locations.

BNDGTT

This subroutine calculates the flatwise and edgewise bending stiffness characteristic of the torque tube component of a bearingless rotor, as required for the redundant analysis calculation (see RDNANL).

COEFF3

This subroutine calculates various coefficients needed for the UTRC stalled unsteady airloads methodology.

CROUTS

This subroutine is a compact simultaneous equations solver used for nonteetered rotor configurations. It uses the Crout Reduction method described in Reference 15.

DEFCOR

This subroutine calculates constants of integration appropriate to the deflection correction functions (Δv , Δw , etc.) to insure orthogonality of these functions with the articulated blade degrees-of-freedom.

DEFLEX

This subroutine evaluates the spanwise deflections, slopes, velocities, etc. from the modal responses, forms the sweep transformations and, for the eigensolutions, forms various deflection partial derivatives. DEFLEX typically operates within the spanwise loop of the calling subroutine.

DFYZEA

This subroutine forms the spanwise derivative of the structural sweep angles from the input sweep changes per segment length, or from numerical differentiation.

DISCRT

The purpose of this subroutine is to compute the magnitude of the Fourier coefficient CMAG of a set of time-history data, as part of the transient spectral stability analysis (TSSA).

DMPRTB

This subroutine does a table look-up to implement the nonlinear lag damper angular rate vs damper moment characteristics.

DPCHEK

This subroutine tests the input integration steps size for acceptable accuracy, and automatically decreases it if the value is too large.

DYNNAT

This subroutine forms the modal integration coefficients used for the portions of the equations not requiring explicit spanwise integrations at each time step.

EIGENE

This subroutine performs the eigensolution of the bending portion of the E159 preprocessor for uncoupled blade frequencies and mode shapes. It uses the method of determinant iteration.

ELAST

The purpose of this subroutine is to calculate the elastic coefficients for flatwise and edgewise bending for the E159 eigensolution.

ENDCON

This subroutine serves three main functions associated with the completion of the Part II time-history solution: (1) it completes the calculations for median and 1/2 peak-to-peak stresses, (2) it controls the harmonic analyses of responses hub loads and stresses, and (3) it controls the saving of end conditions and other data for use in either the F389 code or subsequent G400 runs.

EULER

This subroutine performs the coordinate system transformations between the "5" and "6" coordinate system vectors.

EXTRAP

This subroutine effects a "static" solution on any degree-of-freedom whose natural frequency is sufficiently high to approximate the response neglecting the twice time differentiated term in that degree-of-freedom's governing equation.

E159

This subroutine controls the preprocessor calculations of the uncoupled modal frequencies and mode shapes for flatwise and edgewise beam bending, and for torsion responses.

FACT12

This subroutine performs an interpolation function calculation in the use of input tabulated variable inflow.

FFTGEN

This subroutine is a standard Fast Fourier Transform calculator, and is used in the transient spectral stability analysis (TSSA).

F389SU

This subroutine sets up the various blocks of data needed by the (UTRC F389) variable inflow branch of the coupled rotor/fuselage vibration analysis and writes them to appropriate data files. A detailed description of the appropriate data transmitted between the G400PA and F389 portions of the analysis is given in Reference 3.

GETCDS

This subroutine provides internally calculated static aerodynamic drag data in place of user provided static airfoil data for usage in the unsteady stalled airloads calculation.

GETCLS

This subroutine provides internally calculated static aerodynamic lift data for usage in the unsteady stalled airloads calculation.

GETCMS

This subroutine provides internally calculated static aerodynamic moment data for usage in the unsteady stalled airloads calculation.

GJR

This utility subroutine optionally obtains simultaneous equation solutions and/or matrix inversions using the Gauss-Jordan Reduction method.

G400PG

The subroutine is the main G400PA element and directs all major portions of the solution flow.

HARM

This utility subroutine performs a Fourier (harmonic) Analysis of any time history string of data. This harmonic analysis uses a negative cosine and sine definition for the harmonic components.

HBINRT

This subroutine calculates components of inertial acceleration, as measured in the rotating blade coordinate system, from the prescribed harmonics of hub motion.

HEYSDL

This subroutine calculates interference factors needed for subroutine ALFCOR.

HEYSK

This subroutine calculates induced velocity functions for subroutine HEYSDL.

HHCANG

This subroutine calculates contributions to the total blade pitch angle and its first and second time derivatives accruing from higher harmonic control angle inputs.

HUBSUM

This subroutine provides a printout of the rotor hub loads and impedance matrix calculations which are transmitted to the coupled matrix/fuselage vibration analysis program.

HYSDMP

This subroutine calculates the increment to blade edgewise bending moment to account for hysteretic structural damping. This formation of structural damping is dependent on edgewise deflection and the signs of rate and acceleration, but not their magnitudes.

INISH

This subroutine initializes arrays and logic variables, and nondimensionalizes parameters, as required for the time-history solution.

INTERP

This subroutine is a general purpose linear interpolation calculator.

INVERT

This subroutine is a general purpose matrix inversion, determinant calculator used by the E159 eigensolution.

LFCT

This subroutine finds the prime decomposition of any integer for use with the Fast Fourier Transform subroutine, FFTGEN.

LINFIT

This subroutine performs a least-square fit to results from the transient spectral stability analysis routine, WAKUCZ.

LNAERO

This subroutine calculates partial derivatives of airfoil section coefficients with respect to angle-of-attack and Mach number.

LOADER

The purpose of this subroutine is the loading of the generic loader portion of the input data.

MAJITR

This subroutine provides the structuring needed to produce a trimmed configuration, and to calculate the impedance matrices. Specifically, this subroutine provides the iterative loop structure to perturb various system parameters in a systematic manner to form numerical partial derivatives, both those needed for trim and those needed for the impedance matrices.

MAXIMZ

The purpose of this subroutine is to maximize the magnitude of the Fourier coefficient as a function of frequency in the vicinity of an identified high response frequency, as part of the transient spectral stability analysis.

MODEIN

This utility subroutine inputs the blade bending and torsion mode shapes and their derivatives with respect to span.

MODULS

The purpose of this utility subroutine is to form the modulus of a vector of Fourier transforms.

MOMNTM

This function evaluates an empirical function joining the two branches of the actuator disk momentum equation across the vortex ring state based on a function given in Reference 16.

MOTION

This subroutine controls the time-history solution flow.

MYKSTD

This subroutine calculates the static flatwise bending deflection and spanwise derivative distributions for the blade for unit load on the inboard and of the cantilever mounted torque tube (for bearingless rotor applications only).

NFMS

This subroutine controls the calculation of the uncoupled beam bending vibration modes within the E159 eigensolution preprocessor.

NIAM

This subroutine performs the following functions:

1. Completes the input of the required data; specifically (a) the inertia, elastic, geometric and other operational data, (b) the blade mode shape data, (c) the variable inflow data, and (d) the saved initial conditions, from an appropriate data file.
2. Performs some initializations and/or nondimensionalizations of logic and system parameters.
3. Calculates the deflection correction functions which accrue from structural twist and sweep.

NPRM

This utility subroutine finds the next prime number given the vector of previous primes. It is intended for use with subroutine LFACT.

NUTRIM

This subroutine calculates the combined partial derivative matrices used for the trim (major iteration) calculations and performs the simultaneous equations solution for each major iteration.

PABSSU

This subroutine sets up parameters and provides appropriate nondimensionalizations as required for the prescribed hub motions and simulations of the pendular absorbers.

PCHDAT

This utility subroutine output punches spanwise array elastomechanical data from the E159 portion of the program for subsequent optional explicit input to the G400 proper part of the program.

PCHMOD

This utility subroutine putput punches spanwise mode shape data from the E159 portion of the program for subsequent optional explicit input to the G400 proper portion of the program.

PRNT

This subroutine provides an echo print output of the Part II input data which pertains to the Inertia, Elastic, Geometric and other Operational Data.

PTFLLG

This subroutine calculates the parameters used to define the pitch-flat, pitch-edge and pitch-flap couplings.

QPPCAL

This subroutine calculates the array of response accelerations for output print.

QPPTST

This subroutine tests the system degrees-of-freedom for numerical instabilities. The criteria used to identify such an instability are the occurrence of three sign changes of increasing amplitude in three time steps.

QSTHRM

This subroutine performs harmonic analyses (using subroutine HARM) of the blade modal responses, pendular absorber responses, hub shears and moments, and blade stresses, after the responses have converged to periodicity.

QUADFT

This subroutine fits a quadratic function to any set of three ordinates corresponding to three equally spaced abscissae.

RDNANL

This subroutine makes the redundant analysis calculations needed for simulations of bearingless rotor configurations.

RESETG

This subroutine resets torsion mode shapes which might be displaced by the formation of the pseudo-torsion mode.

RESETQ

This subroutine places selected terminal conditions into an array and writes them to a data file for use as initial conditions for subsequent runs.

REVERS

This subroutine is used for subscript scrambling and unscrambling as required for the FFT calculation.

RSPNSS

This subroutine performs the following time-dependent calculations:

1. Forms the blade azimuth angle and various harmonics
2. Sets the impressed control angle and its time derivatives.
3. Sets the modal response variables from various optional sources.

SBSCRIP

This subroutine finds the mixed radix representation of an integer for use in the Fast Fourier Transform.

SCTAB

This utility subroutine exponentiates an angle multiplied by the imaginary vector i .

SEARCH

This subroutine is used in the TSSA solution to search a vector of Fourier transforms to identify frequencies at which the Fourier transform is a maximum.

SETUP

This subroutine sets up the inertia coupling matrix and excitation vector for the modal responses of a given blade.

SETUAL

This subroutine saves and inputs end (initial) conditions on spanwise inflow angle and the component time variables comprising the unsteady decay parameter α_w .

SHLDM

This subroutine analytically approximates the NACA 0012 airfoil aerodynamic coefficients as functions of angle-of-attack and Mach number.

SIMUL

This utility subroutine performs a simultaneous equations solution as part of the E159 calculations.

SPANS

This subroutine implements the loop over spanwise station in forming the blade response equations. The spanwise inertia, aerodynamic and gravity load distributions are formed in this subroutine.

SPNWIZ

This function performs a numerical integration between blade section centers of a specific integrand type as required for forming the deflection corrections functions due to structural twist.

SPRINT

This subroutine outputs (as optionally requested) the spanwise integration coefficients. Although most of these coefficients were required only for the (deleted) flutter, coupled mode eigensolution, some are used in the time-history solution. For completeness all coefficients were retained.

STALM

This function approximates the variation of static moment coefficient stall angle with Mach number for the NACA 0012 airfoil.

STALN

This function approximates the variation of static normal force (lift, to close approximation) coefficient stall angle with Mach number for the NACA 0012 airfoil.

STRSSS

This subroutine calculates the spanwise stresses and integrated hub loads optionally using the force-integration or mode deflection methods.

SUBS

This subroutine computes appropriate subscripts and exponents for the Fast Fourier Transform.

SYNTH3

This subroutine is a component of the group of elements comprising the unsteady stalled airloads modeling wherein the final calculations of unsteady lift, drag and moment are made.

TABLE

This utility subroutine performs a table look-up and first derivative calculation for use in defining the instantaneous control angle.

TCOUPL

This subroutine calculates the coupled torsion modes arising from optional use of the rigid body degree-of-freedom with the E159 calculated elastic (normal) torsion modes.

TEETR

This subroutine combines the inertia coupling matrices and excitation vectors for a two-bladed rotor to effect the teetered rotor boundary conditions at the blade roots.

TIMINT

This utility subroutine is used for interpolation of input control functions which are prescribed functions of time.

TMARCH

This subroutine controls the solution flow for obtaining the time-history solutions. It furthermore tests for numerical instabilities and convergence to periodicity.

TMSS

This subroutine calculates the uncoupled torsion mode shapes and natural frequencies within the E159 eigensolution.

TRFLX1

This subroutine calculates the torsion deflection characteristics of the flexbeams (for bearingless rotor configurations) due to spanwise varying torques resulting from the concentrated shears and moments at junction point of the flexbeam, torque tube and blade proper.

TWOF

This function performs a least-square curve fit calculation on blade twist to facilitate subroutine NIAM in the numerical differentiation of blade twist.

ULSTAL

This subroutine performs a table look-up of the input airfoil data to obtain (1) derivatives of section unstalled lift and moment coefficients with respect to angle-of-attack, and (2) static lift and moment stall angles, for use in subroutine COEFF3.

UNDATA

This element contains the empirical coefficients required by subroutine COEFF3 for using the unsteady stalled airloads calculation.

UNSTCF

This subroutine controls the implementation of the unsteady stalled airloads calculation.

WAKUCZ

This subroutine performs the transient spectral stability analysis (TSSA) for extracting such stability indicators as characteristic exponent and time to half amplitude from the time-history solutions (see Reference 17).

PROGRAM INPUT DESCRIPTION

The required input to the program consists of the following major data blocks in order of loading:

- I. Airfoil Data
- II. Loader Data Descriptions
- III. Blade Modal Data
- IV. Variable Inflow Data

In addition, there are descriptions of optional data entries which augment the utility of the code:

- V. Rotor Inflow Program F389 Required Data
- VI. Multiple Case Runs
- VII. Initial Conditions
- VIII. Input/Output File Unit Numbers
- IX. General Information to Facilitate Operation and Improve Efficiency

Details which define and describe pertinent preparation procedures for these data are given in the subsections which follow.

I. Airfoil Data

This data block consists of sets of tables of two-dimensional lift, drag and pitching moment coefficients versus angle-of-attack for up to ten (maximum) Mach numbers. Such sets of angle-of-attack, Mach number variable data can be obtained for up to five (5) arbitrary spanwise locations. Additionally, if unsteady aerodynamics are used, the static stall angles, both lift curve slope and pitching moment curve slope (C_M against α) may be included in this table.

Input Format for First Card(s)

While actual set-up of this data block follows a basic format (described below), specific variations are required on the first card(s) of this block depending on optional usage. These variations denote whether multiple data sets are to be input for respective spanwise locations, a single set is to be input for use on all spanwise locations, or an analytic representation of the NACA 0012 airfoil is to be used for all spanwise locations. Each of these optional usages is described below.

Multiple Spanwise Airfoils

For the case of distinct airfoil characteristics being defined at up to five (5) spanwise locations, the first card image format is as follows:

card #1A:

NZ	NRCL	NRC	NRCM	TITLE (optional)	(4I2,A72)
----	------	-----	------	------------------	-----------

NZ (normally the number of Mach number groups) on card 1A is not used when defining multiple spanwise airfoils i.e. G400 automatically ignores NZ on card 1A if the sum of the absolute values of NRCL, NRC and NRCM is 4 or greater. See card 1B for specification of the number of Mach number groups. The quantities NRCL, NRC and NRCM are, respectively, the number of radial stations for which c_l , c_d and $c_{mc}/4$ airfoil data tables to be input. NRCL, NRC and NRCM each must fall between a minimum absolute value of 1 and a maximum absolute value of 5. Normally, NRCL, NRC and NRCM are input as positive integer numbers. The program also provides for the optional input of NRCL as a negative value, in which case the printout of the entire data table, (part of the normal case printout) is suppressed. Note that at least one of these three inputs must have an absolute value of 2 or greater. For multiple spanwise section properties, an additional card, following the one described above, is then required, which begins the input of the c_l airfoil data:

card #1B:

NZ(1) RADCL(1)	TITLE(optional)	(I2, F8.0, A70)
----------------	-----------------	-----------------

where NZ(1) is the number of Mach numbers, 12 (maximum), for which groups of c_g data are to be read in for the first radial station; RADCL(1) is the nondimensional radial station at which the airfoil no. 1 data is defined.

For a blade with three distinct constant airfoil sections along the span the quantities NRCL, NRCD and NRCM would be set to 4. For example, if the airfoils change abruptly at $x/R = .4$ and $x/R = .8$, the change is modeled by entering four complete airfoil tables for the four radial locations adjacent to $x/R = .4$ and $x/R = .8$ of the blade. Thus, the airfoil data should be assigned as follows: (Note that the #2 airfoil data is entered twice)

- 1) airfoil no. 1 from $x/R = 0.$ to $.399$ (RADCL(1) = $.399$)
- 2) airfoil no. 2 from $x/R = .401$ to $.799$ (RADCL(2) = $.401$) and (RADCL(3) = $.799$)
- 3) airfoil no. 3 from $x/R = .801$ to 1.0 (RADCL(4) = $.801$)

It is not necessary to specify a radial station at the blade tip or at the root. For the present example airfoil no. 3 data, which is entered in the c_g vs. α table that follows card 1B (which has RADCL(4) = $.801$), will automatically be assumed to extend to the blade tip. Similarly the data of the table with RADCL(1) = $.399$ will be assumed to extend to the root subject to the parameters (A)5 and (R)421 which are often used to render the airfoil ineffective in the region inboard of the true airfoil.

Single Airfoil Description

For the case of a single airfoil to be used for all spanwise locations, a single first card image is input. This card is similar to the card #1A described above, except that the quantities NRCL, NRCD AND NRCM are input as zero (or the columns are left blank):

card #1

NZ(1) 0 0 0	TITLE(optional)	(4I2, A72)
-------------	-----------------	------------

In this case the card is interpreted as the first card of the c_g data with the RADCL(1) information omitted (see description above for card #1B). NZ is required and defines the number of c_g Mach number groups to follow.

Analytic Airfoil Description

For those optional cases wherein the analytic NACA 0012 airfoil option is specified, (see "S" array location 63 discussed in subsequent sections) the first card image must be a single card with blank or zeroed columns 1 through 8. For this option, the remainder of the airfoil data is omitted.

Input Format for Subsequent Cards

For those cases wherein tabulated airfoil data are to be input, the subsequent inputs continue the airfoil c_g data initiated with the #1A and/or #1B cards. Thus, the card image set-up defined by cards 1B, 2, and 2+ is then input NRCL times (or only once, if NRCL = 0):

card #2: J N M A(1) CL(1) A(2) CL(2) ... A(4) CL(4) (I2, 10F7.0)

cards #2+: A(5) CL(5) ... (F9.0, 9F7.0)

.
.
.

... A(N) CL(N) ALSTAL DCLDAO (F9.0,9F7.0)

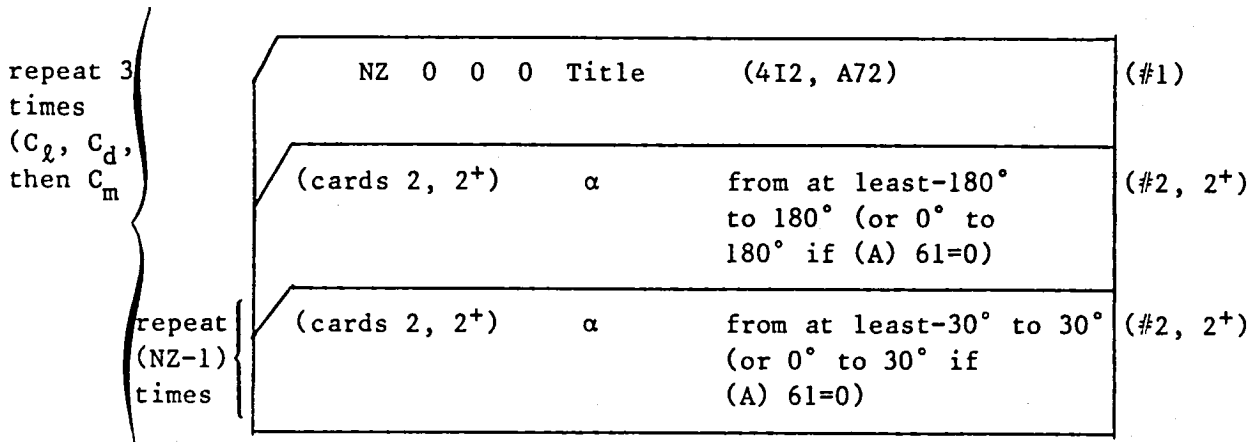
where: J is the number of data entries to be input for this Mach number group. N is the number of angle-of-attack- c_l (abscissae - ordinate) pairs to be input. Normally, a maximum of thirty-four (34) α - c_l pairs may be input; up to thirty-three (33) pairs can be input if the unsteady option is chosen. Note that $J = N \times 2 + I$, where $I = 2$ without invoking the unsteady option, and $I = 4$ with the use of the unsteady option (i.e. ALSTAL, DCLDAO input) M is the Mach number appropriate to the data group. A(i) are the N angle-of-attack abscissae in degrees and CL(i) are the N lift coefficient ordinates. ALSTAL and DCLDAO are, respectively, the static stall angle (α at C_l max), in degrees, and the lift curve slope at zero angle-of-attack, in per degree units; these items are needed only if the unsteady airloads option, (A)64, is invoked with a value of 2. Note that J is an integer, but N and M are floating point formatted.

Cards 2 and 2+ are then repeated for each successively higher Mach number. A maximum of 12 Mach numbers is allowed and the lowest and highest Mach numbers need not define the total working range as the search technique uses the boundary data for Mach numbers beyond the range input. Thus, repeated data for zero and supersonic Mach numbers are not needed. The lowest Mach number table must contain an angle-of-attack range from -180° to 180° or from 0° to 180° depending on whether or not unsymmetric airfoil data is expected by G400 according to (A)61; all higher Mach number data need extend only from -30° to 30° if (A)61 = 1 or from 0° to 30° if (A)61 = 0.

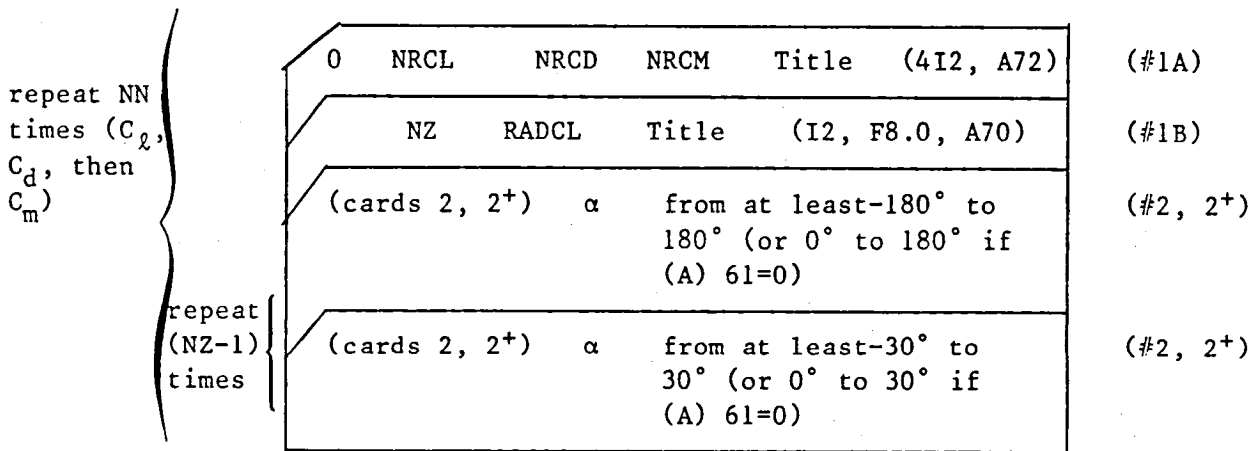
The general format described above is repeated for the c_d and $c_{mc}/4$ sub-blocks in that order but with either card image #1B or #1A, depending on whether multiple airfoil section data are or are not input and used. The static stall angles and aerodynamic coefficient curve slopes at zero angle-of-attack are not entered for the for the c_d subblock. Lastly, the total storage allocated for the combined airfoil data is 5000 locations. The total airfoil data consists of several sets each comprised of two data items (no. of point pairs and Mach number) and point pair data, one set defined for each Mach number. The maximum number of abscissa-ordinate point pair data available is therefore equal to 2500 less the total number of Mach number sets. For applications requiring extensive airfoil data, the data should be "budgeted" among the various spanwise sections, as appropriate.

Combining the previous discussions we arrive at the following airfoil data input sets. Note that the Mach numbers should be input in increasing order.

Single Airfoil



Multiple Airfoil



where: $NN = |NRCL| + |NRCD| + |NRCM|$

II. Loader Data Descriptions

Most of the data used by G400 is entered by using the "loader blocks" discussed in this section. Each loader block is assigned a letter designation. Each block groups items that are similar in nature. For example, the A-block includes only (A)erodynamic data while the D-block contains only (D)ynamic data. Since a particular data block usually contains a substantial volume of data, a particular entry is referred to by both it's block letter and by numerical designation. For example (A)28 is item 28 of the A-block or the rotor collective pitch while (D)2 is the number of edgewise modes to be used. It should be noted that it is not always obvious which data block a particular item should belong to although a conscious attempt has been made to group similar items into the same block. Subsequent sections briefly describe the items available in each data block. Note that the blocks are arranged in alphabetical order (with some letters missing, i.e. there is no I-block) for convenience even though the user need not order the input alphabetically in the input deck or file.

Since the capabilities of the various G400 versions vary slightly, some of the input quantities are not appropriate for all versions. For such cases where a G400 data entry from one version of G400 is loaded to another version where it is inappropriate, the data entry will be accepted and treated only as a data file comment, not to be used.

Card Format

The following card format must be adhered to for loader block data entries:

```
ZZ NN L DATA(L) DATA(L+1) ... DATA(L+4) (A1,I1,I4,5F12.0)
```

where: ZZ is the block letter for the data on this card, A, B, C...etc

NN is the number of data items on this card, max = 5. For example, if NN is 3 only DATA(L), DATA(L+1) and DATA(L+2) will be used. Any data entered in the fields corresponding to DATA(L+3) and/or DATA(L+4) when NN = 3 will be ignored

L is the loader location of DATA(L). For example if ZZ = A, NN = 3 and L = 28 then the DATA () fields on this card correspond to (A)28, 29, 30 respectively.

Although not a requirement it is recommended practice to group the A-block, D-block etc. cards together in a particular deck to aid input interpretation. This order is particularly useful since loader data can be redefined in the same deck. For example if loader location (D)2 is defined early in the file it may still be redefined later in the deck. If the data from many blocks are interspersed it becomes more difficult to assure which (D)2 data was the last to be loaded.

Overriding Data

There are some loader locations in the R, G and D-blocks that are automatically overridden by the E159 preprocessor generated block data if (E)1195 = 1.0. Any values loaded into these R, G and D-block locations will be replaced with the E159 generated block values. In subsequent sections a dagger superscript (†) flags the entries that are overridden in this way. When the E159 preprocessor and associated E-block data is not used, (E)1195 = 0., the daggered values are used.

Title and Comment Cards

Provision has been made for the input of title and comment cards in the loader block data. The first 15 (or less) cards encountered with an asterisk, '*', in column 1 will be read and stored as the job title. The title will be printed at the beginning of the loader block input echo, before the beginning of the time history solution, and before the beginning of the TSSA solution. If the code encounters a character in column 1 other than an asterisk or one of the data block characters (e.g. A, C, D. etc.) the card will be treated as a comment card. It will be read and ignored. It is therefore useful in labeling a particular input deck, but nowhere will it be printed. For example, the code would treat a card with a "dollar sign", or even a blank, in column 1 as a comment card.

(A) <u>Location</u>	<u>Item</u>	<u>Description</u>
1	ρ	Air density. [lb-sec ² /ft ⁴]
2	a_{∞}	Speed of sound. [ft/sec]
3	B	Tip loss, used to define equivalent momentum area and three-dimensional airloads near the blade tip. Usually set to .97 but when using variable inflow (see (A)66 (A)3 should be set to 1.0). [ND]
4	Δc_{d_0}	Increment added to all values of c_d obtained from tabulated airfoil data or from the analytic NACA 0012 data. Airfoil data generally correspond to smooth wind tunnel models and Δc_{d_0} is often used to adjust for the higher drag of production blades. [ND]
5	$N_{\text{cut-out}}$	Number of blade segments, starting at inboard end and defining the cut-out region for which the lift and moment coefficients are set to zero.
6	$(c_d)_{\text{cut-out}}$	The drag coefficient used on the first $N_{\text{cut-out}}$ segments. [ND]
7	κ_{vim}	Effectivity factor of the induced velocities calculated using actuator disk momentum considerations in calculating inflow angle at a local blade section. Default value is 1., corresponding to conventional usage of momentum actuator disk inflow. This input quantity can be used to approximate the effects caused by real inflow characteristics as modeled by more accurate theories. For such usage, the effectivity would typically be in the range of 1.0 to 1.1. [ND]

(A)			
<u>Location</u>	<u>Item</u>		<u>Description</u>
8	h		Height of positively thrusting rotor from ground or wind tunnel floor for purposes of evaluating Heyson corrections to rotor angle of attack (see Ref. 14). [ft]
9	H _{WT}		Height of wind tunnel test section for purposes of evaluating Heyson corrections. Note that zero values for the wind tunnel test section dimensions implies that ground effect corrections, rather than wind tunnel wall corrections, are to be made. [ft].
10	W _{WT}		Width of wind tunnel test section for purposes of evaluating Heyson corrections. [ft]
11-20	—		Intentionally blank.
21	V		Forward flight velocity. See also (V)23. Should be a positive value. [kts] (1 kt=1.689 ft/sec=.5148 m/sec)
22	α_s		Aerodynamic shaft angle-of-attack measured with respect to the relative air velocity. The shaft angle of attack will be varied if major iterations ((A)41 \neq 0) are performed and trim is on propulsive force (see (A)48). Typical input values are -90° for a forward thrusting propeller, +90° for a wind turbine with a horizontal nacelle, 0° for the main rotor of a helicopter in hover, and -90° < α_s < 0 for the main rotor of a helicopter in forward flight. [deg]
23	R/C		Rate of climb. If (A)23 is nonzero then (V)21 becomes the total net 'forward' velocity. [ft/min]

(A)			
<u>Location</u>	<u>Item</u>		<u>Description</u>
24	Ω_x		Fixed roll rate. [deg/sec]
25	Ω_y		Fixed pitch rate. [deg/sec]
26	A_{1s}		Longitudinal cyclic pitch, coefficient of minus $\cos\psi$ term in Fourier expansion of blade control pitch angle. [deg]
27	B_{1s}		Lateral cyclic pitch, coefficient of minus $\sin\psi$ term in Fourier expansion of blade control pitch angle. [deg]
28	$\theta_{.75R}$		Blade collective pitch angle as defined at the 75% radius. [deg]
29	λ		Mean rotor inflow ratio. Used only if (A)68=0. Usually should be set to zero for variable inflow cases. [ND]
30-32	$\bar{v}_o, \bar{v}_{1c}, \bar{v}_{1s}$		Initial conditions on the "momentum" induced velocity components comprising a Glauert-like variable inflow description (used only when (A)68>0). Note that the variable inflow controlled by locations (A)65 and (A)66 and the momentum variable inflow can be used separately or simultaneously, see (A)68. [ND]
33	$A_{(b-1)s}$		Amplitude of minus cosine term of (b-1)/rev cyclic pitch. The number of blades is b. [deg]
34	$B_{(b-1)s}$		Amplitude of minus sine term of (b-1)/rev cyclic pitch. [deg]

(A)		
<u>Location</u>	<u>Item</u>	<u>Description</u>
35	$A(b)_s$	Amplitude of minus cosine term of b/rev cyclic pitch. [deg]
36	$B(b)_s$	Amplitude of minus sine term of b/rev cyclic pitch. [deg]
37	$A(b+1)_s$	Amplitude of minus cosine term of b+1/rev cyclic pitch. [deg]
38	$B(b+1)_s$	Amplitude of minus sine term of b+1/rev cyclic pitch. [deg]
39-40	—	Intentionally blank.
41	N_{MI}	Maximum number of major trim iterations to be made in an attempt to achieve trim. A zero value will deactivate the major iteration. G400 will not print a complete transient time history if major iteration fails, see (S)12.
42	(Control)	<p>Calculation rate (by sequential control angle perturbations) for trim partial derivative matrix. Base value here is problem dependent, 2. is typical. (A)42 has a strong affect on CPU time. 0=calculate partial derivative matrix for the first major iteration only and use this matrix for all remaining major iterations. If table (A)351 is not completely empty use the table for the first iteration and recalculate the matrix according to (A)42 for the remaining major iterations.</p> <p>1.=recalculate for every major iteration. 2.=recalculate for every other major iteration.</p>

(A)	<u>Location</u>	<u>Item</u>	<u>Description</u>
43		f_w	Nonstandard correction weighting factor. Usually G400 will attempt to drive the trim error completely to zero at every major iteration using the trim partial derivative matrix. (A)43 can be used to moderate the size of this large step (usual values are .5 or 1.0); default=1.0. [ND]
44		—	Intentionally blank.
45		L_{req}	Requested values of lift to be used in major iteration. [lb]
46		ϵ_{lift}	Tolerance lift for major iteration. A zero value deactivates trimming on lift (1% to 3% on total lift is typical). [lb]
47		PF_{req}	Requested value of propulsive force to be used in major iteration. [lb]
48		ϵ_{PF}	Tolerance on propulsive force for major iteration. A zero value deactivates trimming on propulsive force. The automatic trim calculation (major iteration) must trim either to a required propulsive force or to a required shaft angle of attack; therefore, a deactivation of trim to propulsive force automatically directs the trim calculation to trim to requested shaft angle, location (A)22. [lb]
49		PM_{req}	Requested value of pitching moment for major iteration (positive nose up). [lb-ft]
50		ϵ_{PM}	Tolerance on pitching moment for major iteration. A zero value deactivates trimming on pitching moment. [lb-ft]

(A)	<u>Location</u>	<u>Item</u>	<u>Description</u>
	51	RM_{req}	Requested value of rolling moment for major iteration (positive port side up). [lb-ft]
	52	ϵ_{RM}	Tolerance on rolling moment for major iteration. A zero value deactivates trimming on rolling moment. [lb-ft]
	53-59	—	Intentionally blank.
	60	$\Delta\psi_{F389}$	Delta psi for F389 aerodynamic (W1) data transferral. Note that this value is only used as a data transfer "frequency" and is not actually used <u>during</u> F389 execution. See also (S)33, (S)23, (A)65, (A)66. (A)60 must be greater than (S)8. Also, (A)60 must be \leq 15 deg; G400 will set to 15 deg if criterion is violated. [deg]
	61	(Control)	Make nonzero (1.) if <u>airfoil data for a nonsymmetrical airfoil</u> are to be used.
	62	(Control)	Make 1., to invoke the <u>radial flow, swept airfoil option</u> , see (R)461-(R)500, R(221-300).
	63	(Control)	<u>Analytic (static) airfoil option</u> . Make nonzero (1.) to use the built-in analytic approximation to the static NACA 0012 airfoil data. A zero value results in the use of the input tabular data.
	64	(Control)	Unsteady airfoil data option. 0.=use conventional quasi-static airloads (this is the default value). See (A)63. 1.=generalized Wagner function to define effective angle-of-attack; assumes <u>unstalled</u> aerodynamics. Tabular airfoil data look-up in t-h solution. 2.=UTRC synthesized α , A , α_w method in the t-h solution; assumes dynamic stalled aerodynamics (see locations (R)521- (R)540, (A)300-(A)308, and (A)63).

(A) <u>Location</u>	<u>Item</u>	<u>Description</u>
65	(Control)	Make nonzero (1.) to <u>load</u> velocity distributions from the F389 code. See (S)33, S(23), (A)66. The velocity distributions from F389 are the induced velocities only.
66	(Control)	Make nonzero (1.) to <u>use</u> the F389 velocity distributions loaded as per input locations (A)65 and (S)33. If (A)68 is nonzero, momentum induced velocities will be added to the loaded velocities. This option is often referred to as the variable inflow option.
67	(Control)	Variable inflow shape option. A value of (0., 1.) causes the inputted variable inflow azimuthal distributions to be used in a (continuous point-to-point, stepped pulse) manner.
68	(Control)	Generalized Glauert (momentum derived) inflow option. A zero value deactivates usage. A value of 1. causes the input ((A)30-32) induced velocity components to be used as constants; a value of 2. causes the induced velocities to be varied to satisfy momentum considerations.
69	(Control)	Input nonzero (1.) to activate use of the tabulated time histories of incremental control angles. $\Delta\theta_{75}$ in table (A)101, [deg] ΔA_{1s} in table (A)151, [deg] ΔB_{1s} in table (A)201, [deg]

(A) <u>Location</u>	<u>Item</u>	<u>Description</u>
70	(Control)	Gust wave option. 0.=Disable this option. 1.=(F) is a time history of gust factor. This factor is multiplied by the velocity of (A)21. Abscissa of table (A)251 is time (sec). 2.=(F) is a time history of gust velocity increment that is added to the velocity of (A)21. Abscissa of table (A)251 is time (sec). 3.=(F) is the gust velocity vs. ft imbedded in the air mass. Similar to option (2) but abscissa of table (A)251 is ft.
71	α_{Gw}	Inclination angle of the gust wave; a positive value implies a relative velocity component up in the vertical direction. Also see (A)251,(A)70. [deg]
72	β_{Gw}	Side flow angle of the gust wave; a positive value implies a relative lateral velocity component in the direction to port. Also see (A)70, (A)251, (A)501. [deg]
73-100	—	Intentionally blank.
101	$N_{\Delta\theta.75}$	Number of abscissa-ordinate point pairs used to define time-history of $\Delta\theta.75(t)$. $\Delta\theta.75$ calculation is bypassed if $N_{\Delta\theta.75}$ is zero. Max pairs 24. (See (A)69, (A)28).
102-149	(T, $\Delta\theta.75$)	Table of $\Delta\theta.75$ abscissa-ordinate pairs; [U(T)=sec; $\dot{U}(\Delta\theta.75) = \text{deg}$]. Note that the pairs are input with time first, $\Delta\theta.75$ second.
150	—	Intentionally blank.

(A) <u>Location</u>	<u>Item</u>	<u>Description</u>
151	$N_{\Delta A_{1s}}$	Number of abscissa-ordinate point pairs used to define time history of ΔA_{1s} . $\theta = \theta_{.75} - A_{1s} \cos \Omega t - B_{1s} \sin \Omega t - \dots$. ΔA_{1s} calculation is bypassed if $N_{\Delta A_{1s}}$ is set to zero. Max pairs 24 (see (A)69, (A)26).
152-199	$(T, \Delta A_{1s})$	Control angle increment ΔA_{1s} time history tabulation. [U(T)=sec, U(ΔA_{1s}) = deg]
200	—	Intentionally blank.
201	$N_{\Delta B_{1s}}$	Number of abscissa-ordinate point pairs used to define the time history of ΔB_{1s} , $\theta = \theta_{.75} - A_{1s} \cos \Omega t - B_{1s} \sin \Omega t - \dots$. ΔB_{1s} calculation is bypassed if $N_{\Delta B_{1s}}$ is set to zero. Max pairs 24. (See (A)69, (A)27).
202-249	$(T, \Delta B_{1s})$	ΔB_{1s} control angle increment time history tabulation. [U(T)=sec; U(ΔB_{1s}) = deg]
250	—	Intentionally blank.
251	N_{gust}	Number of abscissa-ordinate point pairs used to define the time-history of the gust wave function; calculation is bypassed with a zero value. (See (A)70).
252-299	(T, f_{gust})	Table of gust wave function abscissa-ordinate pairs; (see input loc. (A)70 for definition of f_{gust}) [(sec, ND), (sec, ft/sec), or (ft, ft/sec)]

(A) <u>Location</u>	<u>Item</u>	<u>Description</u>
		<u>Locations (A)300-(A)308 are for unsteady stalled airloads option, when (A)64=2.</u>
300	(Control)	Static aerodynamic data utilization for use with the UTRC α -A- α_w synthesized unsteady stalled airloads; used if (A)64=2. 1.=using static data according to (A)63. 2.=using built-in static data. See (A)304 to enable sweep effects.
301	M_{lower}	Lower Mach number below which the UTRC unsteady airloads method is suppressed (0.=no lower limit). [ND]
302	M_{upper}	Upper Mach number above which the UTRC unsteady airloads method is suppressed (0.=no upper limit). [ND]
303	(Control)	Inclusion of nonuniform inflow in inflow rate $\dot{\phi}$ calculation. 0.=nonuniform inflow is included 1.=nonuniform inflow is omitted
304	(Control)	Swept data option (see (A)300) for unsteady stalled aero. 0.=do not use swept data 1.=use swept data
305	(Control)	Input/Output unit code number for both input/output of unsteady parameters (for restart purposes) (0.=input/output is suppressed).
306	(Control)	An input value of (0.,1.) causes the unsteady stalled airloads method to (omit, include), respectively, the calculation of unsteady drag.
307	$ A _{max}$	Maximum (absolute) value of A parameter used in UTRC unsteady stalled airloads method (0.=no limit). [rad]

(A)		
<u>Location</u>	<u>Item</u>	<u>Description</u>
308	$ \alpha_w _{\max}$	Maximum (absolute) value of unsteady decay parameter, α_w , used in unsteady airloads formulations (0.=no limit). [rad]
309	$\bar{\omega}_\phi^*$	Frequency used for numerically differentiating inflow angle to calculate 'A' parameter. Typical nonzero values would be blade 1st or 2nd torsion mode frequency. Zero value invokes numerical differentiation algorithm based on standard backward differentiation techniques. [ND]
310-350	—	Intentionally blank.
351-399	[T]	Trim partial derivative matrix obtained as output from a previous trim calculation. Any nonzero value in this table will suppress recalculation for first major iteration. (See (A)41-(A)55).
400-600	—	Intentionally blank.

(C)

<u>Location</u>	<u>Item</u>	<u>Description</u>
1	NSPSTR	Innermost torsionally flexible segment of flexbeam. Default is 1. Twist will always be zero for segments <(C)1. This entry is always used to define the pseudo torsion mode shape and twist regardless of (C)15.
2	$\theta_{B_{FB}}$	Built-in twist angle of the flexbeam, positive leading edge up at outboard end of flexbeam, deg. Note that $\theta_{B_{FB}}$ is defined relative to the inputted twist angle distribution (only when using (G)7, which in turn is defined for zero collective angle). Used only when <u>all</u> of (R)361-(R)381=0. [deg]
3	θ_R	Built-in flexbeam pitch angle at flexbeam root, defined relative to structural twist input only when using (G)7, positive leading edge up. Only used if <u>all</u> of (R)361-(R)381=0. [deg]
4	$\kappa_{T_{FB}}$	Equivalent or critical torsion stress coefficient for flexbeam (i.e., stress per unit average torsion strain as defined by total flexbeam twist). [in-psi]
5	C/t	Flexbeam aspect ratio parameter, where C is flexbeam width and t is flexbeam thickness. This parameter is used to determine plate-like deflection for torsion "pseudo-mode". A zero value gives a rod-like deflection shape. Max value = 12.5 to avoid under flow. A larger value will be reset to zero. Used always, regardless of (C)15. [ND]

(C) <u>Location</u>	<u>Item</u>	<u>Description</u>
6	(Control)	Torque tube snubbing control 0.=torque tube is snubbed to the flexbeam at location (G)15 1.=torque tube is snubbed to the hub extension at location (G)15 of torque tube. (C)6 is used only if (C)15=1.
7	(Control)	Snubber stiffness alignment option. Used only if (C)15=1 0.=snubbers are oriented vertically and horizontally, see (C)8, (C)9 1.=snubbers are oriented parallel and perpendicular to local torque tube angle. Usually used for cantilevered torque tube configurations, see (C)8, (C)9.
8	K_{sz5} (K_{sF})	Snubber vertical (torque tube flatwise) spring rate, see (C)7. Used only if (C)15=1. [lb/ft]
9	K_{sy5} (K_{sE})	Snubber horizontal (torque tube edgewise) spring rate, see (C)7. Used only if (C)15=1. [lb/ft]
10	K_{wOB}	Spring rate of rotational spring connecting outboard end of torque tube to the blade spar about chordwise axis. A zero value implies zero stiffness for pinned-pinned torque tube configurations ((C)14=(C)15=0) and infinite stiffness for snubbed configurations. Used only if (C)15=1. [ft-lb/rad]
11	K_{vOB}	Spring rate of rotational spring connecting the outboard end of the torque tube to the blade spar about an axis perpendicular to the chord line. Used only if (C)15=1. A zero value implies infinite stiffness. [ft-lb/rad]

(C) <u>Location</u>	<u>Item</u>	<u>Description</u>
12	(Control)	When the torque tube flexbeam redundant analysis is enabled, location (C)15=1 the <u>torque tube</u> is assumed to be in (tension, compression) as location (C)12 is (0.,1.). Default = 0.
13	(Control)	Used to weigh the effectiveness of nonlinear EI bending excitation of torsion over flexbeam span. The effectiveness is taken to be 100%, 0%, 100%*pseudo-torsion mode shape, as location (C)13 is 0.,1.,2., respectively. Default is 0. Used always regardless of (C)15, on all segments \leq (G)16-1.
14	(Control)	1=include wobble mode for cantilevered torque tube configurations. Valid only (G)15=(G)16 and (G)16>1. (C)15=1 will disable this option. Use option (D)34 instead of (E)1189.
15	(Control)	0.=disable redundant analysis, do either a cantilevered torque tube analysis with wobble mode (C)14=1, or a simple pitch-horn analysis without wobble, (C)14=0. 1.=Use flexible torque tube flexbeam redundant analysis snubbing to the flexbeam or to the hub extension, see (C)6. G400 will default to (C)15=0. if C-block inconsistencies are detected. See limitations on (D)1, (D)3. For (C)15=1 the following input constraints must be followed: (G)15=1, (G)15=(C)16, (G)16>(G)15, (G)16>2., (G)16>(C)16, (G)18 >0, (D)3>2, (D)1>1. Use option (D)34 instead of option (E)1189.
16	NTQTBI	Innermost segment of torque tube, also the snubber location and the pitch horn attachment segment. Used only if (C)15=1. This entry also defines the first value in tables (C)71,(C)81 etc. that is actually used.

(C) <u>Location</u>	<u>Item</u>	<u>Description</u>
17	D _{SNUB}	Optional snubber attachment distance below flexbeam. Used only when (C)15=1 (Usually used on main rotors). [in]
18	ψ_{DR}	Optional built-in torque tube droop angle at the flexbeam-torque tube juncture. Used only if (C)15=1. [deg]
19-30	—	Intentionally blank.
31-40	D	Optional flexbeam plate bending stiffness for each flexbeam segment. Where $D = Et^3/12(1-\nu)^2 \approx EI/C$. t = segment flexbeam thickness, C = segment flexbeam width of (C)51. D is used to correct the flexbeam <u>torsional</u> equation for secondary warping effects. [lb-ft]
41-50	GJ _{FB}	Flexbeam torsion (St. Venant) stiffness for each flexbeam segment. Flexbeam is torsionally flexible between segment (G)16-1 and segment (C)1 or first nonzero value in table (C)41, whichever has highest segment number. In this way G400 can redefine (C)1 to be as large as (G)16. (Note that (E)737-(E)886 defines the torque-tube torsional stiffness). Only used if (G)15=1. Flexbeam is centrifugally stiffened using (R)161. [lb-ft ²]

(C)

<u>Location</u>	<u>Item</u>	<u>Description</u>
51-60	W_{FB}	Optional flexbeam section width for each flexbeam segment. This is used with table (C)31 to define incremental stiffness changes due to flat plate effects. [ft]
61-70	---	Intentionally blank.
71-80	EI_{FTT}	Torque-tube flatwise bending stiffness, EI (Note that (E)253 defines the flexbeam flatwise stiffness; also note that no unique segments are defined for the torque tube. The torque tube segments are defined in the (E)4-(E)23 table and therefore have lengths identical to the flexbeam lengths). Used only when (C)15=1. [lb-ft]
81-90	EI_{ETT}	Torque-tube edgewise bending stiffness. (Note that (E)454 defines the flexbeam stiffness; also see note on (C)71-(C)80.) Used only when (C)15=1. [lb-ft]
91-100	M_{TT}	Mass of each torque-tube segment (see notes on (C)71-(C)80 for segment length definitions). Used only when (C)15=1. [lb-sec /ft]
101-110	$y_{TT_{CG}}$	Distance from torque-tube elastic axis to torque tube c.g. for each segment (see notes of (C)71-(C)80 for segment length definitions). Presently not functional. [ND,R]

<u>(C)</u>		
<u>Location</u>	<u>Item</u>	<u>Description</u>
111-120	(I/c) _F	Torque-tube flatwise bending modulus (see notes of (C)71-(C)80 for segment length definitions). Used only when (C)15=1. [in ³]
121-130	(I/c) _E	Torque-tube edgewise bending modulus (see notes of (C)71-(C)80 for segment length definitions). Used only when (C)15=1. [in ³]
131-150	—	Intentionally blank.

(D)

<u>Location</u>	<u>Item</u>	<u>Description</u>
1	NFM	Number of flatwise bending modes to be used not including rigid modes if blade is articulated (see (G)10). Note that it is not necessary to use all of the bending modes that were calculated by E159. For articulated rotors (D)1<(E)24-1 (when E159, G400 run simultaneously). For cantilevered rotors (D)1<(E)24. If (C)15=1, (D)1 must be ≥ 1 , default=0. Max value = 5.
2	NEM	Number of edgewise bending modes to be used not including rigid modes if blade is articulated (see (G)11). Note that it is not necessary to use all of the bending modes that were calculated by E159. For articulated rotors (D)2<(E)25-1 (when E159, G400 run simultaneously). For cantilevered rotors (D)2<(E)25. Default=0. Max value = 3.
3	NTM	Number of elastic torsion modes to be used. (D)3<(E)26 (when E159, G400 run simultaneously). Note that even if (D)3=0, G400 permits use of a rigid body torsion mode. See (D)34. If (C)15=1, (D)3 must be ≥ 1 , default=0. Max value = 2.
4-8	$\dagger\omega_i$	Flatwise bending modal frequencies, non-dimensional with respect to Ω , in ascending modal order. A negative value will cause $q_{\omega_i}^{**}$ inertia blade forces to be neglected while retaining all elastic terms in the time history solution. Max values = 5. [ND]
9	—	Intentionally blank.

\dagger G400 will obtain these values from the E159 preprocessor if (E)1195=1.0. In this case (D) input values entered by user will be ignored.

(D)

<u>Location</u>	<u>Item</u>	<u>Description</u>
10-12	$\dagger\omega_k$	Edgewise bending modal frequencies, non-dimensional with respect to Ω , in ascending modal order. A negative value will cause $q_{v_k}^{**}$ inertia blade forces to be neglected while retaining all elastic terms in the time-history solution. Max values = 3. [ND]
13	—	Intentionally blank.
14-15	$\dagger\omega_j$	Torsion modal frequencies, nondimensional with respect to Ω , in ascending modal order (not including rigid body feathering mode). A negative value will cause $q_{\theta_j}^{**}$ inertia blade forces to be neglected while retaining all elastic terms in the time history solution. Max value = 2. [ND]
16-30	—	Intentionally blank.
30	(Control)	Edgewise structural damping option. 0.=use (D)31 in viscous damping formulation 1.=use (D)31 in nonviscous hysteretic damping formulation 2.=use distribution of nonviscous hysteretic damping. See (R)501 for distribution table.
31	$\zeta_{v_{se}}$	Viscous ((D)30=0.) damping equivalent critical damping ratio used to approximate <u>structural damping</u> in all <u>edgewise bending modes</u> . If (D)30=1., this item is a non-viscous, hysteretic constant. If (D)30=2., this item is not used, see (R)501. Caution: typically some nonzero damping is required here to dampen the lightly damped edgewise modes. [ND]

\dagger G400 will obtain these values from the E159 preprocessor if (E)1195=1.0. In this case (D) input values entered by user will be ignored.

(D)			
<u>Location</u>	<u>Item</u>		<u>Description</u>
32	$\zeta_{w_{sf}}$		Critical (viscous) damping ratio for <u>structural damping in flatwise bending modes</u> . [ND]
33	$\zeta_{\theta_{se}}$		Critical (viscous) damping ratio for <u>structural damping in torsion modes</u> . [ND]
34	K_{root}		Torsional spring rate connecting root of blade to fixed structure to represent control system flexibility. A nonzero value will automatically introduce the rigid-body feathering degree-of-freedom as an additional "torsion mode". Do not use in tandem with (E)1189-(E)1190. See comments in (E)1189. (D)34 must be used instead of (E)1189 for bearingless rotor applications when (C)15=1. [ft-lb/rad]
35-37	$\frac{DTHETA}{DQVK}$		Direct pitch-edge coupling for edgewise <u>bending modes</u> only. 3 max, one value for each edgewise bending mode. See (G)13 for a similar value for the rigid lead lag mode. Nondimensional where DTHETA is pitch angle per unit of edgewise modal amplitude DQVK (which in turn is nondimensional with respect to R). Unlike (G)12 this entry functions with cantilevered blade modal data. [ND]
38	—		Intentionally blank.
39	g		Acceleration due to gravity; a negative value implies inverted flight. Default = 32.2 ft/sec ² . [ft/sec ²]
40	C_{LD}		Linear lag damper rate. Provides lag damping moment at blade root proportional to root angular velocity, see (D)49. [lb-ft-sec]

(D) <u>Location</u>	<u>Item</u>	<u>Description</u>
41-46	L1-L6	Six lag damper geometrical dimensions. Currently this option is not functional.
47	N_D	Lag damper attaches to center of this segment, default=1. Currently not functional.
48	(Control)	Make (0.,1.) as the outboard lag damper attachment is (inboard, outboard) of the feathering bearing.
49	(Control)	1.=Use tabulated damper properties, table (D)51. 0.=Use linear lag damper rate ((D)40).
50	N_{LD}	Number of root angular velocity - root damping moment pairs (abscissa-ordinate) to be inputted in table (D)51-98.
51-98	(\dot{A}, M)	Table of blade root angular velocity, \dot{A} , vs. root damper moment, M, pairs. Max pairs = 24. Usually velocity and moment are given same sign. Values for both positive and negative root velocities must be entered. [U(\dot{A})=rad/sec; U(M)=ft-lb]
99	—	Intentionally blank.
<u>The following five items are for teetered rotors only.</u>		
100	β_1	Limit stop angle below which there is no constraint on teetering (a zero input is treated as infinity). [deg]
101	K_{β_1}	Initial limit stop flapping spring rate defined when the β_1 limit stop is first reached. [ft-lb/rad]

(D)

<u>Location</u>	<u>Item</u>	<u>Description</u>
102	β_2	Saturation limit stop angle above which the limit stop constraint is defined by a second constant spring rate. [deg]
103	M_{β_2}	Saturation moment when the β_2 limit stop is reached. [ft-lb]
104	K_{β_2}	Flapping spring rate of limit stop for teeter angles in excess of β_2 . (Note that locations (D)100-104 provide a general representation of a nonlinear limit stop spring). [lb-ft/rad]
105-150	—	Intentionally blank.

(E)			
<u>Location</u>	<u>Item</u>		<u>Description</u>
1	R		Rotor radius, from center of rotation to blade tip. [ft.]
2	\bar{e}		Offset distance of start of elastically deformable portion of rotor blade. Must be zero for a teetered rotor. [ND,R]
3	NSEG		Number of segments into which the blade is partitioned; min of 5., max of 20.
4-23	Δr		Blade segment lengths, in order from root to tip; sum of segment lengths plus the offset must equal the rotor radius. [in.]
24	NFMC		Number of flatwise bending modes to be calculated, including rigid flapping mode if any; min of 0., max of NSEG. See (D)1, (E)26. (E)24 must be >0. if (C)15=1.
25	NEMC		Number of edgewise bending modes to be calculated, including rigid lag mode if any; min of 0., max of NSEG. See (D)2, (E)26.
26	NTMC		Number of torsion modes to be calculated. Torsion mode(s) alone cannot be requested (i.e., (E)24+(E)25 cannot be zero); min of 0., max of NSEG. (E)26 must be ≥ 1 . if (C)15=1. See (D)3.
27	(Control)		Make nonzero (1.) to output punch loader block data and uncoupled mode shape data for direct input in subsequent runs.
28-47	(I/c) _F		Section moduli for flatwise bending for segments defined in locations (E)4-23, root to tip, cannot be zero. [in ³]
48-67	(I/c) _E		Section moduli for edgewise bending for segments defined in locations (E)4-23, root to tip, cannot be zero. [in ³]

(E)			
<u>Location</u>	<u>Item</u>		<u>Description</u>
69	Ω_R		Rotor tip speed. [ft/sec]
70	(Control)		Make nonzero (1.) to output intermediate E159 calculations for debug purposes.
71	$\Delta\omega_{FE}$		Frequency scan interval for flatwise and edgewise bending frequency iteration; default value is 0.5. See (E)1192 for torsion scan interval [rad/sec]
72-99	—		Intentionally blank.
100	N_w		Number of elements in weight distribution table (equal to twice the number of ordinate-abscissa pairs in table (E)101-(E)250).
101-250	$(w', \Delta s)$		Weight distribution table, taken as sequential ordinate-abscissa pairs, root to tip. Generally, this and all other tables should include an extended final (tip) spanwise increment so that the sum of the spanwise increments plus the offset exceeds the radius by a sufficient amount to preclude diminution due to numerical round-off. [U(w' _k) = lb/in; U(Δs_k) = in]
251	—		Intentionally blank.
252	N_{I_F}		Number of elements in flatwise area moment of inertia table (equal to twice the number of ordinate-abscissa pairs in table (E)253-(E)452.
253-452	$(I_F, \Delta s)$		Flatwise area moment of inertia table (see remarks for w', Δs table). [U(I _{Fk}) = in ⁴ , U(Δs_k) = in]
453	N_{I_E}		Number of elements in edgewise area moment of inertia table (equal to twice the number of ordinate-abscissa pairs in table (E)454-(E)653.

(E)		
<u>Location</u>	<u>Item</u>	<u>Description</u>
454-653	$(I_E, \Delta s)$	Edgewise area moment of inertia table (see remarks for w' , Δs table); $[U(I_{Ek}) = in^4, U(\Delta s_k) = in]$
654	—	Intentionally blank.
655-674	$(x_i)_{NS}$	Stations other than those defined by the input breakup (E)4-23 for purposes of evaluating the mode shapes. [ND,R]
675	—	Intentionally blank.
676-695	ΔM_i	Discrete incremental lumped masses added to centers of blade segments defined by inputs (E)4-23. [lb-sec ² /ft]
696-715	K_{F_i}	Explicit flatwise hinge spring rates at inboard ends of selected blade segments to replace values obtained from input flatwise bending stiffness considerations. Note: (E)696 and (E)716 should both be sufficiently large to approximate infinite stiffness retention if a cantilever beam root boundary condition is desired. If an articulated (hinged) joint is desired a small nonzero value is recommended. See item (G)10. [lb-ft/rad]
716-735	K_{E_i}	Explicit edgewise hinge spring rates at inboard ends of selected blade segments, to replace values obtained from input edgewise bending stiffness considerations (see note for K_{F_i}), see (G)11. [lb-ft/rad]
736	N_{GJ}	Number of elements in the St. Venant torsion stiffness (GJ) table (equal to twice the number of ordinate-abscissa pairs in (E)737-(E)886). (For flexbeam type rotor include the torque-tube GJ and GJ of spar outboard of the torque tube in this table, GJ of flexbeam is entered in (C)41-(C)50).

(E)		
<u>Location</u>	<u>Item</u>	<u>Description</u>
737-886	(GJ, Δs)	Torsion stiffness table, G is the shear modulus, J is the area polar moment of inertia about the elastic axis (see remarks for w', Δs table). [U(GJ _k) = lb-in ² , U(Δs _k) = in]
887	N _{kA}	Number of elements in tension area radius of gyration table (equal to twice the number of ordinate-abscissa pairs in (E)888-(E)1037).
888-1037	(k _A , Δs)	Tension carrying area polar radius of gyration table. Taken about the elastic axis this parameter adds the torsional stiffness caused by centrifugal forces to the elastic, GJ, stiffness (see remarks for w', Δs table). [U(k _{AK}) = in, U(Δs _k) = in]
1038	N _{Iθ}	Number of elements in torsional mass inertia distribution table (equal to twice the number of ordinate-abscissa pairs in (E)1039-(E)1188).
1039-1188	(I _θ , Δs)	Torsional mass inertia per inch distribution table (see remarks for w', s table). [U(I _θ) = lb-sec ² , U(Δs _k) = in]
1189	(Control)	Default value implies that the blade is torsionally cantilevered at the root. Make (-1.) to active root torsional spring restraint (input item (E)1190). Note that this input and (D)34 define a redundant capability. (E)1189 and (E)1190 enable the flexible torsion mode to have root flexibility directly. Alternatively, (E)1189 can be set to zero. In this way E159 will calculate a cantilevered torsion mode. If a rigid body component is required due to control system flexibility (D)34 may be entered. G400 will then include a rigid body feathering d.o.f. in subsequent calculations. (E)1189 and (D)34 should not be used simultaneously. Option (D)34 should be used for bearingless rotors when (C)15=1. or when (C)14=1.

(E) <u>Location</u>	<u>Item</u>	<u>Description</u>
1190	K_{θ_R}	Torsion root spring rate. See (E)1189 and (D)34. [lb-in/rad]
1191	(Control)	Innermost segment which is active in torsion. Segments inboard of this are assumed not to twist elastically, default=1. (Note: For bearingless rotors this entry defines the innermost torsionally flexible torque tube segment).
1192	$\Delta\omega_T$	Frequency scan interval for torsion frequency iteration; default value is 5. See (E)71 for flatwise-edgewise scan interval. [rad/sec]
1193	E	Modulus of elasticity; default value is 1×10^7 . [lb/in ²]
1194	BSCALE	Factor used to scale the stiffness matrix to avoid erroneous zero evaluation of the determinant due to computer underflow or overflow; default value is 10^4 . In addition to under and over flow messages, an indication of a need to vary this input is the calculation of bending modes with frequencies equal to multiples of the scan interval (E)71. [ND]
1195	(Control)	Make nonzero (1.) to activate the E159 uncoupled mode preprocessor branch of the program. If this item is set to zero, modes must be loaded from an existing file, see (S)15 and (E)27.
1196-1540	—	Intentionally blank.
1541-1560	k_{y10}	Thickness wise mass radii of gyration evaluated about the chordwise axis for selected blade breakup. Note that G400 will use inputted values of torsional mass inertia (E)1039-1188 and the thicknesswise mass radii of gyration to calculate chordwise mass radii of gyration (R)141-160; anything entered by the user in (R)141-160 is replaced if E159 is run. [in]

(E)

<u>Location</u>	<u>Item</u>	<u>Description</u>
1561-1999	—	Intentionally blank.
2000	(Control)	Case number for output generated by E159 branch of the program. Used in printout and on modal output file.

(G) <u>Location</u>	<u>Item</u>	<u>Description</u>
1	$\dagger \Omega_R$	Rotor tip speed. [ft/sec]
2	$\dagger R$	Rotor radius from center of rotation to blade tip. [ft]
3	b	Number of blades. Must be 2. for a teetered rotor ((S)5=1.)
4	$\dagger e$	Nondimensional offset distance to start of deformable and/or deflectable portion of rotor blade; this distance added to the sum of the segment lengths must exactly equal R. [ND,R]
5	$\dagger N_{SEG}$	Number of blade segments used to define spanwise variable arrays, min of 1., max of 20.; sum of (E)5 plus the rotor offset (G)4*R must be equal to the rotor radius (G)2.
6	σ	Rotor area solidity (bc/R). Will calculate internally if not input [ND]
7	θ_{lequ}	Linear equivalent blade twist angle (i.e., difference between tip and center of rotation built-in angles, positive when tip angle is greater than root angle). Note, this input is the default value used when both the aerodynamic ((R)361) and structural ((R)381) built-in twist angle radial distributions have <u>all</u> zero values. (G)7 not used if non-zero values are entered; in (R)361 <u>or</u> (R)381. When (G)7 is used, (C)2 and (C)3 are also used to define span and/or flexbeam twist. (C)1 always defines the first segment to have nonzero twist for bearingless rotors. [deg]

\dagger G400 will obtain these values from the (E) block if the E159 preprocessor is invoked.

(G)			
<u>Location</u>	<u>Item</u>	<u>Description</u>	
8	c	Blade chord if chord is constant. If a non-zero value is entered here (G)8 will be used instead of the chord distribution of table (R)421. [ft]	
9	—	Intentionally blank.	
10	β_B	Built-in precone angle. An identically zero value denotes a rotor blade articulated in flapping in which case the first mode input (from E159 or direct input) will be a calculated "rigid-like" mode but will be discarded in favor of an analytic rigid flapping mode regardless of any root spring entered in (E)696; similarly, a finite nonzero value signifies a nonarticulated blade with built-in precone, see (D)1. [deg]	
11	δ_B	Built-in prelead angle. An identically zero value denotes a rotor blade articulated in lead-lag in which case the first mode input (from E159 on direct input) will be a calculated "rigid-like" mode but will be discarded in favor of an analytic rigid lead-lag mode regardless of any root spring entered in (E)716; similarly a finite nonzero value signifies a nonarticulated blade with built-in prelead, see (D)2. [deg]	
12	$\Delta\theta/\Delta\beta$	"Direct" value of pitch-flap coupling ($=\Delta\theta/\Delta\beta$). A nonzero value will suppress a calculation of this quantity from the inputted pitch-horn/push-rod geometry, see (G)17, (G)18. It will also suppress the printout of the push-rod force harmonic analysis. Since this option pitches the blade in proportion to the blade root shape, (G)12 doesn't function for flatwise cantilevered modes. A positive value is flap-up, pitch-up. [ND]	

(G)		
<u>Location</u>	<u>Item</u>	<u>Description</u>
13	$\Delta\theta/\Delta\delta$	Pitch-lead coupling forward. A positive value represents lead-pitch up. This entry is for rigid lead-lag only. The following constraints must be met to enable (G)13; (D)34 \neq 0., (G)11=0., (C)14=0., (C)15=0. See (D)35 for edgewise bending mode pitch coupling values. [ND]
14	θ_{BPR}	Built-in elevation angle (from horizontal) of push-rod attachment point, measurable when $\theta_{.75} = 0$. [deg]
15	NDEL31	The center of this segment number is the inboard attachment point of pitch input structural members (pitch horn, feathering cuff, or torque tube) to blade spar. If (G)16 $>$ 0., (G)15 will default to 1.0. For redundant torque tube analysis, (C)15=1., (G)15 should be set to (C)16.
16	NDEL30	The center of this segment number is the outboard attachment point of pitch input structural member to blade spar. Note that if this pitch input member is attached to the blade spar at a single point (cantilevered configuration as for a typical articulated blade with a pitch horn) NDEL31 and NDEL30 must both be inputted with the same appropriate value. For bearingless rotor (C)15=1. applications (G)16 serves the additional function of defining the outer limit of the flexbeam; this limit is taken as the inner boundary segment (G)16. If (C)15=1., the torque tube attaches to the center of (G)16. When (C)15=1., (G)16 must be \leq 11.
17	r_{PR}	Radial location of push-rod to pitch input structural member attachment point. (G)12 must be zero to enable use of this entry for pitch-flap coupling. [in]

(G) <u>Location</u>	<u>Item</u>	<u>Description</u>
18	Y _{10PR}	Location forward of feathering axis of pitch input point (pitch link to pitch horn point). Note that input items (G)15-(G)18 together with the input modal data provide the geometric data from which pitch-flap, and pitch-edge couplings are calculated. These calculations are bypassed if either of locations (G)16 or (G)18 are inputted identically zero. (G)12 must be set to zero to enable use of this entry for pitch-flap, pitch-edge coupling. For a redundant flexbeam analysis, (C)15=1., (G)18 must be nonzero. [in]

Input (G)19-21 used only for teetered rotor ((S)5=1.)

19	SN _{FB}	Feathering bearing segment number. Segments 1 thru SN _{FB} are fixed in torsion for the pseudo-torsion mode (but not necessarily for the elastic modes).
20	H _{USL}	Hub undersling distance. This is the distance from the teeter hinge to the hub (and rotor) apex. Positive for an undersling rotor [in]
21-50	—	Intentionally blank.

(N)	<u>Location</u>	<u>Item</u>	<u>Description</u>
1		N_{pend}	Number of blade appended pendular vibration absorbers activated per blade, maximum of 2.
2-4		—	Intentionally blank.
			<u>5-24 Data for pendular absorber No. 1</u> (see V-block for pendular absorber initial conditions)
5		r_{PAH}	Radial location of pendular absorber hinge attachment. [in]
6		$Z_{10\text{PAH}}$	Location of pendular hinge point in direction normal to the section chord (+ upward). [in]
7		l_p	Pendular absorber arm length (i.e., distance from hinge point to mass center). [in]
8		M_{PA}	Mass of pendular absorber. [lb-sec ² /ft]
9		I_p	Rotary inertia of pendular absorber about the hinge point. [lb-sec ² -ft]
10		K_p	Discrete rotary spring restraining the pendular absorber about the hinge point. [ft-lb/rad]
11		C_p	Rotary damping about hinge point. [lb-sec-ft]
12		S_p	Frictional moment about the hinge point. [lb-ft]
15-24		—	Intentionally blank.

(N)	<u>Location</u>	<u>Item</u>	<u>Description</u>
13		$\bar{\omega}_{PA}$	Integration frequency for the pendular absorber. This frequency should be close to the natural frequency of the absorber. Default value is calculated from the inputted mechanical properties. [ND]
14		θ_{oPA}	Built-in (+, nose up) pitch angle, relative to section chord line for the pendular absorber hinge axis. [deg]
25-49			Repeat of locations (N)5 through (N)24, but for the second pendular absorber. See V-block for pendular absorber initial conditions.

(R)		
<u>Location</u>	<u>Item</u>	<u>Description</u>
1-20	$\dagger \Delta \bar{x}$	Nondimensional blade segment lengths, in order from root to tip, minimum of 5, maximum of 20 values, starting from the offset location. Accuracy is generally improved if the last segment is small (≤ 0.03). [ND]
21-40	$\dagger M_i$	Mass of each blade segment. [lb-sec ² /ft]
41-60	$\dagger (EI)_F$	Flatwise bending stiffness evaluated about bending neutral axis. [lb-in ²]
61-80	$\dagger (EI)_E$	Edgewise bending stiffness evaluated about bending neutral axis. [lb-in ²]
81-100	$\dagger (I/c)_F$	Section moduli for flatwise bending, root to tip. [in ³]
101-120	$\dagger (I/c)_E$	Section moduli for edgewise bending, root to tip. [in ³]
121-140	$\dagger \bar{k}_{y10}$	Thicknesswise mass radii of gyration of blade segments about the chordwise axis, root to tip. [ND]
141-160	$\dagger \bar{k}_{z10}$	Chordwise mass radii of gyration of blade segments about an axis perpendicular to the chord line and through the elastic axis, root to tip. [ND]
161-180	$\dagger \bar{k}_A$	Tension carrying area polar radii of gyration about elastic axis, root to tip. [ND]

†G400 will obtain these values from the (E) block output from the E159 preprocessor if it is run simultaneously with G400

(R)			
<u>Location</u>	<u>Item</u>	<u>Description</u>	
181-200	\bar{y}_{10CG}	Distances from elastic axis forward in the chordwise direction to airfoil section mass centers for each segment, root to tip. [ND]	
201-220	\bar{z}_{10CG}	Distances from elastic axis "upward" in thicknesswise direction to airfoil section mass centers for each segment, root to tip (presently inactive). [ND]	
221-240	\bar{y}_{5EA}	Distances forward in in-plane (y_5) direction from the (extended) root pitch axis to the built-in elastic axis for each section (defined herein as the locus of section shear centers). [ND]	
241-260	$\Delta\bar{y}_{5EA}$	Built-in in-plane elastic axis offset change over each segment (i.e., the difference in nondimensionalized y_{5EA} between the two ends of a segment) table. This item is used to determine the chordwise (forward) structural sweep angle distribution; if all values of this distribution are input as zero, the sweep angle distribution is computed internally using numerical methods from the offset data (R)221-(R)240. [ND]	
261-280	\bar{z}_{5EA}	Distances in out-of-plane (z_5) direction from the root pitch axis to the built-in elastic axis (see above items (R)221-(R)240), positive in the normally thrusting direction. [ND]	
281-300	$\Delta\bar{z}_{5EA}$	Built-in out-of-plane elastic axis offset change per segment table. The comments made for $\Delta\bar{y}_{5EA}$ apply for this item (except that it is for the out-of-plane sweep). [ND]	

(R)		
<u>Location</u>	<u>Item</u>	<u>Description</u>
301-320	EB ₁	Torsional stiffness (to be multiplied by twist rate squared), as defined in Ref. 18. [lb-ft ⁴]
321-340	EB ₂	Torsion to edgewise elastic coupling stiffness (to be multiplied by twist rate), as defined in Ref. 18. [lb-ft ³]
341-360	τ/M	Constants relating torsional moment to torsional stress, root to tip. Default is 1 if all values are entered as zero. If the default is used, this means that what the code prints out as torsional stress is really the torsional moment. [in ⁻³]
361-380	θ_{B_a}	Aerodynamic built-in nonlinear twist (at the center of each segment) angle distribution, root to tip. Since collective angle is defined at the 75% span location, θ_{B_a} should have a zero value at 75% span. Should the structural twist angle distribution differ from θ_{B_a} , the appropriate data must be loaded into locations (R)381-(R)100; otherwise, θ_{B_a} will be used for both aerodynamic and structural applications, (G)7 is ignored if nonzero values are entered in this table. [deg]
381-400	θ_{B_s}	Structural built-in nonlinear twist angle (at center of each segment) distribution, root to tip, if different from aerodynamic twist. (G)7 is ignored if anything nonzero is entered in this table. If (R)381-400 is input then (R)361-380 must be input. See remarks above for aerodynamic built-in twist, locations (R)361-(R)380. [deg]

(R) <u>Location</u>	<u>Item</u>	<u>Description</u>
401-420	$\Delta\theta_B$	Built-in (structural) twist angle change over each segment, root to tip. (i.e., the difference in twist between the two ends of a segment). Note that this item is used directly to define the built-in twist rate distribution, θ'_{BS} ; if all values of this item are input as zero, the twist rate distribution is computed internally using numerical methods from the input twist angle distributions, locations (R)361-(R)380 or (R)381-(R)400, as appropriate. [deg]
421-440	c	Blade chord at center of each segment (use for nonconstant chord blades only). For constant chord blades, use (G)8, root to tip. Nonzero (G)8 will override this table. [ft]
441-460	$\bar{y}_{10c/4}$	Distances from elastic axis forward to airfoil quarter chord position, root to tip. [ND]
461-480	Λ_s	Aerodynamic built-in sweep angle distribution, positive aft. [deg]
481-500	c_{dsf}	Blade airfoil section spanwise <u>skin friction drag coefficient</u> , for use with the radial flow, swept airfoil option, (A)62=1. [ND]
501-520	ζ_{vse}	Distribution of edgewise nonviscous structural damping ratio. These entries provide hysteresis damping proportional to the local edgewise moment. Used when (D)30=2. [ND]

(R)

<u>Location</u>	<u>Item</u>	<u>Description</u>
521-540	(Control)	Distribution of explicit airfoil shape similarity index for each segment for use with the <u>unsteady stalled airloads</u> option, (A)64=2. A zero value denotes a default quasi-static airloads modeling whereas a value of (1. through 6.) denotes respective unsteady stalled airfoil similarity with the following sections. 0.=suppresses α -A- α_w method at this section. 1.-3.= inactive 4.= NACA 0012 5.= SC1095 6.= inactive
541-560	—	Intentionally blank.
561-580	ΔC_l	Incremental lift coefficient ΔC_l coefficient to be added to the airfoil tables. [ND]
581-600	ΔC_m	Incremental pitching moment coefficient, ΔC_m , to be added to the airfoil tables. [ND]
601-620	\bar{e}_A	Distances from reference (elastic) axis forward to neutral axis of tension carrying area for each segment, root to tip. [ND]
621-640	—	Intentionally blank.

(S)	<u>Location</u>	<u>Item</u>	<u>Description</u>
	1	CASE	Case number (can be any noninteger, for labeling purposes).
	2-4	—	Intentionally blank.
	5	(Control)	1.=teetering rotor, only if two-bladed. See (G)3, (G)19, and (G)20.
	6	(Control)	Make nonzero (1.) to print the <u>modal integration</u> constants used to a limited extent in the time-history solution.
	7	—	Intentionally blank.
	8	$\Delta\psi$	<u>Azimuth increment</u> used in the <u>numerical integration</u> of the dynamic equations. Usually, $30./F_{\max}$ where F_{\max} is the largest natural blade frequency (cycles/rev) of (D)4-(D)15. To minimize computer time (S)8 should be as large as possible. [deg]
	9	N_F	Number of "flap trials" (i.e., maximum number of rotor revolutions for which the blade time history will be computed in an attempt to obtain convergence to periodicity). If a transient response is desired for only a portion of one rotor revolution the program will compute a time history solution for any nonzero fractional N_F value (<1.) input. Normally N_F is input as an integer value. An identically zero value will cause the time-history solution to be bypassed entirely. Usually an input value in the range of 7.-10. is sufficient for helicopter applications requiring convergence to periodicity.

(S)	<u>Location</u>	<u>Item</u>	<u>Description</u>
10		ϵ_F	Flapping tolerance to within which the aeroelastic/dynamic responses must repeat on successive revolutions in order for the motion to be considered converged to periodicity. (Generally use .001 to .002). Flatwise and torsional modal displacements and velocities are compared to this tolerance. Edgewise displacements and velocities are compared to ϵ_F as well, except when the blade is cantilevered edgewise and articulated flatwise. Then for the highest edgewise mode alone, periodicity is checked using $5*\epsilon_F$. (S)10 should be set to a small nonzero value for transient analyses. [ND]
11		$\Delta\psi_{\text{print}}$	<u>Azimuth increment</u> used to present <u>printed output</u> of various pertinent aerodynamic, dynamic, and elastic load distributions as well as aeroelastic responses and stresses. This input quantity should be an integral multiple of location (S)8. [deg]
12		(Control)	Make nonzero (1.) if the total (<u>transient</u>) <u>time-history</u> is to be output (i.e., responses calculated before convergence to periodicity is obtained). If a major iteration is performed ((A)41>0) and succeeds, all of the final rotor revolutions of the final major iteration are printed. If major iterations fail, only the last rotor revolution of the last major iteration is printed. When (S)7=0 the rotor initial conditions at the initial azimuth are always printed regardless of (S)12.
13,14		—	Intentionally blank.
15		(Control)	Make greater than zero (1.) for all cases wherein <u>new blade modal data</u> are to be input. Program automatically sets this control number to (-1.) after each loading of modal data. Set (E)1195=0 when (S)15>0.

(S)	<u>Location</u>	<u>Item</u>	<u>Description</u>
	16-20	---	Intentionally blank.
	21	(Control)	Blade stress calculation method 0.=integrate forces on blade to evaluate stresses (recommended option) 1.=superpose modal deflections (strains) to evaluate stresses
	22	(Control)	Blade number for stress calculations Default is 1.
	23	(Control)	Make nonzero (1.) if the <u>modal responses</u> and <u>hub shears</u> and <u>moments</u> are to be (negative) <u>Fourier analyzed</u> and output after periodicity has been obtained. Must be set to one if coupling to F389 is desired so that flapping harmonics may be transferred to F389. See (S)52.
	24	(Control)	Input nonzero (1.) to (negative) Fourier analyze and output harmonics of flatwise and edgewise bending stresses, see (S)52.
	25	(Control)	Input nonzero (1.) to (negative) Fourier analyze and output harmonics of torsional stresses, see (S)52.
	26	$\Delta\psi_{\text{plot}}$	<u>Azimuthal increment</u> used to form the data strings for <u>plotting purposes</u> and for use with the transient spectral stability analysis (input locations (S)41 through (S)50). This input quantity should be an integral multiple of location (S)8. [deg]
	27-31	(Control)	Spanwise segment numbers for which stress data are to be saved for plotting (or TSSA) purposes (max number of values = 5.); see Ref. 17 for SA version plotting.
	32	(Control)	Unit code number of file into which the saved <u>time data strings</u> are to be stored for subsequent plot (or TSSA) purposes (default = 12.)

(S)			
<u>Location</u>	<u>Item</u>		<u>Description</u>
33	(Control)		File unit number control for interaction with the F389 variable inflow program. 0.=all inputs and outputs are via card images (file units 1 and 5). 1.=inputs from file unit 14, outputs to files 13, 16 and 23.
34	(Control)		File unit number control for use in <u>saving end conditions</u> for use as initial conditions in subsequent runs (or restarting when using the F389 code). 0.=end conditions only are output via card images (file unit 1). 1.=end conditions and restart initial conditions are input to and output from unit 26.
35	(Control)		Stress calculation suppression option. Make value equal to (0.,1.,2.) to cause suppression of stress calculations for (nonoutputted responses only, nonoutputted responses and all transient responses, all responses), respectively.
36-40	—		Intentionally blank.
41	SR		<u>Sample rate</u> for Transient Spectral Stability Analysis (TSSA) (see Ref. 17 for a discussion of this technique). Every (SR) th point in a transient time-history is saved for use in a TSSA. A zero value bypasses the TSSA.
42-44	(Control)		Channel selection for each of three available for the TSSA. The channels available are: 1-5, flatwise bending modal responses; 6-8, edgewise bending modal responses; 9,10 torsion modal responses; 11,12,13 blade tip vertical, inplane, and torsion deflections, respectively. In addition, channels 14-28 are available for stability analysis of the blade stresses as selected by input locations (S)27-31. Thus, channels 14-18 contain the five flatwise stresses, channels 19-23 contain the five edgewise stress, and channels 24-28 contain the five torsion stresses. 3 values max.

(S) <u>Location</u>	<u>Item</u>	<u>Description</u>
45	—	Intentionally blank.
46	ω_L	Lower bound of frequency band chosen for TSSA. [ND]
47	ω_U	Upper bound of frequency band chosen for TSSA. [ND]
48	(Control)	Initial estimate of percentage of total transient data used in each time displaced data sample block in TSSA. [ND]
49	(Control)	Number of transient (time displaced) Fourier coefficient calculations made to establish modal damping in TSSA; maximum value is 200.
50	N_{FREQ}	Number of desired resonant frequencies to be extracted from frequency band defined by input locations (S)46 and (S)47.
51	—	Intentionally blank.
52	(Control)	Make nonzero (1.) to analyze and print <u>harmonics of spanwise airloads</u> in negative cosine Fourier series. See (S)23-25.
53-59	—	Intentionally blank. <u>(S)60-(S)70 control calculation of hub impedance matrix and excitation vector</u>
60	m	Multiple of number of blades to determine the harmonics of hub motion and resulting loads and impedance, thus, resulting frequency, ω , would be $\omega=mb\Omega$.

(S)		
<u>Location</u>	<u>Item</u>	<u>Description</u>
61	Δa	<u>Perturbational amplitude</u> used for incrementing each of the components of <u>linear hub acceleration</u> (x,y,z) to calculate the impedance matrix numerically. [ft/sec ²]
62	$\Delta \alpha$	<u>Perturbational amplitude</u> used for incrementing each of the components of <u>angular hub acceleration</u> ($\theta_x, \theta_y, \theta_z$) to calculate the impedance matrix numerically. [rad/sec ²]
63	NSTAVB	Number of blade radial stations for which harmonics of vibratory stresses are to be included in augmented impedance matrix, maximum of 3.
64-66	ISTAVB	The (NSTAVB) radial station segment numbers for utilizing vibratory stresses in the augmented impedance matrix.
67	(Control)	Make (1.) to include <u>vibratory push-rod loads</u> in the augmented impedance matrix.
68-69	—	Intentionally blank.
70	$\Delta \theta_{HHC}$	<u>Perturbational amplitude</u> used for incrementing the components of <u>higher harmonic control</u> (locations (A)33 through (A)38) to calculate the augmented impedance matrix numerically. A zero value will retain the inputted higher harmonics of pitch control, but will suppress this portion of the impedance matrix calculation. [deg]

(S)

<u>Location</u>	<u>Item</u>	<u>Description</u>
71-98	—	Intentionally blank.
99	(Control)	<p>Location used to <u>end a case</u> or series of cases. Input (+1.) to end the Loader format data block for the case defined by the loader data and load additional cases at the conclusion of that case. Make (-1.) to end the loader data and read no further cases. In both instances the combined alpha-numeric code and word count, ZZ NN (see beginning of this section) should be either (S1) or (-1). Note: this entry must appear singly on an input card, and that card must be the last card for the case. This card image must have one of the following forms (with A1, I1, I4, F12.0 format):</p> <p>S1 99 1. S1 99 -1. -1 99 1. -1 99 -1.</p>

(V)		
<u>Location</u>	<u>Item</u>	<u>Description</u>
1-20	—	Intentionally blank.
21	ϕ_H	Hub Euler roll (helicopter) angle used to orient hub relative to gravity vector. Positive is right-hand rule rotation about the negative x_1 axis. Since Euler angles may be large, the order in which they are applied is important; in G400 the order is ψ_H , θ_H , then ϕ_H . [deg]
22	θ_H	Hub Euler pitch (helicopter) angle used to orient hub relative to gravity vector. Positive is rotation about the Y_0 axis (right-hand rule). [deg]
23	ψ_H	Hub Euler yaw (helicopter) angle used to orient hub relative to gravity vector. Positive is right-hand rule rotation about the negative z_0 axis. [deg]
24	ψ	Initial condition on rotor azimuth. [deg]
25-40	—	Intentionally blank.
41-45	$^*q_{wi}$	Initial conditions on i^{th} flatwise bending mode rates (blade no. 1); max value = 5., see (D)4. [ND]
46-48	$^*q_{vk}$	Initial conditions on k^{th} edgewise bending mode rates (blade no. 1); max value = 3., see (D)10. [ND]

(V)	<u>Location</u>	<u>Item</u>	<u>Description</u>
	49,50	$q_{\theta_j}^*$	Initial conditions on j^{th} torsion mode rates (blade no. 1); max value = 2., see (D)14. [ND]
	51	—	Intentionally blank.
	52	β^*	Articulated rigid flap rate initial condition for rotors with a rigid flapping mode (blade no. 1). [ND]
	53	δ^*	Articulated rigid lead rate initial condition for rotors with a rigid lag degree-of-freedom (blade no. 1). [ND]
	54	$p_{P_1}^* (1)$	Initial flap rate of pendular absorber number one on blade no. 1, see N-block (also see (V)94 for initial conditions on blade 2 of a teetered rotor). [ND]
	55	$p_{P_2}^* (1)$	Initial flap rate of pendular absorber number 2 on blade 1, see N-block (also see (V)95 for initial conditions on blade 2 of a teetered rotor). [ND]
	56-60	—	Intentionally blank.
	61-65	q_{w_i}	Initial conditions on i^{th} flatwise bending mode deflection (blade no. 1); max value = 5. see (D)4. [ND]
	66-68	q_{v_k}	Initial conditions on k^{th} edgewise bending mode deflections (blade no. 1); max value = 3. see (D)10. [ND]

(V)		
<u>Location</u>	<u>Item</u>	<u>Description</u>
69,70	$q_{\theta j}$	Initial conditions on j^{th} torsion mode deflections (blade no. 1); max value = 2. (blade no. 1), see (D)14. [rad]
71	—	Intentionally blank.
72	β	Articulated rigid flap angle initial condition, positive upward (i.e., in the direction of the Z_1 , axis). [rad]
73	δ	Articulated rigid lead angle, positive forward (i.e., in the direction of rotation). [rad]
74	$\beta_{P_1}^{(1)}$	Initial flap angle of pendular absorber no. 1 on blade no. 1, see N-block. [rad]
75	$\beta_{P_2}^{(1)}$	Initial flap angle of pendular absorber no. 2 on blade no. 1, see N-block. [rad]
76-80	—	Intentionally blank.
81-115		Initial conditions for blade 2 for a teetered rotor. Same format as (V)41-(V)75. See (S)2, (S)5.

III. Blade Modal Input Data

Included in this data are the radial distributions of the blade (uncoupled) flatwise, edgewise and torsion normal mode shapes and their derivatives. These quantities are either calculated internally by the (activated) E159 branch of the program (and not input as part of the input data) or are explicitly input from some previous source. This previous source can be either the output from the E159 branch itself (from some previous run), or an equivalent analysis. In either case, these data are then input in the following card image format:

```
NFM NEM NTM NSEG (4I4)
```

subsequent cards:

```
F(i) F(i+1) F(i+2) F(i+3) F(i+4) (F18.0, 4F12.0)
```

where: NFM, NEM, and NTM are, respectively, the numbers of flatwise bending, edgewise bending and torsion normal modes whose mode shapes and derivatives are to be input. See (D)1-3 to limit the number of those modes actually used to be a subset of NFM, NEM and NTM. NSEG is the number of blade spanwise stations for which the input modal data are defined. F(i) are the modal functions listed below (defined at the i'th spanwise stations). Five entries per card are made for each F function input for NSEG total entries. The modal functions must be loaded in the following order (note that the natural frequencies for the following modes are entered in locations (D)4,10,14):

γ_{w1} (NSEG values, root to tip)

γ'_{w1} (" " " " ")

γ''_{w1} •

γ_{w2} •

•

•

•

γ_{v1}

γ'_{v1}

γ''_{v1}

γ_{v2}

•

•

•

$\gamma_{\theta1}$

$\gamma'_{\theta1}$

$\gamma_{\theta2}$

•

•

•

} (NFM flatwise modes)

} (NEM edgewise modes)

} (NTM torsion modes)

IV. Variable Inflow Data

If location (A)65 of the Loader block of operational data is nonzero, the following block of variable harmonic inflow is input:

card #1: NHARML (I3)

card #2: XLAMO(I) (F14.0)

card #3: XLAMC(I,1) XLAMC(I,2)... (5F14.0)

card #3 + (NHARML/5):

XLAMS(I,1) XLAMS(I,2)... (5F14.6)

Subsequent cards repeat the pattern wherein "I", the spanwise station index, varies from 1 to NSEG. NHARML is the number of harmonics of inflow to be input, and XLAMO(i), XLAMC(i,n) and XLAMS(i,n) are, respectively the zeroth, n'th cosine and n'th sine components of harmonic inflow at the i'th radial station, wherein a positive Fourier series is assumed. The inflow is defined positive up and has the units of ft/sec.

V. Rotor Inflow Program F389 Required Data

The UTRC Prescribed Wake Rotor Inflow and Flow Field Prediction Analysis (F389) is described in detail in Reference 3. This analysis determines the induced velocities of a rotor if provided with the rotor flight condition, airfoil lift curves shapes, blade motion, and geometry. G400 can be linked to F389 to provide the data as discussed in Reference 3. The typical run sequence is to execute G400 using it's internal inflow model (constant or Glauert), while trimming to a specified flight condition. Upon G400 convergence, the airfoil data, blade data, and aeroelastic blade responses are automatically transferred through various files to F389. However, F389 requires a small amount of card image input data.

The user may optionally save the G400 aeroelastic rotor conditions for use in the second pass through G400 ((S)34>0.). F389 calculates induced velocity harmonics and writes this data to a file. Then, G400 is executed a second time retrieving that variable inflow file. If an initial condition file was generated and saved during the previous pass through G400, it can also be retrieved and used to speed convergence.

Entry (S)33 triggers G400 to save blade geometric data, flapping harmonics and airfoil data on units 16, 13 and 23 respectively for subsequent use by F389. Entry (S)34 enables G400 final conditions to be written upon completion of the first G400 pass and to be read as initial conditions at the beginning of the second G400 pass. (E)27 will trigger G400 to write modal data to unit 1 to be subsequently transferred (by JCL) into G400 as unit 5 data, during the second G400 pass. Upon completion of F389, G400 will read the resulting variable inflow harmonics if (A)65>1.

It should be emphasized that some control parameters in the G400 loader must be changed between the first and second G400 passes. The following tables, adapted from Reference 3, summarize these G400 entries.

TABLE II

LOADER DATA TRANSFERRED FROM G400 TO F389

Entry	Description	First Pass	Later Passes
(A)3	Tip Loss Factor	.97 (typically)	1.0
(A)29	Inflow Ratio	proper values	0.0
(or (A)30-32 when (A)68>0)			
(A)60	$\Delta\psi$ F389	multiple of (S)8	same
(A)65	Load Variable Inflows	0.	1.
(A)66	Use Variable Inflows	0.	1.
(S)23	Output Blade Responses	1.	1.
(S)26	Write Plot File	Unused when (S)32=0	$\Delta\psi$ optionally
(S)32	Unit No. for Plotfile	0.	as appropriate
(S)33	Mode of data transferred with F389	1.	1.
(S)34	Create/Use Initial Condition File	1. optionally	1.

As previously mentioned, F389 not only receives input from files but also a small volume of data via cards. Using the JCL of Reference 3, the data is transferred through files to F389 with no user interaction, aside from properly setting the entries in the table above. The following table summarizes the additional card data required by F389 aside from the automatically transferred data. See Reference 3 for details of card formats.

TABLE III

REQUIRED F389 DATA NOT AUTOMATICALLY
TRANSFERRED FROM G400

<u>Entry</u>	<u>Item</u>	<u>Brief Description</u>
4	DPSI	Azimuthal increment $DPSI < 15^\circ$, $360 / (\text{No. of blades} * DPSI)$ must be an integer. [deg]
23	STNS	No. of blade segments for inflow solution (not necessarily same as G400 segments) max=15 but usually set to 9.0.
24-38	RS	Radial coordinates of segment <u>centers</u> . These are very sensitive entries, see Reference ___. [ND]
88	XLINK	Set to 1.0 to couple with G400.

<u>Entry</u>	<u>Item</u>	<u>Brief Description</u>
185	XNH	Number of harmonics of induced velocity to be printed. Must not be greater than 180/DPSI. Max=12.
187	RUN	Set to 1.0
189	REV	Number of wake revolutions for hover set $\mu >$ 8.0 revs $\mu = .0 - .05$ set = 6.0 revs $\mu = .05 - .15$ set = 4.0 revs $\mu = .15 - .20$ set = 3.0 revs $\mu > .25$ set = 2.0 revs
200	TRUNC	Angle of rollup of tip vortex. TRUNC/DPSI must be an integer. Usually TRUNC=15.
202	RCORE	Tip vortex filament core radius. Usually RCORE \approx .1 x chord. RCORE must be less than .5* outer segment length. [ND]
203	RCOREI	Vortex filament core radius for filaments inboard of tip. RCOREI must be less than .5* smallest nontip segment length. [ND]
206	WLOPT	Set to 1.0 since flapping harmonics are provided by G400.
210	PUNCH	Set to -1.0 to "punch" induced axial velocities
221	DEBUGP	Set to 1.0 to trigger intermediate printout
227	HARMOP	Usually set to zero
366-380	THICK	Not used

All other F389 entries typically used are automatically transferred to F389 by G400. At the conclusion of a G400-F389-G400 sequence, the user should compare the thrust coefficient of the last G400 pass with that of the first pass. If they are significantly different, then more passes between F389 and G400 are required to achieve convergence.

VI. Multiple Case Runs

The above described data setup defines the correct ordering of required data blocks for a general G400 case, or for the G400 portion of a more complicated multi-program run stream. When multiple cases are run (while remaining within the G400 portion of the run stream) the second and subsequent cases utilize most of the data input for the first case. The following rules apply to the running of multiple cases:

1. Airfoil data is loaded only for the first case; all subsequent cases within the run use the same tabular data, if analytic data is not used.
2. Only those items within the operational generic (loader) data which are to be changed from case to case need to be input.
3. Item (S)99 of the operational data controls the running of subsequent cases; a (+1.) value causes a subsequent case to be loaded whereas a (-1.) value terminates the computer run after the current case.
4. Unless otherwise specified (by a +1. value for operational data item (S)15) the input modal array data block is used for all cases within the run.
5. Similarly, unless otherwise specified (by a +1. value for operational data item (A)65) and appropriate additional variable inflow data, the input variable inflow data block is used for all cases within the run.
6. Operational data items (S)15 and A(65) discussed above are both automatically set to zero at the conclusion of the data input for every case.
7. Terminal conditions on the blade azimuth angle, item (V)24, and on the degrees-of-freedom, items (V)41-50 and (V)51-70, for any case are carried over as initial conditions on these quantities for the subsequent case. Thus, for some applications, e.g., investigations of unstable responses, it would be appropriate to reinitialize these items on the subsequent cases.

When solution flow leaves the G400 portion of a complex run stream, the ability to carry over terminal conditions (as initial conditions for a subsequent case) and/or any other quantities associated with trim is lost. However, a need still exists for preserving these initial conditions for subsequent reentries to the G400 portions of the run stream. As per loader locations (S)34 these initial conditions are written to and read from the file indicated in this input location.

VII. Initial Conditions

The initial conditions for a G400 run can be specified via the loader block input or by triggering the code to read the initial conditions from a file, which was created from a previous run. If the initial conditions are read from a file they override values input by the user in the same locations in the loader block. End conditions (to be used as initial conditions for a subsequent run) are also output by the ENDCON subroutine onto card images in the punch file (unit 1) in loader block format. The user could merge this data with the other loader block data to restart a run. Alternately, the data can be transferred via file (unit 26) as activated by (S)34) eliminating the need to modify the basic loader data file. This can be useful for cases where iteration is done between codes in one job stream (i.e., F389). This separate file is written onto unit 26 by the RESETQ subroutine and contains a string of data stored with an (8E15.6) format. The following list indicates what data are stored on this file.

(A)21-38, (A)65, (A)66, (A)351-399, (A)60, (S)33, (V)21-120

Unsteady Stalled Parameters Needed for Restart

It should be noted that a separate file is used to transfer initial and end conditions for use with the unsteady stalled aerodynamic modeling ((A)64=2).

The subroutine SETVAL saves the end conditions on inflow angle and components of the unsteady decay parameter (α_w) on the unit specified in (A)305. The file is written as 5F10.5 and contains the following information:

((PHISAV(I,J), J=1,3), XALFW(I), YALFW(I), I=1,NSEG)

VIII. Input/Output File Unit Numbers

The following list indicates which logical unit numbers are used by G400 for the input and output of data. No attempt is made here to specify how the job control language (JCL) is to be set up for the execution of G400. The user must make sure that the appropriate units are available to G400 for input and output.

<u>Unit</u>	<u>Input/Output</u>	<u>Relates to</u>	<u>Function</u>
5	Input	(A)63,(S)15,(E)1159	Obtain airfoil data, loader block data, mode shape data
14	Input	(A)65,(S)33	Input variable inflow data
26	Input/Output	(S)34	Input initial conditions from file. Output end conditions to same unit
(A)305*	Input/Output	(A)305	Input initial conditions for unsteady aero calculations. Output end conditions for same to the same unit
1	Output	(E)27,(E)1195	Output E159 mode shapes and ENDCON generated end conditions to the punch file (unit 1)
(S)32	Output	(S)32,(S)26	Save time-histories for plotting (or TSSA) purposes. Default is file unit 12.
6	Output	---	All printed output

*Care must be exercised if the user wants to save initial conditions files, since the code will overwrite the initial conditions with the end conditions (on the same file).

G400 Data File Output

The G400 program outputs to a number of data files for use with other programs and for restart purposes. They are listed here for completeness. Refer to an above subsection for the logical unit numbers which need to be defined in the job control language for creation of this output.

1. End conditions at the completion of a time history analysis (normal completion only). The end conditions are written to the same file used to read in initial conditions (written in RESETQ subroutine). This file can be read into a subsequent run without modification of the input loader block data.
2. End conditions, for unsteady aero calculations, at the completion of a time history analysis (normal completion only). This file is written only if (A)64=2. The end conditions are written to the same file used to read in initial conditions.
3. Mode shapes generated by E159 and end conditions at the completion of a time history analysis (normal completion only). The purpose of these end conditions is the same as that for item 1. The end conditions here are written on card images in loader block format (written by the ENDCON subroutine). To use these conditions, the card images must be merged into the input loader block data of a subsequent run.
4. Plot file containing time history information.
5. Rotor impedance matrix.
6. Explicit W1 velocity distributions for F389.
7. Blade data for F389.
8. Airfoil data for F389.

Specific I/O units for this purpose are given below:

<u>Unit</u>	<u>Input/Output</u>	<u>Relates to</u>	<u>Function</u>
11	Output	S(60)	Output Rotor Impedance Matrices
13	Output	(S)33	Output explicit W1 velocity distributions for F389
16	Output	(S)23,(S)33	Output blade data for F389
23	Output	(S)33	Output airfoil data for F389

Recommended Values

(A)305 = 15

(S)32 = 12

IX. General Information to Facilitate Operation of Program and Improve Efficiency

Aside from the details of the aeroelastic modeling which are covered in previous sections, and in references 1, 2 and 7, additional considerations exist in maximizing both the efficiency and accuracy of the implemented numerical solutions of the dynamic equations. This subsection presents material concerning these numerical methods, and more importantly, ways of dealing with them by proper input procedures.

Blade Segment Selection

Two decisions must be made in selecting a proper distribution of blade segment lengths: how many segments should be used, and where segments should be either sparsely or densely packed. The G400 code incorporates a maximum number of twenty segments, up from the maximum of fifteen offered in the earlier versions of G400 (references 1 and 2). Capability to use twenty segments should not be confused with a general need to use all this capability in every application.

Various criteria can be used to guide the program user in making an efficient blade breakup selection:

1. Generally any one segment should not exceed 15 percent of the span. This criterion is subjective in that it is based on accumulated user experience.
2. The segment density should be greatest at the innermost portion of the blade for the E159 part of the program (uncoupled mode calculations) and at outermost portion for the G400 proper part of the program. The requirement for greater blade detail at the root blade portion in the E159 calculation stems from the fact that here at least for hingeless rotors the elastic strain energy is most heavily concentrated and has the most variability. It follows that accurate modeling of the equivalent springs used in E159 is enhanced by a finer breakup here. The requirement for greater blade detail in the blade tip portion in the G400 proper calculations stems from the concentration here of inertial and aerodynamic loadings. The aerodynamic loads are especially subject to greatest variability at the tip sections.
3. The segment density should be also guided by the specific details of the blade in question. Any blade portion which has locally concentrated properties should have greater segment density. Also, segment boundaries should be selected to conform to the geometry inherent in the blade planform.

4. With some initial extra effort in the preparatory stage, an efficient breakup can be used wherein the need for a dense breakup at any portion of the blade can be relaxed in the G400 proper portion of the code. This effort consists of first running the E159 preprocessor separately with a dense breakup to maximize the accuracies of the natural frequencies. Then, various inboard segments are selectively eliminated or modified from the mode shapes and other distributed data before subsequent input to G400 proper part of the code. In this manner the elastic modeling accuracy is preserved (through retention of the accurate natural frequencies) while reducing the all over segment count used in the more expensive G400 proper aeroelastic calculation.

Input of Differentiated Data

The coordinate transformations formulated for G400 require two sets of spanwise differentiated data which must be explicitly gleaned from the geometry of the blade design: structural twist rate and structural sweep rate. Although the G400 code provides for internal numerical differentiations of these quantities, actual designs often include abrupt spanwise variation which cannot be so differentiated efficiently. Consequently, the G400 input list includes a direct input of rate related data, and use of this input is generally recommended for increased accuracy.

The method selected for input of rate data on these items is based on the assumption that the rates are constant over their respective segment lengths. To make the input numbers more meaningful and to minimize data preparation calculations by the user, the rate data are input as respective changes in the variables (either twist angle and/or elastic axis offset) over each segment length. Thus, the actual derivatives are calculated internally by division by each segment length and the user is freed of this chore. One advantage of this input format is that the resulting numerical values input provide quick checks of the data. All such changes can be easily summed to yield the integrated change over the whole blade, for comparison with input root to tip values of the variables themselves.

Temporal Numerical Integration

As discussed in reference 1, temporal integration of the higher differentiated response variables to obtain the lower ones is achieved in the G400 program using a variant of the Adams integration algorithm. The selected algorithm is defined by means of the azimuthal integration step size, $\Delta\psi$, and the integration frequency, $\bar{\omega}$.

The integration step size should be an integral divisor of 360; a proper choice depends on the maximum coupled frequency inherent in the various aero-elastic responses. A reasonable upper limit for $\Delta\psi$ is 30 divided by the maximum such frequency in per rev. Values of $\Delta\psi$ greater than this upper limit will compromise the integration accuracy and, for sufficiently large values, will cause the computed responses to develop "numerical" instabilities. As a corollary, a check on any response which is predicted to be unstable by the analysis, is to rerun the case with a reduced integration step size to test for the possibility of the unstable response being merely a numerical instability.

For each response degree-of-freedom a different integration frequency, $\bar{\omega}$, is used in the integration algorithm; this frequency is, for each of the elastic modes, the respective input natural frequencies (locations (D)4-8, (D)10-12, and (D)14,15). In addition to defining modal stiffnesses and integration frequencies, the input frequencies serve yet another purpose. As noted above, the proper value of integration step size, $\Delta\psi$, varies inversely with the maximum modal frequency. Thus, run times (caused by reduced step size) will significantly increase as any one modal frequency increases. Since any degree-of-freedom exhibiting a large natural frequency tends to respond quasi-statically, i.e., as if the acceleration (**q) term were negligible, a reasonable approximation to the response calculation is to avoid the numerical integration of the **q term entirely and treat the response quasi-statically. This option can be invoked for any such high frequency mode by input of a negative frequency; a negative sign will not affect the proper usage of the frequency in the calculation of the dynamic equations. Note that this optional response calculation can be invoked singly or in combination for any of the elastic modal responses (negative values in any of locations (D)4-8, 10-12, and 14-15).

State Vector Initial Conditions

For many applications useful results can be obtained from the G400 code with little or no attention paid to the input of initial conditions (all elements of the (V) Loader block and locations 30-32 of the (A) Loader block). Two situations exist, however, wherein appropriate and accurate initial conditions should be input to maximize the usefulness of the analysis.

Calibrated Excitations of Transients

For those cases wherein aeroelastic instabilities are to be investigated using the time-history solution, the initial conditions provide a convenient method for exciting the transient responses in an unambiguous and calibrated manner. This can be accomplished by selecting a critical degree-of-freedom and assigning to it a rate initial condition ((V) loader block locations 41-50) equal to its (nondimensional) natural frequency times an appropriate amplitude (in radians).

Restart Calculations

For some cases involving time-history calculations, insufficient rotor revolutions may have been selected to define the dynamic phenomenon under study, and a continuation of the case is required. To this end, use should be made of the built-in feature of the G400 code to record end conditions on the control angles, components of induced velocity, and the blade deflection state vector. The code provides for automatic output of punched card images at the end of the run and, if Loader location (S)34 is input with a nonzero value for file unit number, to that file as well. Note, however, that these end conditions will be so recorded only if the run makes a normal completion. Premature aborting of the run because of excessive response amplitudes, for example, will suppress this output. Finally, once the end conditions are recorded they can then be used as initial conditions for subsequent runs.

Hub Force and Moment Trim

Operation of the trim or major iteration feature of the program is controlled by input locations (A)41 through (A)43 and (A)45 through (A)52. The main control for the major iteration is location (A)41, the number of major iterations, N_{MI} . A zero value causes the major iteration feature to be completely deactivated. On the basis of past usage, a reasonable range for this input appears to be from 5 to 10, depending on the tightness of the convergence tolerances selected and the "goodness" of the initial guesses on the control parameters. Convergence of the major iteration is adversely affected by any lack of convergence of the responses to periodicity within each trim iteration and by incursion of the rotor into a significantly stalled flight regime. Should a major iteration fail to converge within any one run the last used control angles and initial conditions on response variables are generally available in output card image form and/or partially in the output printed records of each major iteration for use in subsequent major iterations.

The trim iteration is operationally flexible as to what hub loads it will drive to requested values. Generally, the various requested hub loads, lift, propulsive force, pitching and rolling moment are activated in turn by specifying nonzero values for each of their respective tolerances. Specifically, the following table describes the optional combinations of hub loads and rotor shaft angle available with the G400PA trim capability.

TABLE IV

SUMMARY OF OPTIONAL BASIC TRIM COMBINATIONS

Option	Lift	Prop. Force	Pitch. Moment	Roll Moment	$\theta .75R$	A_{1s}	B_{1s}	α_s
1	S	U	U	U	V	F	F	S, (V)
2	S	S	U	U	V	F	F	V
3	U	U	S	S	F	V	V	S, (V)
4	S	U	S	S	V	V	V	S, (V)
5	S	S	S	S	V	V	V	V
6	U	U	S	U	F	V	F	S, (V)
7	S	U	S	U	V	V	F	S, (V)
8	S	S	S	U	V	V	F	V

where:

- F: Control parameter kept fixed
- V: Control parameter varied
- S: Trim parameter specified and trimmed to
- U: Trim parameter unspecified and ignored

PROGRAM OUTPUT DESCRIPTION

The complete printed output generated by the G400PA program can be classified into the following six major categories:

- I. Listing of Input Data
- II. Uncoupled Blade Mode Calculation
- III. Parameters Calculated from the Input Data
- IV. Results of Time-History Solution
- V. Impedance Matrices
- VI. Transient Spectral Stability Analysis

This section describes the pertinent output associated with each of these categories. While output will always be generated for the first, third and fourth categories, output for the remaining categories depends upon the options selected.

Listing of Input Airfoil Data

A series of pages listing the airfoil data will be generated providing that: (1) the user inputs a zero (0.) in the "A" array location 63, thereby revoking the static airfoil option, (2) the user specifies no negative values in the first airfoil data card image, and (3) the user provides the static airfoil data as input. A negative value or values on the first card would imply that the optional suppression of the airfoil data was desired.

If static airfoil data is input, then a listing of this data will be output for c_l , c_d , and $c_{mc}/4$ with the formats shown in sample pages 1, 2, and 3. First, the aerodynamic section coefficient type is appropriately identified with a label. Next, if multiple spanwise airfoil data is input, the blade radial station at which the data is defined is output. This value is nondimensional with respect to rotor radius. If a single airfoil is to be used for all spanwise locations, a 1.0 is output in place of the blade radial station to signify that the data can be used for the entire blade span.

The remaining airfoil data is presented as 12 columns of information (some of which may be zeros). The output closely follows the input format description described earlier. Each column represents data at one Mach number. Within each column, the first line gives the number of angle-of-attack/aerodynamic coefficient pairs. The second line in the column is the Mach number, and the ensuing

line pairs are the angle-of-attack/aerodynamic coefficient pairs presented vertically. The angles-of-attack are in degrees, and the aerodynamic coefficients are dimensionless. As soon as the specified number of pairs of data have been listed vertically, one may encounter a final pair of static stall angle/lift curve slope data values, providing the unsteady airloads option, (A)64 is invoked with a value of 2. The static stall angle is in degrees, and the lift curve slope is in per-degree units (at zero angle-of-attack).

If the maximum of 34 pairs of data values are not entered, the remainder of the column will consist of zeros. Similarly, if the maximum of 12 Mach numbers are not entered, the remainder of the column will consist of zeros.

The above format is repeated for all the blade airfoil stations (at most 5 values of XCEN), and for all 3 aerodynamic coefficient types (CL, CD, and CM). The only exception to the above format is that in the CD table, there will never be the final pair of static stall angle/aerodynamic coefficient curve slope data values which sometimes do occur in the CL and CM tables.

Results of Uncoupled Blade Mode Calculation Processor E159

A requirement for the use of the basic G400 analysis is a set of uncoupled blade modal data consisting primarily of natural frequencies and normal mode shapes (and their spanwise derivatives). Since the initial development of the G400 code (reference ___), the United Technologies Corporation program E159 has been added to the G400 code in the form of a preprocessor. Since the output from the E159 preprocessor impacts on the Loader data used in the G400 proper portion of the code, E159 must be run before the output of the Loader data. Hence, this output category precedes the output of the remaining input data.

The first page of output from the E159 portion of the program follows the format of sample page 4. The first line consists of a statement of the case number for the output generated by the E159 branch of the program (see entry (E)2000). This is followed by a line stating the total number of flatwise, edgewise, and torsional frequencies generated by the E159 portion of the code. Next, the modulus of elasticity in lb/in^2 is presented.

The principal output on the remainder of this page consists of six pairs of columns defining the distributions of pertinent elasto-mechanic properties starting at the blade root and progressing outward to the blade tip. These distributions of weight (lbs/in.), area radius of gyration of the tension carrying (spar) portion of the blade (in.), torsional inertia (lb-sec^2), edgewise

and flatwise area moments of inertia (in^4), and St. Venant torsion stiffness (lb-in^2) echo the data input in the (E)101-150, (E)888-1037, (E)1039-1188, (E)454-653, (E)253-452, and (E)737-886 locations, respectively. At the bottoms of the columns representing distance out along the blade (columns 2, 4, 6, 8, 10, and 12) are presented summations at the spanwise increments plus the offset. These summations are presented to show that indeed the distribution extends slightly beyond the blade radius, to preclude numerical round-off.

Finally, on sample page 4 is a line which defines at which segment the torsion stiffness, GJ, becomes finite (location (E)1191) and at what segment the push-rod is located (if present).

Sample page 5 shows the second page of output from E159. First, the rotor tip speed (ft/sec), rotor radius (ft), and offset distance (nondimensionalized by rotor radius) are printed. Then the rotor speed in RPM is presented. Next, the frequency scan intervals for flatwise and edgewise bending frequency iteration, and for torsion frequency iteration, are printed (rad/sec). Also, on the same line is an item called the frequency nondimensionalization scale factor. This has the units of $1/\text{sec}^2$ and is either a duplicate of location (E)654 (if present and nonzero) or is internally computed as rotor tip speed (divided by rotor radius) squared. Finally, in this line is a statement of whether the root is modeled as cantilevered (rigid), or as possessing a spring restraint (flexible) in which case the torsion root spring rate is then printed (in-lb/rad). Input items (E)1189 and (E)1190 define the root flexibility.

The lower portion of sample page 5 consists of 4 columns of information. The first column represents the selected blade segment breakup (locations (E)4-(E)23) nondimensionalized by blade radius. However, an additional first item in this column is presented if a cantilever root boundary condition is desired. If locations (E)696 and (E)716 are both nonzero, an extra nondimensional first segment length of .0001 is internally added to the blade, to make the total number of E159 segments greater than the number of G400 proper segments by 1.

The second column represents the lumped equivalent masses ($\text{lb-sec}^2/\text{ft}$) at each of the selected radial stations. If a cantilever root is assumed, as defined by input items (E)696 and (E)716, the mass at the first "segment" is defined as 0.0. The remainder of the masses are either computed internally based upon the weight distribution table inputted in locations (E)101-150, or explicitly from the discrete incremental masses which are inputted in locations (E)676-695. These masses are located at the blade segment centers.

The third and fourth columns represent the effective flatwise and edgewise elastic coefficients, or spring rates (ft-lbs/rad). These values are computed

using the inputted distributions of flatwise and edgewise moments of inertia (locations (E)253-(E)653) and the modulus of elasticity. The values may be replaced with input explicit flatwise and edgewise hinge springs if any of locations (E)696-735 are made nonzero. The elastic coefficients are used only internally to calculate the natural modes.

At the bottom of sample page 5 is a summation of the nondimensional spanwise intervals plus the nondimensional offset. If this sum is not within the range of 0.99 to 1.01, a message will appear: "sum not equal to one." This is to ensure that the number of specified blade segments actually cover the blade radius specified, with some tolerance for round-off error.

Sample page 6 consists of 5 columns of data. The first column again represents the blade segment breakup nondimensionalized by blade radius, without the extra first "segment." Columns 2 and 4 display the flatwise and edgewise section bending stiffnesses (lb-in²/in.), as determined from the input area moments of inertia and the modulus of elasticity, as well as from the radial locations specified in the distribution tables. Columns 3 and 5 show the flatwise and edgewise section bending moduli (in³) as input in locations (E)28-67.

Sample page 7 contains 4 columns of torsionally relevant elastic information. The first column is the blade segment breakup nondimensionalized by blade radius including the extra first segment, if present. The next two columns are distributions of torsion stiffnesses, (lb-in²/in), determined from the radial distributions, the inputted torsion stiffnesses (locations (E)737-(E)886), and (for GJEFF) from the inputted area radii of gyration of the tension carrying blade portions (locations (E)888-1037) and from appropriate nondimensionalizing factors. Actually, GJEFF reflects "centrifugal" torsional stiffening and is formed from a combination of terms used in the torsion loading equation:

$$GJEFF = GJ + \bar{k}_A^2 T$$

where GJ is the torsion stiffness, k_A is the spar radius of gyration, and T is the local tension in the blade. Finally, a column representing the spar radius of gyration (nondimensionalized by rotor radius) is output. This is determined as the square root of the difference between GJEFF and GJ, divided by T:

$$KA/R = \sqrt{(GJEFF-GJ)/T}$$

Sample Page 8 begins the output of the actual calculations for the bending modes. The format of Sample Page 8 is used for both flatwise and edgewise modes

and the type of modal data being output is clearly indicated. The first two rows of Sample Page 8 give the natural frequencies of the flatwise modes in increasing order. The units of these frequencies, as given in the first row, are either in rad/sec or per rotor rev depending on whether the input rotor speed is zero or nonzero, respectively. The second row values are always the same respective frequencies, but in units of Hz (cycles/sec). The twelve columns which follow on this sample page consist first of descriptors for the selected blade radial stations. The second column (labeled X) gives the nondimensional spanwise stations as measured from the axis of rotation, whereas the third column (labeled XFH) gives the similar information, but instead from the offset point. The remaining three groups of three columns give, for up to three modes, the mode shape and the 1st and 2nd mode shape spanwise derivative information, as indicated.

The mode shapes are determined from the E159 eigensolution preprocessor, using the method of determinate iteration. These uncoupled beam bending vibration modes are normalized with respect to the blade tip. For all applications except the semi-articulated or articulated rotors, the mode shapes and derivatives are calculated at the additional first "segment" (N=0) as well as at the remaining the radial stations. The mode shapes and derivatives are provided at the additional first segment to define a more refined blade breakup at the root for cantilever applications.

The remaining three columns of output at the bottom of the sample page give, for each respective mode, various summations of internally calculated modal integration constants (integration over the blade span). These E159 integration constants are provided as a "back of the envelope" list of terms which could be used in various simplified, linearized aeromechanical dynamics calculations. G refers to the respective mode shape array given directly above each of these three lower columns. The integrals for the flatwise modes are respectively:

$\int_m \gamma_{w_i} dr$ (coupling of the flatwise mode with hub translation),

$\int_m \gamma_{w_i} r dr$ (coupling of the flatwise mode with hub rotation or rigid flapping),

$\int_m \gamma_{w_i}^2 dr$ (generalized mass of the flatwise mode),

$$\left. \begin{aligned}
 & \int \gamma_{wi} \, dr \\
 & \int \gamma_{wi} \, r dr \\
 & \int \gamma_{wi} \, r^2 dr \\
 & \int \gamma_{wi} \, r^3 dr \\
 & \int \gamma_{wi} \, r^4 dr \\
 & \int \gamma_{wi} \, r^5 dr
 \end{aligned} \right\} \text{(simplified aerodynamic integrations terms),}$$

$$\int \gamma_{wi}^2 \, r dr \quad \text{(aerodynamic damping term),}$$

and

$$\int \gamma_{wi}^2 \, r^2 dr \quad \text{(used in aerodynamic terms).}$$

The units of the first three integrals are lb-sec²/ft², and the remainder of the units are nondimensional. These integrals are not used in the G400 proper portion of the code but are potentially useful in simplified aeromechanical analyses (other than G400).

Sample Page 9 presents 5 columns of torsionally relevant inertial information, beginning again with the blade segment breakup including the extra first segment, if present. The second column (labeled IXX) presents the section polar torsion inertia (in-lb-sec²), which is the sum of the chordwise and thicknesswise mass moments of inertia. These values are determined from the spanwise locations and from the input torsional inertia table (locations (E)1039-(E)1188). The third column presents the difference between the chordwise and thicknesswise mass moments of inertia, ΔIXX (in-lb-sec²). This difference of inertia distribution is the one which determines the so-called "propeller moment" torsional stiffening effect. The remaining columns are the thicknesswise and chordwise mass radius of gyration distributions which, along with the output lumped equivalent masses, produce the IXX and ΔIXX values. The thicknesswise mass radii of gyration (in) are input in locations (E)1541-(E)1560.

Sample Page 10 summarizes modal results for the torsion modes. As with bending mode output, the first two rows of Sample Page 10 give the modal natural frequencies first in either rad/sec or per rotor rev, and then in the second row, cycles/sec. The remaining columns follow closely the format discussed above for

the bending modes, except that only the first spanwise derivative is given for each mode. The second derivatives of the torsion mode shapes are not provided because they are not used in the torsion equation. (The flatwise and edgewise bending equations on the other hand require both first and second derivatives of the flatwise and edgewise mode shapes). Therefore, up to four torsion mode shapes and first derivatives may be presented. No modal integrations (summations over blade span) are performed for the torsion modes.

Listing of Remaining Input Data

Sample page 11 illustrates a listing of the variable inflow input originating from a data file prepared by the F389 code. The first group of information on this page shows the harmonic components, at each spanwise station, of the coefficients VLAMO, VLAMA, and VLAMB which are superimposed to yield the inflow LAMBDA. The second group of information shows the azimuthal variation of the inflow LAMBDA at each of the blade segments. The inflow is defined positive up, has the units of ft/sec, and a conventional positive Fourier series representation is used.

INPUTED VARIABLE INFLOW DISTRIBUTIONS (OUTPUT FROM PROGRAM F389 OR EQUIVALENT), FPS

HARMONIC COEFFICIENTS: $LAMBDA(X(J),PSI) = RMLAMB + (VLAMB(J) + \text{SUM}(VLAMB(J,N) \cdot \text{COS}(N \cdot \text{PSI}) + VLAMB(J,N) \cdot \text{SIN}(N \cdot \text{PSI})) / \text{OMEGA-R}$

SEG. N. J =	1	2	3	4	5	6	7	8	9	10	11	12	13	14	15
VLAMB 0	AX.XX	AX.XX	AA.YA	XX.XX	AX.XX	XX.VX	XX.XX	XX.XX	XX.XX	AA.XX	AX.XX	AX.XX	AX.XX	XX.XX	AX.VY
VLAMB 1	AX.XX	AX.XX	AA.YA	XX.XX	AX.VA	XX.VX	XX.XX	XX.XX	XX.XX	AX.XX	AX.XX	AX.XX	AA.XX	XX.XX	AX.VY
VLAMB 2	AX.XX	AX.XX	AA.YA	XX.XX	AX.VA	XX.VX	XX.XX	XX.XX	XX.XX	AX.XX	AX.XX	AX.XX	AA.XX	XX.XX	AX.VY
VLAMB 3	AX.XX	AX.XX	AA.YA	XX.XX	AX.VA	XX.VX	XX.XX	XX.XX	XX.XX	AX.XX	AX.XX	AX.XX	AA.XX	XX.XX	AX.VY
VLAMB 4	AX.XX	AX.XX	AA.YA	XX.XX	AX.VA	XX.VX	XX.XX	XX.XX	XX.XX	AX.XX	AX.XX	AX.XX	AA.XX	XX.XX	AX.VY
VLAMB 5	AX.XX	AX.XX	AA.YA	XX.XX	AX.VA	XX.VX	XX.XX	XX.XX	XX.XX	AX.XX	AX.XX	AX.XX	AA.XX	XX.XX	AX.VY
VLAMB N	AX.XX	AX.XX	AA.YA	XX.XX	AX.VA	XX.VX	XX.XX	XX.XX	XX.XX	AX.XX	AX.XX	AX.XX	AA.XX	XX.XX	AX.VY

AZIMUTHAL VARIATION

SEG. N. J =	1	2	3	4	5	6	7	8	9	10	11	12	13	14	15
PSI 0.	AX.XX	AA.XX	AA.XX	XX.XX	AA.VA	XX.VX	XX.XX	XX.XX	XX.XX	AA.XX	AX.XX	AX.XX	AX.VA	XX.XX	AX.VA
XX.	AX.XX	AA.XX	AA.XX	XX.XX	AX.VA	XX.VX	XX.XX	XX.XX	XX.XX	AA.XX	AA.XX	AX.XX	AA.XX	XX.XX	AX.VA
XX.	AX.XX	AA.XX	AA.YA	XX.XX	AX.VA	XX.VX	XX.XX	XX.XX	XX.XX	AA.XX	AA.XX	AX.XX	AA.XX	XX.XX	AX.VA
XX.	AX.XX	AA.XX	AA.YA	XX.XX	AX.VA	XX.VX	XX.XX	XX.XX	XX.XX	AA.XX	AA.XX	AX.XX	AA.XX	XX.XX	AX.VA
XX.	AX.XX	AA.XX	AA.YA	XX.XX	AX.VA	XX.VX	XX.XX	XX.XX	XX.XX	AA.XX	AA.XX	AX.XX	AA.XX	XX.XX	AX.VA
XX.	AX.XX	AA.XX	AA.YA	XX.XX	AX.VA	XX.VX	XX.XX	XX.XX	XX.XX	AA.XX	AA.XX	AX.XX	AA.XX	XX.XX	AX.VA
XX.	AX.XX	AA.XX	AA.YA	XX.XX	AX.VA	XX.VX	XX.XX	XX.XX	XX.XX	AA.XX	AA.XX	AX.XX	AA.XX	XX.XX	AX.VA

Parameters Calculated from the Input Data

Sample Pages 12, 13, 14, and 15 list a variety of intermediate parameter calculations which apply to the bearingless, semi-articulated, and teetered rotors. If a bearingless redundant rotor analysis is specified by setting (C)15=1., sample pages 12, 13 and 14 appear. For a cantilevered bearingless analysis enabled by setting (C)14=1., sample page 15 is printed. If semi-articulated rotors are input, only sample page 14 is produced. The semi-articulated (or fully articulated) application is specified by locations (G)10 and (G)11, and by locations (V)52, (V)53, (V)72, and (V)73. The teetered rotor applications are activated primarily by input locations (G)3, (G)19-(G)21, (A)22, and (S)5.

Sample page 12 presents the matrices and vectors used to define, respectively, the elastic bending characteristics of the torque tube and the inboard (snubber) end vertical deflection of the torque tube. The second and third lines of this page show, in equation form, the relationships of the various matrices and vectors to the total bending stiffness matrix (FDEFLL) and the total inboard deflection vector (Z5I). In the equations presented, TTHO (radians) represents the total blade pitch angle at the 75 percent span. All the results outputted for FDEFLL and Z5I are nondimensional.

The first matrix presented on this page consists of 8 rows and 7 columns of information with regard to the first component (FDEFLO) of the quadratic representation of the stiffness matrix. The rows represent, at the torque tube respectively; in-plane shear loads in the "5" coordinate system at the snubber and juncture points, moment out of the plane defined by the torque tube section at the juncture, in-plane slope in the "5" system at the snubber, out-of-plane shear loads in the "5" system at the snubber and juncture points, moment in the plane defined by the torque tube section at the juncture, and out-of-plane slope in the "5" system at the snubber. The columns represent, at the flexbeam respectively; in-plane deflections at the snubber and juncture points, in-plane slope at the juncture, out-of-plane deflections at the snubber and juncture, out-of-plane slope at the juncture, and the force of the push-rod, all in the "5" coordinate system.

The next row defines the first component (Z5I0) of the quadratic representation of the inboard torque tube deflection vector. Its seven values represent the same items as did the columns making up the stiffness matrix. These matrices and vectors are repeated two more times, to define FDEFLL1, Z5I1, FDEFLL2; and Z5I2.

Finally, at the bottom of this page are evaluations of FDEFLL and Z5I, using the quadratic representations, at a pitch angle equal to the inputted collective angle (location (A)28). First, the collective angle is printed, in degrees.

TORQUE-TUBE BENDING STIFFNESS MATRICES AND SNUBBER ATTACHMENT POINT DEFLECTION VECTORS:

$$FDEFL(I,J) = FDEFLO(I,J) + TTHO*(FDEF1(I,J) + TTHO*FDEF2(I,J))$$

$$Z5I(J) = Z5I0(J) + TTHO*(Z5I1(J) + TTHO*Z5I2(J))$$

FDEFLO(I,J):	X.XXXXX	X.XXXXX	X.XXXXX	X.XXXXX	X.XXXXX	X.XXXXX	X.XXXXX
	X.XXXXX	X.XXXXX	X.XXXXX	X.XXXXX	X.XXXXX	X.XXXXX	X.XXXXX
	X.XXXXX	X.XXXXX	X.XXXXX	X.XXXXX	X.XXXXX	X.XXXXX	X.XXXXX
	X.XXXXX	X.XXXXX	X.XXXXX	X.XXXXX	X.XXXXX	X.XXXXX	X.XXXXX
	X.XXXXX	X.XXXXX	X.XXXXX	X.XXXXX	X.XXXXX	X.XXXXX	X.XXXXX
	X.XXXXX	X.XXXXX	X.XXXXX	X.XXXXX	X.XXXXX	X.XXXXX	X.XXXXX
	X.XXXXX	X.XXXXX	X.XXXXX	X.XXXXX	X.XXXXX	X.XXXXX	X.XXXXX
	X.XXXXX	X.XXXXX	X.XXXXX	X.XXXXX	X.XXXXX	X.XXXXX	X.XXXXX
Z5I0(J):	X.XXXXX	X.XXXXX	X.XXXXX	X.XXXXX	X.XXXXX	X.XXXXX	X.XXXXX
FDEF1(I,J):	X.XXXXX	X.XXXXX	X.XXXXX	X.XXXXX	X.XXXXX	X.XXXXX	X.XXXXX
	X.XXXXX	X.XXXXX	X.XXXXX	X.XXXXX	X.XXXXX	X.XXXXX	X.XXXXX
	X.XXXXX	X.XXXXX	X.XXXXX	X.XXXXX	X.XXXXX	X.XXXXX	X.XXXXX
	X.XXXXX	X.XXXXX	X.XXXXX	X.XXXXX	X.XXXXX	X.XXXXX	X.XXXXX
	X.XXXXX	X.XXXXX	X.XXXXX	X.XXXXX	X.XXXXX	X.XXXXX	X.XXXXX
	X.XXXXX	X.XXXXX	X.XXXXX	X.XXXXX	X.XXXXX	X.XXXXX	X.XXXXX
	X.XXXXX	X.XXXXX	X.XXXXX	X.XXXXX	X.XXXXX	X.XXXXX	X.XXXXX
	X.XXXXX	X.XXXXX	X.XXXXX	X.XXXXX	X.XXXXX	X.XXXXX	X.XXXXX
	X.XXXXX	X.XXXXX	X.XXXXX	X.XXXXX	X.XXXXX	X.XXXXX	X.XXXXX
Z5I1(J):	X.XXXXX	X.XXXXX	X.XXXXX	X.XXXXX	X.XXXXX	X.XXXXX	X.XXXXX
FDEF2(I,J):	X.XXXXX	X.XXXXX	X.XXXXX	X.XXXXX	X.XXXXX	X.XXXXX	X.XXXXX
	X.XXXXX	X.XXXXX	X.XXXXX	X.XXXXX	X.XXXXX	X.XXXXX	X.XXXXX
	X.XXXXX	X.XXXXX	X.XXXXX	X.XXXXX	X.XXXXX	X.XXXXX	X.XXXXX
	X.XXXXX	X.XXXXX	X.XXXXX	X.XXXXX	X.XXXXX	X.XXXXX	X.XXXXX
	X.XXXXX	X.XXXXX	X.XXXXX	X.XXXXX	X.XXXXX	X.XXXXX	X.XXXXX
	X.XXXXX	X.XXXXX	X.XXXXX	X.XXXXX	X.XXXXX	X.XXXXX	X.XXXXX
	X.XXXXX	X.XXXXX	X.XXXXX	X.XXXXX	X.XXXXX	X.XXXXX	X.XXXXX
	X.XXXXX	X.XXXXX	X.XXXXX	X.XXXXX	X.XXXXX	X.XXXXX	X.XXXXX
	X.XXXXX	X.XXXXX	X.XXXXX	X.XXXXX	X.XXXXX	X.XXXXX	X.XXXXX
Z5I2(J):	X.XXXXX	X.XXXXX	X.XXXXX	X.XXXXX	X.XXXXX	X.XXXXX	X.XXXXX
TTHO = THETA-75 =	X.XX DEG.						
FDEF1(I,J):	X.XXXXX	X.XXXXX	X.XXXXX	X.XXXXX	X.XXXXX	X.XXXXX	X.XXXXX
	X.XXXXX	X.XXXXX	X.XXXXX	X.XXXXX	X.XXXXX	X.XXXXX	X.XXXXX
	X.XXXXX	X.XXXXX	X.XXXXX	X.XXXXX	X.XXXXX	X.XXXXX	X.XXXXX
	X.XXXXX	X.XXXXX	X.XXXXX	X.XXXXX	X.XXXXX	X.XXXXX	X.XXXXX
	X.XXXXX	X.XXXXX	X.XXXXX	X.XXXXX	X.XXXXX	X.XXXXX	X.XXXXX
	X.XXXXX	X.XXXXX	X.XXXXX	X.XXXXX	X.XXXXX	X.XXXXX	X.XXXXX
	X.XXXXX	X.XXXXX	X.XXXXX	X.XXXXX	X.XXXXX	X.XXXXX	X.XXXXX
Z5I(J):	X.XXXXX	X.XXXXX	X.XXXXX	X.XXXXX	X.XXXXX	X.XXXXX	X.XXXXX

Then an 8 row by 7 column matrix is printed, displaying the total stiffness matrix, FDEFL, when TTHO is set equal to the input collective angle. And finally, the seven values for the total deflection vector, Z5I, are presented at the same input collective angle.

Sample page 13 defines the nonlinear torsional stiffness characteristics of the flexbeam. First, the equation is presented relating the outboard torsional deflection to the spanwise varying torques resulting from the shears and moments at the outboard end of the flexbeam and from the spatial curvature of its torsion axis. Then, the seven nondimensional deflection dependent coefficients defining the nonlinear torsional stiffness characteristics are presented in row form (THTHP, THMX, THSX, THMO, THM1, THSO, and THS1).

Sample page 14 shows the quadratic functionality coefficients for the pitch-flat couplings (AWO, AW1, and AW2) and pitch-edge couplings (AVO, AV1, and AV2) for each flatwise and edgewise mode. Each row represents respective modal content. Also presented are the angular motions of the torque tube relative to the flexbeam, at the juncture, for each of the selected flatwise (RELMW) and edgewise (RELMV) bending modes.

The quadratic representations based on pitch angle for AW and AV are as follows:

$$AW(I) = AWO(I) + TTHO * (AW1(I) + TTHO * AW2(I))$$

$$AV(K) = AVO(K) + TTHO * (AV1(K) + TTHO * AV2 (K))$$

As with the quadratic representations of the torque tube bending stiffness matrix (FDEFL), TTHO again represents the total blade pitch angle at the 75 percent span in radians. RELMW and RELMV are calculated only on the basis of an infinitely rigid torque tube and are therefore not calculated (left as zeros) when the torque tube-flexbeam redundant analyses is operative (i.e. for the cases when a flexible torque tube is employed).

A final line appears on sample page 15 only for the semi-articulated or fully-articulated applications. This is a statement of the pitch-flap coupling, i.e. $\Delta\theta/\Delta\beta_F$, where $\Delta\beta_F$ is the change in flap angle. This value is determined as follows:

FLEX-BEAM TORSIONAL STIFFNESS CHARACTERISTICS

$$\text{THETA-JCT} = (\text{THTHP}) * \text{THETAP-JCT} + (\text{THTMX}) * \text{MX5} + (\text{THTSX}) * \text{SX5} * (\text{Y5} * \text{Z5}' - \text{Z5} * \text{Y5}')$$

$$+ (\text{THTMO}) * (\text{MY5} * \text{Y5} + \text{MZ5} * \text{Z5}) + (\text{THTM1}) * (\text{MY5} * \text{Y5}' + \text{MZ5} * \text{Y5}') + (\text{THTSO}) * (\text{SZ5} * \text{Y5} - \text{SY5} * \text{Z5}) + (\text{THTS1}) * (\text{SZ5} * \text{Y5}' - \text{SY5} * \text{Z5}')$$

THTHP	THTMX	THTSX	THTMO	THTM1	THTSO	THTS1
X.XXX	X.XXX	X.XXXX	X.XXX	X.XXX	X.XXX	X.XXX

COEFFICIENTS FOR QUADRATIC VARIATIONS OF PITCH-FLAT AND PITCH-EDGE COUPLINGS WITH PITCH ANGLE

I	AWO(I)	AW1(I)	AW2(I)	RELMW(I)
1	XX.XXXXX	X.XXXXX	X.XXXXX	.XXXXX
2	XX.XXXXX	X.XXXXX	X.XXXXX	.XXXXX
3	XX.XXXXX	XX.XXXXX	XX.XXXXX	.XXXXX
K	AVO(K)	AV1(K)	AV2(K)	RELMV(K)
1	X.XXXXX	X.XXXXX	X.XXXXX	.XXXXX
2	X.XXXXX	X.XXXXX	X.XXXXX	.XXXXX
PITCH-FLAP COUPLING (DERIVED), DTHETA/DBETA				X.XXX

$$\frac{\Delta\theta}{\Delta\beta_P} = \frac{-(\text{location (G)17} - e)}{\text{location (G)18}}$$

where location (G)17 is the push-rod radial location (in), location (G)18 is the push-rod chordwise location (in), and e is the (dimensionalized) blade root offset (in).

Sample page 15 will vary depending upon whether the "wobble" mode is included by setting (C)14=1.0. If (C)14=1.0 two parameters and a table are printed. The two parameters are respectively the displacement at the inboard edge of a cantilevered torque tube due to a unit load at the same location yielding, ZZ, a flexibility (in/lb) and, secondly, the blade tip deflection resulting from the same unit load applied to the torque tube inner edge. Below these two values a table is printed summarizing the nondimensional spanwise blade deflections, slopes and curvatures arising from the unit load on the torque tube's innermost edge. To dimensionalize the blade displacements under the column GW, multiply the printed values by the ZZ parameter described above. This will result in units of in/lb, interpreted as the displacement at each station along the span due to a unit force on the inner torque tube edge.

When (C)14=0.0, the aforementioned two parameters and the table described above are not printed since the "wobble mode" is disabled. The remainder of sample page 15 shows the effective torsional springs (KTHETA1, KTHETA2, and KTHETA3) and the effective flex-beam torsional stiffnesses (GJ-EFF and TKA2) in row form. KTHETA1 represents the flex-beam torsional stiffness or spring (lb-ft/rad). KTHETA2 represents the equivalent root torsion spring due to control system flexibility (lb-ft/rad). KTHETA3 is the actual control system stiffness or spring (lb-ft/rad). The flex-beam torsional stiffnesses (lb-ft²) together form the coefficient of the twist rate in the flex-beam torsional differential equation.

Sample page 16 presents data pertinent to the built-in elastic axis offset (structural sweep). The first two columns present the spanwise distribution as identified by segment number (N), and by the non-offset radial location of the spanwise segment center, X, (nondimensional with respect to rotor radius). Columns 3 and 5 give the edgewise and flatwise offset distances of the elastic axis from the X₅ axis, respectively, (nondimensional with respect to rotor radius). Columns 4 and 6 represent derived quantities. For small angles, these quantities become the slopes (first derivatives) of the offset locations (Y10EA and Z10EA). The quantity DUEAO represents the foreshortening array needed to

PSEUDO-FLATWISE MODE SHAPE (DEFLECTIONS DUE TO UNIT LOAD AT INBOARD END OF CANTILEVERED TORQUE TUBE)

ZZ = X.XXXXX XX IN/LB BLADE TIP DEFLECTION = .XXXXX XX IN/LB

N	X	GW	GWP	GWPP
1	X.XXXXX	X.XXXXX	X.XXXXX	XX.XXXXX
2	X.XXXXX	X.XXXXX	X.XXXXX	XX.XXXXX
3	X.XXXXX	X.XXXXX	X.XXXXX	XX.XXXXX
.
.
.
.
.
.
.
.
.
.
.
.
.
.
N

TORSIONAL RETENTION SPRINGS AND EFFECTIVE FLEX-BEAM TORSIONAL STIFFNESSES

KTHETA1	KTHETA2	KTHETA3	GJ-EFF	TKA2
XXXX.XXXXX	XXXXX.XXXX	X.X	XXXX.XXXXX	XXXX.XXXXX

177

ELASTIC AXIS OFFSET DISTRIBUTIONS AND DEFLECTION VECTORS

N	X	Y10EA	Y10EAP	Z10EA	Z10EAP	DUEAO
1	.XXXXX	.XXXXX	.XXXXX	.XXXXX	.XXXXX	.XXXXX
2	.XXXXX	.XXXXX	.XXXXX	.XXXXX	.XXXXX	.XXXXX
3	.XXXXX	.XXXXX	.XXXXX	.XXXXX	.XXXXX	.XXXXX
4	.XXXXX	.XXXXX	.XXXXX	.XXXXX	.XXXXX	.XXXXX
5	.XXXXX	.XXXXX	.XXXXX	.XXXXX	.XXXXX	.XXXXX
6	.XXXXX	.XXXXX	.XXXXX	.XXXXX	.XXXXX	.XXXXX
7	.XXXXX	.XXXXX	.XXXXX	.XXXXX	.XXXXX	.XXXXX
8	.XXXXX	.XXXXX	.XXXXX	.XXXXX	.XXXXX	.XXXXX
9	.XXXXX	.XXXXX	.XXXXX	.XXXXX	.XXXXX	.XXXXX
10	.XXXXX	.XXXXX	.XXXXX	.XXXXX	.XXXXX	.XXXXX
11	.XXXXX	.XXXXX	.XXXXX	.XXXXX	.XXXXX	.XXXXX
12	.XXXXX	.XXXXX	.XXXXX	.XXXXX	.XXXXX	.XXXXX
13	.XXXXX	.XXXXX	.XXXXX	.XXXXX	.XXXXX	.XXXXX
14	.XXXXX	.XXXXX	.XXXXX	.XXXXX	.XXXXX	.XXXXX
15	.XXXXX	.XXXXX	.XXXXX	.XXXXX	.XXXXX	.XXXXX
16	.XXXXX	.XXXXX	.XXXXX	.XXXXX	.XXXXX	.XXXXX
17	.XXXXX	.XXXXX	.XXXXX	.XXXXX	.XXXXX	.XXXXX
18	.XXXXX	.XXXXX	.XXXXX	.XXXXX	.XXXXX	.XXXXX
19	.XXXXX	.XXXXX	.XXXXX	.XXXXX	.XXXXX	.XXXXX
20	.XXXXX	.XXXXX	.XXXXX	.XXXXX	.XXXXX	.XXXXX

restore the equivalent straight beam back to the originally structurally swept position. It is determined from the input elastic axis offset data, and from the radial distribution of the blade segments.

Sample page 17 shows typical modal information for the input flatwise and edgewise bending modes. For each mode, the modal frequency (per rotor rev) is printed. Also on this line, for all applications except that of the propeller, is a statement defining the total pitch-flat or pitch-edge coupling (AW(I) or AV(K)) for the mode. And finally on this line, is a statement of whether the mode type is hinged or hingeless. This is determined internally by evaluating:

$$\frac{EI_F^{(2)}}{R} \gamma_{wi}''^{(2)} - \frac{EI_F^{(1)}}{R} \gamma_{wi}''^{(1)}$$

where the superscripts (2) and (1) refer to the second and first spanwise segments. The EI_F terms represent the section bending stiffnesses in the flatwise direction, and γ_{wi} refers to the second spanwise derivative of the flatwise mode shape, similarly for edgewise modes. If this difference is negligible, the mode type is defined as hingeless. Otherwise the mode type is presented as hinged.

Next, for all applications, thirteen columns of information follow. The first two columns present the spanwise distribution, with X being the non-offset radial location of the segment center (nondimensionalized by rotor radius). Columns 3 through 5 echo El59 output of mode shapes, mode shape derivatives, and mode shape second derivatives at each of the spanwise segments. The remaining columns on the sample page, for each mode, present the various derived incremental deflection correction function vectors which account for blade twist and for radial foreshortening. All values are nondimensional.

Column 6 presents the DVB array, which corresponds to the first order Δv_B spanwise function due to built-in twist. This set of values makes up the linear portion (in terms of the modal time variables) of the Δv deflection correction function defined in the structural twist analysis. The array is presented in the flatwise modal information group because it is defined using the flatwise deflections. Column 7 presents the DV2BP array, which contains the first spanwise derivatives of the second integrals defining the Δv_B spanwise function (Δv_B is made up of two integrals in its definition). Column 8 presents the DWBB (ΔW_B) array, which corresponds to the built-in twist portion of the second order ΔW functions defined in the structural twist analysis. The next column

LINEAR AND NONLINEAR MODAL DEFLECTION VECTORS

FLATWISE MODE 1 MODAL FREQUENCY = XXX.XXXX PITCH-FLAT COUPLING, AW(1)=X.XXXX MODE TYPE=XXXXXX

N	X	GW	GWP	GWPP	DVB	DV2BP	DWVBB	DWV2BBP	DWVBC	DWV2BCP	DWVCC	DWV2CCP
1	X.XXXXX	X.XXXXX	X.XXXXX	X.XXXXX	X.XXXXX	X.XXXXX	X.XXXXX	X.XXXXX	X.XXXXX	X.XXXXX	X.XXXXX	X.XXXXX
2	X.XXXXX	X.XXXXX	X.XXXXX	X.XXXXX	X.XXXXX	X.XXXXX	X.XXXXX	X.XXXXX	X.XXXXX	X.XXXXX	X.XXXXX	X.XXXXX
3	X.XXXXX	X.XXXXX	X.XXXXX	X.XXXXX	X.XXXXX	X.XXXXX	X.XXXXX	X.XXXXX	X.XXXXX	X.XXXXX	X.XXXXX	X.XXXXX
.	X.XXXXX	X.XXXXX	X.XXXXX	X.XXXXX	X.XXXXX	X.XXXXX	X.XXXXX	X.XXXXX	X.XXXXX	X.XXXXX	X.XXXXX	X.XXXXX
.	X.XXXXX	X.XXXXX	X.XXXXX	X.XXXXX	X.XXXXX	X.XXXXX	X.XXXXX	X.XXXXX	X.XXXXX	X.XXXXX	X.XXXXX	X.XXXXX
.	X.XXXXX	X.XXXXX	X.XXXXX	X.XXXXX	X.XXXXX	X.XXXXX	X.XXXXX	X.XXXXX	X.XXXXX	X.XXXXX	X.XXXXX	X.XXXXX
N	X.XXXXX	X.XXXXX	X.XXXXX	X.XXXXX	X.XXXXX	X.XXXXX	X.XXXXX	X.XXXXX	X.XXXXX	X.XXXXX	X.XXXXX	X.XXXXX

LINEAR RADIAL DEFLECTION VECTOR DUE TO ELASTIC AXIS OFFSET (DUEAF), AND

QUADRATIC DEFLECTION VECTORS DUE TO TORSION MODAL TWIST (DVE(1,J), DV2EP(1,J)) AND TO FLATWISE BENDING (UWE(1,M))

N	X	J = (1) (2) (3) / M = (1) (2) (3) (4)				UWE								
		DUEAF	DVE	DV2EP	DVE	DV2EP	DVE	DV2EP	DVE	DV2EP	DVE	DV2EP	DVE	DV2EP
1	X.XXXXX	X.XXXXX	X.XXXXX	X.XXXXX	X.XXXXX	X.XXXXX	X.XXXXX	X.XXXXX	X.XXXXX	X.XXXXX	X.XXXXX	X.XXXXX	X.XXXXX	X.XXXXX
2	X.XXXXX	X.XXXXX	X.XXXXX	X.XXXXX	X.XXXXX	X.XXXXX	X.XXXXX	X.XXXXX	X.XXXXX	X.XXXXX	X.XXXXX	X.XXXXX	X.XXXXX	X.XXXXX
3	X.XXXXX	X.XXXXX	X.XXXXX	X.XXXXX	X.XXXXX	X.XXXXX	X.XXXXX	X.XXXXX	X.XXXXX	X.XXXXX	X.XXXXX	X.XXXXX	X.XXXXX	X.XXXXX
.	X.XXXXX	X.XXXXX	X.XXXXX	X.XXXXX	X.XXXXX	X.XXXXX	X.XXXXX	X.XXXXX	X.XXXXX	X.XXXXX	X.XXXXX	X.XXXXX	X.XXXXX	X.XXXXX
.	X.XXXXX	X.XXXXX	X.XXXXX	X.XXXXX	X.XXXXX	X.XXXXX	X.XXXXX	X.XXXXX	X.XXXXX	X.XXXXX	X.XXXXX	X.XXXXX	X.XXXXX	X.XXXXX
.	X.XXXXX	X.XXXXX	X.XXXXX	X.XXXXX	X.XXXXX	X.XXXXX	X.XXXXX	X.XXXXX	X.XXXXX	X.XXXXX	X.XXXXX	X.XXXXX	X.XXXXX	X.XXXXX
N	X.XXXXX	X.XXXXX	X.XXXXX	X.XXXXX	X.XXXXX	X.XXXXX	X.XXXXX	X.XXXXX	X.XXXXX	X.XXXXX	X.XXXXX	X.XXXXX	X.XXXXX	X.XXXXX

EDGEWISE MODE 1 MODAL FREQUENCY = XXX.XXXX PITCH-EDGE COUPLING, AV(1)=X.XXXX MODE TYPE=XXXXXX

N	X	GV	GVP	GVPP	DWB	DW2BP	DVVB	DV2BBP	DVVC	DV2BCP	DVCC	DV2CCP
1	X.XXXXX	X.XXXXX	X.XXXXX	X.XXXXX	X.XXXXX	X.XXXXX	X.XXXXX	X.XXXXX	X.XXXXX	X.XXXXX	X.XXXXX	X.XXXXX
2	X.XXXXX	X.XXXXX	X.XXXXX	X.XXXXX	X.XXXXX	X.XXXXX	X.XXXXX	X.XXXXX	X.XXXXX	X.XXXXX	X.XXXXX	X.XXXXX
3	X.XXXXX	X.XXXXX	X.XXXXX	X.XXXXX	X.XXXXX	X.XXXXX	X.XXXXX	X.XXXXX	X.XXXXX	X.XXXXX	X.XXXXX	X.XXXXX
.	X.XXXXX	X.XXXXX	X.XXXXX	X.XXXXX	X.XXXXX	X.XXXXX	X.XXXXX	X.XXXXX	X.XXXXX	X.XXXXX	X.XXXXX	X.XXXXX
.	X.XXXXX	X.XXXXX	X.XXXXX	X.XXXXX	X.XXXXX	X.XXXXX	X.XXXXX	X.XXXXX	X.XXXXX	X.XXXXX	X.XXXXX	X.XXXXX
.	X.XXXXX	X.XXXXX	X.XXXXX	X.XXXXX	X.XXXXX	X.XXXXX	X.XXXXX	X.XXXXX	X.XXXXX	X.XXXXX	X.XXXXX	X.XXXXX
N	X.XXXXX	X.XXXXX	X.XXXXX	X.XXXXX	X.XXXXX	X.XXXXX	X.XXXXX	X.XXXXX	X.XXXXX	X.XXXXX	X.XXXXX	X.XXXXX

LINEAR RADIAL DEFLECTION VECTOR DUE TO ELASTIC AXIS OFFSET(DUEAE), AND,

DEFLECTION VECTORS DUE TO ELASTIC (MODAL) TWIST, DWE(1,J), DW2EP(1,J), AND TO EDGEWISE BENDING, UVE(1,M)

N	X	J = (1) (2) (3)				UVE								
		DUEAE	DWE	DW2EP	DWE	DW2EP	DWE	DW2EP	DWE	DW2EP	DWE	DW2EP	DWE	DW2EP
1	X.XXXXX	X.XXXXX	X.XXXXX	X.XXXXX	X.XXXXX	X.XXXXX	X.XXXXX	X.XXXXX	X.XXXXX	X.XXXXX	X.XXXXX	X.XXXXX	X.XXXXX	X.XXXXX
2	X.XXXXX	X.XXXXX	X.XXXXX	X.XXXXX	X.XXXXX	X.XXXXX	X.XXXXX	X.XXXXX	X.XXXXX	X.XXXXX	X.XXXXX	X.XXXXX	X.XXXXX	X.XXXXX
3	X.XXXXX	X.XXXXX	X.XXXXX	X.XXXXX	X.XXXXX	X.XXXXX	X.XXXXX	X.XXXXX	X.XXXXX	X.XXXXX	X.XXXXX	X.XXXXX	X.XXXXX	X.XXXXX
.	X.XXXXX	X.XXXXX	X.XXXXX	X.XXXXX	X.XXXXX	X.XXXXX	X.XXXXX	X.XXXXX	X.XXXXX	X.XXXXX	X.XXXXX	X.XXXXX	X.XXXXX	X.XXXXX
.	X.XXXXX	X.XXXXX	X.XXXXX	X.XXXXX	X.XXXXX	X.XXXXX	X.XXXXX	X.XXXXX	X.XXXXX	X.XXXXX	X.XXXXX	X.XXXXX	X.XXXXX	X.XXXXX
.	X.XXXXX	X.XXXXX	X.XXXXX	X.XXXXX	X.XXXXX	X.XXXXX	X.XXXXX	X.XXXXX	X.XXXXX	X.XXXXX	X.XXXXX	X.XXXXX	X.XXXXX	X.XXXXX
N	X.XXXXX	X.XXXXX	X.XXXXX	X.XXXXX	X.XXXXX	X.XXXXX	X.XXXXX	X.XXXXX	X.XXXXX	X.XXXXX	X.XXXXX	X.XXXXX	X.XXXXX	X.XXXXX

shows the DWW2BBP array, which lists the first spanwise derivatives of the second integrals defining the built-in twist related ΔW_B spanwise array.

The last four columns correspond to the portions of the second order ΔW functions involving twist due to control inputs. DWWBC (ΔW_{BC}) refers to portions of the second order ΔW functions which contain a coupling of terms due to built-in twist with terms due to twist resulting from control inputs. DWW2BCP represents the first spanwise derivatives of the second integrals defining the ΔW_{BC} spanwise array. DWWCC (ΔW_C) consists of strictly control-related portions of the second order ΔW functions. And finally, DWW2CCP represents the first spanwise derivatives of the second integrals defining the ΔW_C array.

Following these thirteen columns of information appears a statement describing the deflection vectors to be presented next. Again, thirteen more spanwise dependent columns of information are printed. Column 3 presents the DUEAF array corresponding to the flatwise bending deflection linear radial foreshortening accruing from built-in structural sweep. Columns 4 and 5, 6, and 7, 8 and 9 represent pairs of vectors arising due to torsion modal twist, for at most three torsion modes. Above each pair of columns is a label of which torsion mode (J) is being evaluated. For each pair, first the DVE array appears. This array corresponds to the first order Δv_e spanwise function due to torsional modal (elastic) twist. This set of values makes up the nonlinear portion of the Δv deflection correction function. Second, the DV2EP array is printed. This contains the first spanwise derivatives of the second integrals defining the Δv_e spanwise function. Columns 10 through 13 present, for at most four modes (four flatwise or three edgewise - depending on which modal information group is being described) the flatwise (UWE) or edgewise (UVE) bending nonlinear radial foreshortening due to structural sweep.

The above description for the flatwise modal information applies in a similar way to the edgewise modal information group. The various arrays correspond to similarly defined spanwise functions involving twist, structural sweep, and the edgewise modal deflection and spanwise derivative arrays.

Sample page 18 presents typical modal information for the input torsion modes together with the derived pseudo-torsion mode shapes. The pseudo-torsion mode description is output as spanwise variable, as is the case with the conventional normal torsion modal descriptions.

First, the torsion modal frequency (per rotor rev) is printed. Then twelve columns of spanwise distributions are printed. Columns 3 and 4 echo E159 output of mode shapes and mode shape derivatives at each of the spanwise segments. The remaining eight columns present first and second order deflection correction functions accruing from structural sweep. All values are again nondimensional.

DVEA (Δv_{EA}) represents the first order spanwise increments to the edge-wise deflections brought about by the structural sweep of the blade. These values are each defined by two integrals. DV2EAP represents the first spanwise derivatives of the second integrals defining the Δv_{EA} spanwise functions. DWEA (Δw_{EA}) represents the first order spanwise increments to the flatwise deflections, due to structural sweep. DW2EAP represents the first spanwise derivatives of the second integrals defining the Δw_{EA} spanwise functions. DVVEA (ΔV_{EA}) is an array consisting of the second order spanwise increments to the edgewise deflections (due to structural sweep). DVV2EAP displays the first spanwise derivatives of the second integrals defining the ΔV_{EA} spanwise functions. DWWEA (ΔW_{EA}) consists of the second order spanwise increments to the flatwise deflections. And finally, DWW2EAP represents the first spanwise derivatives of the second integrals in the definition of the ΔW_{EA} spanwise functions.

All arrays for the pseudo-torsion mode are defined in a similar manner. In general, the values output for the pseudo-torsion mode shapes have values of 1.0 over the blade span except, for analyses of the bearingless rotor, over the flexbeam-torque tube portion of the blade.

The first line on Sample Page 19 represents coupled torsion information which is produced as a means of suppressing the high frequency coupled mode. This information is printed if either an explicit root torsion spring rate is input (location (D)34), the wobble mode is included (input location (C)14), or the redundant analysis is invoked (input location (C)15). If any of the above items pertain, then the rigid body torsion degree-of-freedom (pseudo-torsion mode) is used with the elastic (normal) torsion modes. The output consists of two coupled frequencies (per rev), the first and third items printed, and the coupled mode shape ratio, A, (nondimensional), computed internally by a simple eigenvalue analysis. The lower of the two coupled frequencies is used in determining the coupled mode shape ratio. This ratio, A, represents a fixed proportion between the cantilevered elastic torsion mode and the rigid pseudo torsion mode. This ratio remains fixed during the time history. Note that when this coupling is enabled by entry (D)34 as discussed above, the time-history printout (Sample page 20) value of QT1 represents the amplitude of the elastic cantilevered component while QT2 is the corresponding rigid pseudo torsion amplitude which is always equal to QT1*A. Also note that the values printed under the heading 'TORSION DEFL.' represent a superposition of QT1 and QT2 converted to degree units.

COUPLED TORSION INFORMATION FOR TORSION MODE 1 ARE X.XXXXXX X.XXXXXX XX.XXXXXX

Results of Solution Part II - Time-History Solutions

Sample Pages 20 through 22 present the pertinent details of the results from the time-history solutions (i.e., transient aeroelastic responses). The first row of parameters following the page title represents, for the subsequent time-history solution, the parameters defining the flight condition. These consist of the various control angles (in degrees), the inflow and advance ratios, LAMBDA and MU, respectively, and the initial nondimensionalized values of the "momentum" induced velocity components. The remainder of Sample Page 20 comprises the typical azimuthal listing; this listing is output for every azimuth angle which is a multiple of the print azimuth increment, loader input (S)11. Regardless of the printout controls ((S)11, (S)12) sample page 30 is always printed for the rotor initial azimuthal angle. In the following discussions each item of pages 30-33 will be discussed.

Azimuthal Printouts

The first line appearing on all subsequent azimuthal printouts gives the rotor azimuth angle, revolution number and time. In addition, the three components of the instantaneous Glauert (momentum induced) inflow, LAMBDAO, LAMBDAIC, LAMBDAIS, are output. The remainder of the azimuthal printout consists of three main groups. The first of the three groups on this sample page lists the spanwise distributions of the pertinent aerodynamic quantities, the format of which depends on the choice of unsteady airloads modeling selected (input location (A)64).

Unsteady Airloads Utilizing an Equivalent Angle-of-Attack

Unsteady airloads options wherein the airloads depend on a single "effective" angle-of-attack are: i) the quasi-static modeling ((A)64 = 0.), ii) the unstalled generalized Wagner functions modeling ((A)64 = 1.), and iii) the UTRC synthesized unsteady stalled modeling ((A)64 = 2.). For these cases, the first seven aerodynamic quantities are: LAMBDA_S, GAMMA, PHI, ALPHA, MACH, A, and ALPHAW. These quantities are, respectively, the aerodynamic sweep angle due only to radial flow (in degrees), the total aerodynamic sweep angle including structural sweep (in degrees), the inflow angle and angle-of-attack (both in degrees), Mach number, nondimensional angle-of-attack rate, and the unsteady decay parameter (in degrees).

Remainder of Azimuthal Printout

The aerodynamic coefficients CL, CD and CM are self-explanatory and nondimensional. The airload distributions in the z₅ and y₅ directions, SAZ5 and SAY5, respectively, have the units of lb/in., the aerodynamic pitching moments about

PART II. TIME HISTORY SOLUTION OF COMPLETE (NONLINEAR) EQUATION SET - AEROELASTIC TRANSIENT RESPONSES

AIS .XXX		BIS .XXX		THETA 75 XX.XXX		LAMBDA .XXXX		MU .XXX		VO .XXXXX		VIC .XXXXX		VIS .XXXXX	
PSI(I)=-		.X DEG		REV- X		TIME- .XX SEC		LAMBDA O = .XXXX		LAMBDA IC = .XXXX		LAMBDA IS = .XXXX			
N	XCEN	LAMBDA S	GAMMA	PHI	ALPHA	MACH	A	ALPHA W	CL	CD	CM	SAZ5	SAYS	MAX5	MAYS
1	.XXXX	.XXX	.XXX	XX.XX	X.XX	.XXX	.XXX	.XXX	.XXX	.XXX	.XXX	.XXX	.XXX	.XXX	.XXX
2	.XXXX	.XXX	.XXX	XX.XX	X.XX	.XXX	.XXX	.XXX	.XXX	.XXX	.XXX	.XXX	.XXX	.XXX	.XXX
3	.XXXX	.XXX	.XXX	XX.XX	X.XX	.XXX	.XXX	.XXX	.XXX	.XXX	.XXX	.XXX	.XXX	.XXX	.XXX
4	.XXXX	.XXX	.XXX	XX.XX	X.XX	.XXX	.XXX	.XXX	.XXX	.XXX	.XXX	.XXX	.XXX	.XXX	.XXX
5	.XXXX	.XXX	.XXX	XX.XX	X.XX	.XXX	.XXX	.XXX	.XXX	.XXX	.XXX	.XXX	.XXX	.XXX	.XXX
6	.XXXX	.XXX	.XXX	XX.XX	X.XX	.XXX	.XXX	.XXX	.XXX	.XXX	.XXX	.XXX	.XXX	.XXX	.XXX
7	.XXXX	.XXX	.XXX	XX.XX	X.XX	.XXX	.XXX	.XXX	.XXX	.XXX	.XXX	.XXX	.XXX	.XXX	.XXX
8	.XXXX	.XXX	.XXX	XX.XX	X.XX	.XXX	.XXX	.XXX	.XXX	.XXX	.XXX	.XXX	.XXX	.XXX	.XXX
9	.XXXX	.XXX	.XXX	XX.XX	X.XX	.XXX	.XXX	.XXX	.XXX	.XXX	.XXX	.XXX	.XXX	.XXX	.XXX
10	.XXXX	.XXX	.XXX	XX.XX	X.XX	.XXX	.XXX	.XXX	.XXX	.XXX	.XXX	.XXX	.XXX	.XXX	.XXX
11	.XXXX	.XXX	.XXX	XX.XX	X.XX	.XXX	.XXX	.XXX	.XXX	.XXX	.XXX	.XXX	.XXX	.XXX	.XXX
12	.XXXX	.XXX	.XXX	XX.XX	X.XX	.XXX	.XXX	.XXX	.XXX	.XXX	.XXX	.XXX	.XXX	.XXX	.XXX
13	.XXXX	.XXX	.XXX	XX.XX	X.XX	.XXX	.XXX	.XXX	.XXX	.XXX	.XXX	.XXX	.XXX	.XXX	.XXX
14	.XXXX	.XXX	.XXX	XX.XX	X.XX	.XXX	.XXX	.XXX	.XXX	.XXX	.XXX	.XXX	.XXX	.XXX	.XXX
15	.XXXX	.XXX	.XXX	XX.XX	X.XX	.XXX	.XXX	.XXX	.XXX	.XXX	.XXX	.XXX	.XXX	.XXX	.XXX
16	.XXXX	.XXX	.XXX	XX.XX	X.XX	.XXX	.XXX	.XXX	.XXX	.XXX	.XXX	.XXX	.XXX	.XXX	.XXX
17	.XXXX	.XXX	.XXX	XX.XX	X.XX	.XXX	.XXX	.XXX	.XXX	.XXX	.XXX	.XXX	.XXX	.XXX	.XXX
18	.XXXX	.XXX	.XXX	XX.XX	X.XX	.XXX	.XXX	.XXX	.XXX	.XXX	.XXX	.XXX	.XXX	.XXX	.XXX
19	.XXXX	.XXX	.XXX	XX.XX	X.XX	.XXX	.XXX	.XXX	.XXX	.XXX	.XXX	.XXX	.XXX	.XXX	.XXX
20	.XXXX	.XXX	.XXX	XX.XX	X.XX	.XXX	.XXX	.XXX	.XXX	.XXX	.XXX	.XXX	.XXX	.XXX	.XXX
N	XCEN	VERT. DEFL.	INPLANE DEFL.	TORSION DEFL.	SDZ5	SDY5	MDX5	MEX9	FLATWISE STRESS	EDGEWISE STRESS	CORNER STRESS	TORSION STRESS	TORSION MOMENT		
1	.XXXX	.XXX	.XXX	.XXX	.XXX	.XXX	XX.XX	.XXX	.XXX	.XXX	.XXX	.XXX	.XXX	.XXX	.XXX
2	.XXXX	.XXX	.XXX	.XXX	.XXX	.XXX	XX.XX	.XXX	.XXX	.XXX	.XXX	.XXX	.XXX	.XXX	.XXX
3	.XXXX	.XXX	.XXX	.XXX	.XXX	.XXX	XX.XX	.XXX	.XXX	.XXX	.XXX	.XXX	.XXX	.XXX	.XXX
4	.XXXX	.XXX	.XXX	.XXX	.XXX	.XXX	XX.XX	.XXX	.XXX	.XXX	.XXX	.XXX	.XXX	.XXX	.XXX
5	.XXXX	.XXX	.XXX	.XXX	.XXX	.XXX	XX.XX	.XXX	.XXX	.XXX	.XXX	.XXX	.XXX	.XXX	.XXX
6	.XXXX	.XXX	.XXX	.XXX	.XXX	.XXX	XX.XX	.XXX	.XXX	.XXX	.XXX	.XXX	.XXX	.XXX	.XXX
7	.XXXX	.XXX	.XXX	.XXX	.XXX	.XXX	XX.XX	.XXX	.XXX	.XXX	.XXX	.XXX	.XXX	.XXX	.XXX
8	.XXXX	.XXX	.XXX	.XXX	.XXX	.XXX	XX.XX	.XXX	.XXX	.XXX	.XXX	.XXX	.XXX	.XXX	.XXX
9	.XXXX	.XXX	.XXX	.XXX	.XXX	.XXX	XX.XX	.XXX	.XXX	.XXX	.XXX	.XXX	.XXX	.XXX	.XXX
10	.XXXX	.XXX	.XXX	.XXX	.XXX	.XXX	XX.XX	.XXX	.XXX	.XXX	.XXX	.XXX	.XXX	.XXX	.XXX
11	.XXXX	.XXX	.XXX	.XXX	.XXX	.XXX	XX.XX	.XXX	.XXX	.XXX	.XXX	.XXX	.XXX	.XXX	.XXX
12	.XXXX	.XXX	.XXX	.XXX	.XXX	.XXX	XX.XX	.XXX	.XXX	.XXX	.XXX	.XXX	.XXX	.XXX	.XXX
13	.XXXX	.XXX	.XXX	.XXX	.XXX	.XXX	XX.XX	.XXX	.XXX	.XXX	.XXX	.XXX	.XXX	.XXX	.XXX
14	.XXXX	.XXX	.XXX	.XXX	.XXX	.XXX	XX.XX	.XXX	.XXX	.XXX	.XXX	.XXX	.XXX	.XXX	.XXX
15	.XXXX	.XXX	.XXX	.XXX	.XXX	.XXX	XX.XX	.XXX	.XXX	.XXX	.XXX	.XXX	.XXX	.XXX	.XXX
16	.XXXX	.XXX	.XXX	.XXX	.XXX	.XXX	XX.XX	.XXX	.XXX	.XXX	.XXX	.XXX	.XXX	.XXX	.XXX
17	.XXXX	.XXX	.XXX	.XXX	.XXX	.XXX	XX.XX	.XXX	.XXX	.XXX	.XXX	.XXX	.XXX	.XXX	.XXX
18	.XXXX	.XXX	.XXX	.XXX	.XXX	.XXX	XX.XX	.XXX	.XXX	.XXX	.XXX	.XXX	.XXX	.XXX	.XXX
19	.XXXX	.XXX	.XXX	.XXX	.XXX	.XXX	XX.XX	.XXX	.XXX	.XXX	.XXX	.XXX	.XXX	.XXX	.XXX
20	.XXXX	.XXX	.XXX	.XXX	.XXX	.XXX	XX.XX	.XXX	.XXX	.XXX	.XXX	.XXX	.XXX	.XXX	.XXX
	QW1	QW2	QW3	QV1	QV2	QV3	QT1	QT2	BETA	DELTA	BETA-P1	BETA-P2			
(+)	.XXX-YYY	.XXX-YYY	.XXX-YYY	.XXX+YYY	.XXX-YYY	.XXX-YYY	.XXX-YYY	.XXX-YYY	.XXX-YYY	.XXX-YYY	.XXX-YYY	.XXX-YYY	.XXX-YYY	.XXX-YYY	.XXX-YYY
(**)	.XXX-YYY	.XXX-YYY	.XXX-YYY	.XXX-YYY	.XXX-YYY	.XXX-YYY	.XXX-YYY	.XXX-YYY	.XXX-YYY	.XXX-YYY	.XXX-YYY	.XXX-YYY	.XXX-YYY	.XXX-YYY	.XXX-YYY
XI	.XXX-YYY	.XXX-YYY	.XXX-YYY	.XXX-YYY	.XXX-YYY	.XXX-YYY	.XXX-YYY	.XXX-YYY	.XXX-YYY	.XXX-YYY	.XXX-YYY	.XXX-YYY	.XXX-YYY	.XXX-YYY	.XXX-YYY

the x_5 and y_5 axes, MAX5 and MAY5, respectively, have the units of lb-in./in. The second of the three groups on Sample Page 20 lists pertinent spanwise distributions of a structural dynamic nature. The vertical and inplane deflections are those, respectively, in the z_5 and y_5 directions and have the units of in. The torsional deflection has the units of deg. The quantities SDZ5, SDY5 and MDX5 are "semi-dynamic" load distributions. These distributions are dimensionally the same as those resulting from aerodynamics, but arise instead from all the dynamic effects except the doubly time differentiated ones. The quantity MEX9 is the nonlinear elastic torsion moment distribution as calculated using the ΔEI implementation; it too has the units of lb-in./in. All stress quantities have the units of lb/in.², whereas the torsion moment has the units of lb-in. The third of the three groups on Sample Page 20 lists the blade modal responses, their nondimensional time derivatives and "right-hand-side" excitations. Specifically, for each blade modal response variable (column) are given the instantaneous displacement, velocity, acceleration and generalized excitation (elements on right-hand side of the modal equation).

If a composite bearingless rotor is modeled, it should be noted that, over the flexbeam-torque tube span, the flatwise and edgewise stresses outputted are those only for the flexbeam whereas the torsion moments and stresses outputted are those only for the torque tube. Also, the items on Sample Page 21 typically occur immediately after the stress quantities are printed, and before the modal responses. The first group of information will appear providing the outboard attachment point (location (G)16) of the pitch-horn is beyond the first segment. If this is the case, the integer identifier and the offset radial location of the center of the segment defined as the innermost flexbeam segment (location (C)1) will first be printed. Then, in the same row, will appear the spar/flexure parameters, i.e. the flatwise stress (lb/in²), edgewise stress (lb/in²), corner stress (lb/in²), torsion stress (lb/in²) and torsion moment (lb-in) at that innermost flexbeam segment. (This segment has an assumed minimum value of 1.) The output torsion moment is for the flexbeam immediately inboard of the juncture.

The next set of values is printed only if the torque tube/flexbeam redundant analysis is used (location (C)15). The five structural quantities (deflection rates, loads, and moments) are outputted at four spanwise locations: outboard of the torque tube-flexbeam-blade juncture, inboard of the flexbeam juncture, inboard of the torque tube juncture, and at the torque tube snubber.

After the time-history solution has either converged to periodicity or run to maximum flapping trials (input location (S)9), various integrated loads are calculated for one additional, final blade revolution to form the aerodynamic

SPAR/FLEXURE PARAMETERS:
 1 X.XXXX

	YY5PM	ZZ5PM	SX5	SY5	SZ5	MX5	MY5	MZ5
OUTB'D OF JUNCTURE	.XXXXXX	.XXXXXX	XXXXX.X	XXX.XXX	XXX.XXX	XXXX.XX	XXXX.XX	XXXX.XXX
INB'D OF J. (FLEXBEAM)	.XXXXXX	.XXXXXX	XXXXX.X	XXX.XXX	XXX.XXX	XXXX.XX	XXX.XXX	XXXX.XXX
INB'D OF J. (T. TUBE)	.XXXXXX	.XXXXXX	XXXXX.X	XXX.XXX	XXX.XXX	XXXX.XX	XXX.XXX	XXXX.XXX
AT SNUBBER (T. TUBE)	.XXXXXX	.XXXXXX	XXXXX.X	XXX.XXX	XXX.XXX	XXXX.XXX		

performance and stress results depicted in Sample Page 22. For each of eight performance quantities, results are presented in nondimensional coefficient form, in nondimensional form divided by solidity, and in actual dimensional form. Note that ten dimensional quantities are listed and the units are lb for forces and lb-ft for moments, as appropriate. LIFT and PROP.FORCE are components of THRUST and H-FORCE that have been rotated through the internally calculated aerodynamic shaft angle printed as ALPHA S. The quantity EQU. DRAG (lb) represents the combined power expended by the rotor due to rotor rotation (torque) and translation (drag) divided by flight speed.

The next line duplicates the parameters defining the flight condition and includes additional quantities which depend on the integrated performance for evaluation. At the beginning of the time-history calculation, it is not known which part of the inflow ratio being used is due to ram effects and which due to momentum induced effects. Once the integrated rotor thrust is calculated, however, the induced portion of the inflow can then be calculated using the simple usual momentum formula derived for flight in an infinite continuum. The complementary portion of the inflow represents the ram effect from which the shaft angle-of-attack, ALPHA S, in degrees, can be calculated. The quantity VEL ACT is the actual forward flight velocity, in knots, consistent with the advance ratio used and the shaft angle-of-attack. For finite forward flight speeds EQU. L/D is the lift divided by the equivalent drag; for hovering cases this quantity is the figure of merit. PAR. AREA, the rotor parasite (drag) area, in square feet is the rotor drag divided by dynamic pressure. The control angles, ALS, BLS, THETA 75 and the shaft angle-of-attack all have the units of degrees. The power absorbed by the rotor from the airstream in kilowatts is given by the quantity KWATT. It will always be of opposite sign from the horsepower. The remainder of Sample Page 22 consists of reductions of the various stresses given in the azimuthal printout in terms of median and 1/2 peak-to-peak values.

Once the time-history solution has converged to periodicity, the program optionally performs harmonic analyses of the azimuthal variations of various response quantities. The outputs of these harmonic analyses are depicted in Sample Pages 23 through 25. In each of these sample pages, the harmonic information for each response variable is contained in the appropriate horizontal band of five rows. The harmonics are listed by columns up to a maximum of ten harmonics. All harmonic analysis output depicted on these sample pages assume a negative harmonic content form in keeping with the (negative) harmonic form conventionally assumed for the blade pitch control and rigid flapping angles. For each harmonic of response variable five quantities are output; these quantities are, respectively, the (negative) cosine and sine components, the equivalent amplitude and phase angle, and lastly, the amplitude of the harmonic relative to all the other harmonic amplitudes output. Sample Page 23 depicts the harmonic analyses of the dimensionless modal response variables selected wherein QW(I),

HARMONIC ANALYSIS OF HUB SLAERS AND MOMENTS

	AO	1	2	3	4	5	6	7	8	9	10
LONG. SHR	XX.X	XXXXX.X XXXXX.X XXXXX.X XXX.XX X.XX	XXX.X XXX.X XXX.X XXX.XX .XX	XXX.X XXX.X XXX.X XXX.XX .XX	XX.X XX.X XX.X XXX.XX .XX	XX.X XX.X XX.X XXX.XX .XX	XX.X XX.X XX.X XXX.XX .XX	XX.X XX.X XX.X XXX.XX .XX	XX.X XX.X XX.X XXX.XX .XX	XX.X XX.X XX.X XXX.XX .XX	XX.X XX.X XX.X XXX.XX .XX
LAT. SHR	XX.X	XXXXX.X XXXXX.X XXXXX.X XXX.XX X.XX	XXX.X XXX.X XXX.X XXX.XX .XX	XXX.X XXX.X XXX.X XXX.XX .XX	XX.X XX.X XX.X XXX.XX .XX	XX.X XX.X XX.X XXX.XX .XX	XX.X XX.X XX.X XXX.XX .XX	XX.X XX.X XX.X XXX.XX .XX	XX.X XX.X XX.X XXX.XX .XX	XX.X XX.X XX.X XXX.XX .XX	XX.X XX.X XX.X XXX.XX .XX
VERT. SHR	XX.X	XXXXX.X XXXXX.X XXXXX.X XXX.XX X.XX	XXX.X XXX.X XXX.X XXX.XX .XX	XXX.X XXX.X XXX.X XXX.XX .XX	XX.X XX.X XX.X XXX.XX .XX	XX.X XX.X XX.X XXX.XX .XX	XX.X XX.X XX.X XXX.XX .XX	XX.X XX.X XX.X XXX.XX .XX	XX.X XX.X XX.X XXX.XX .XX	XX.X XX.X XX.X XXX.XX .XX	XX.X XX.X XX.X XXX.XX .XX
ROLL MOMT	XX.X	XXXXX.X XXXXX.X XXXXX.X XXX.XX X.XX	XXX.X XXX.X XXX.X XXX.XX .XX	XXX.X XXX.X XXX.X XXX.XX .XX	XX.X XX.X XX.X XXX.XX .XX	XX.X XX.X XX.X XXX.XX .XX	XX.X XX.X XX.X XXX.XX .XX	XX.X XX.X XX.X XXX.XX .XX	XX.X XX.X XX.X XXX.XX .XX	XX.X XX.X XX.X XXX.XX .XX	XX.X XX.X XX.X XXX.XX .XX
PITCH MOMT	XX.X	XXXXX.X XXXXX.X XXXXX.X XXX.XX X.XX	XXX.X XXX.X XXX.X XXX.XX .XX	XXX.X XXX.X XXX.X XXX.XX .XX	XX.X XX.X XX.X XXX.XX .XX	XX.X XX.X XX.X XXX.XX .XX	XX.X XX.X XX.X XXX.XX .XX	XX.X XX.X XX.X XXX.XX .XX	XX.X XX.X XX.X XXX.XX .XX	XX.X XX.X XX.X XXX.XX .XX	XX.X XX.X XX.X XXX.XX .XX
YAW MOMT	XX.X	XXXXX.X XXXXX.X XXXXX.X XXX.XX X.XX	XXX.X XXX.X XXX.X XXX.XX .XX	XXX.X XXX.X XXX.X XXX.XX .XX	XX.X XX.X XX.X XXX.XX .XX	XX.X XX.X XX.X XXX.XX .XX	XX.X XX.X XX.X XXX.XX .XX	XX.X XX.X XX.X XXX.XX .XX	XX.X XX.X XX.X XXX.XX .XX	XX.X XX.X XX.X XXX.XX .XX	XX.X XX.X XX.X XXX.XX .XX

HARMONIC ANALYSIS OF FLATWISE STRESSES

N	X	CEN	AO	1	2	3	4	5	6	7	8	9	10
1	.XXXX	XXXX.X	XXXX.X	XXXX.X	XXXX.X	XXXX.X	XX.X	XXX.X	XXX.X	XX.X	XX.X	XX.X	XX.X
				XXXX.X	XXX.X	XXXX.X	XXX.X	XXX.X	XXX.X	XX.X	XX.X	XX.X	XX.X
				XXXX.X	XXX.X	XXXX.X	XXX.X	XXX.X	XXX.X	XX.X	XX.X	XX.X	XX.X
				XX.X	XX.X	XX.X	XX.X	XX.X	XX.X	XX.X	XX.X	XX.X	XX.X
				.XXX	X.XXX	.XXX	.XXX	.XXX	.XXX	.XXX	.XXX	.XXX	.XXX
2	.XXXX	XXXX.X	XXXX.X	XXXX.X	XXXX.X	XXXX.X	XX.X	XXX.X	XXX.X	XX.X	XX.X	XX.X	XX.X
				XXXX.X	XXX.X	XXXX.X	XXX.X	XXX.X	XXX.X	XX.X	XX.X	XX.X	XX.X
				XXXX.X	XXX.X	XXXX.X	XXX.X	XXX.X	XXX.X	XX.X	XX.X	XX.X	XX.X
				XX.X	XX.X	XX.X	XX.X	XX.X	XX.X	XX.X	XX.X	XX.X	XX.X
				.XXX	X.XXX	.XXX	.XXX	.XXX	.XXX	.XXX	.XXX	.XXX	.XXX
3	.XXXX	XXXX.X	XXXX.X	XXXX.X	XXXX.X	XXXX.X	XX.X	XXX.X	XXX.X	XX.X	XX.X	XX.X	XX.X
				XXXX.X	XXX.X	XXXX.X	XXX.X	XXX.X	XXX.X	XX.X	XX.X	XX.X	XX.X
				XXXX.X	XXX.X	XXXX.X	XXX.X	XXX.X	XXX.X	XX.X	XX.X	XX.X	XX.X
				XX.X	XX.X	XX.X	XX.X	XX.X	XX.X	XX.X	XX.X	XX.X	XX.X
				.XXX	X.XXX	.XXX	.XXX	.XXX	.XXX	.XXX	.XXX	.XXX	.XXX
4	.XXXX	XXXX.X	XXXX.X	XXXX.X	XXXX.X	XXXX.X	XX.X	XXX.X	XXX.X	XX.X	XX.X	XX.X	XX.X
				XXXX.X	XXX.X	XXXX.X	XXX.X	XXX.X	XXX.X	XX.X	XX.X	XX.X	XX.X
				XXXX.X	XXX.X	XXXX.X	XXX.X	XXX.X	XXX.X	XX.X	XX.X	XX.X	XX.X
				XX.X	XX.X	XX.X	XX.X	XX.X	XX.X	XX.X	XX.X	XX.X	XX.X
				.XXX	X.XXX	.XXX	.XXX	.XXX	.XXX	.XXX	.XXX	.XXX	.XXX
5	.XXXX	XXXX.X	XXXX.X	XXXX.X	XXXX.X	XXXX.X	XX.X	XXX.X	XXX.X	XX.X	XX.X	XX.X	XX.X
				XXXX.X	XXX.X	XXXX.X	XXX.X	XXX.X	XXX.X	XX.X	XX.X	XX.X	XX.X
				XXXX.X	XXX.X	XXXX.X	XXX.X	XXX.X	XXX.X	XX.X	XX.X	XX.X	XX.X
				XX.X	XX.X	XX.X	XX.X	XX.X	XX.X	XX.X	XX.X	XX.X	XX.X
				.XXX	X.XXX	.XXX	.XXX	.XXX	.XXX	.XXX	.XXX	.XXX	.XXX
6	.XXXX	XXXX.X	XXXX.X	XXXX.X	XXXX.X	XXXX.X	XX.X	XXX.X	XXX.X	XX.X	XX.X	XX.X	XX.X
				XXXX.X	XXX.X	XXXX.X	XXX.X	XXX.X	XXX.X	XX.X	XX.X	XX.X	XX.X
				XXXX.X	XXX.X	XXXX.X	XXX.X	XXX.X	XXX.X	XX.X	XX.X	XX.X	XX.X
				XX.X	XX.X	XX.X	XX.X	XX.X	XX.X	XX.X	XX.X	XX.X	XX.X
				.XXX	X.XXX	.XXX	.XXX	.XXX	.XXX	.XXX	.XXX	.XXX	.XXX

QV(K) and QT(J) are, respectively, the (I) flatwise, (K) edgewise and (J) torsional uncoupled mode responses.

Sample Page 24 depicts the harmonic analyses of the total shears and moments exerted by one blade to the hub. In contrast to the steady hub loads listed in the AERODYNAMIC PERFORMANCE AND STRESSES output (Sample Page 22) which are calculated by integrating only the aerodynamic load distributions, the total hub loads, which are herein harmonically analyzed, are calculated by similarly integrating the combined aerodynamic and the dynamic load distributions. The longitudinal, lateral and vertical hub shears comprising the first three quantities of this sample page all have the dimensions of lb and are defined in the x_1 - (aft), y_1 - (starboard), and z_1 - (up and along axis of rotation) axis directions, respectively. The roll, pitch and yaw moments comprising the latter three quantities on this sample page have the dimensions of lb-ft and are defined positive (using the right-hand rule) about the x_1 -, y_1 -, and z_1 -axes, respectively. Note that the aerodynamic rolling moment whose output is depicted in Sample Page 22 is defined positive starboard side down and is opposite from the harmonically analyzed total rolling moment depicted in Sample Page 24. Sample Page 25 depicts the harmonic analysis of the flatwise stresses at the center of each of the spanwise segments. A similar output listing is provided for both edgewise and torsional stresses.

Should major (trim) iterations be used (see description of input items (A)41 through (A)44) output depicted on Sample Page 26 will be generated by the program. The first line consists of the zeroth, first cosine and first and second sine harmonics of first flatwise mode response, in radians, and an estimate of an effective angle-of-attack on the retreating blade side ($\psi = 270^\circ$), in degrees. The nonzero elements of the depicted (G) MATRIX give, for each row, the partial derivatives of the four trim quantities (C_L , C_{PF} , C_{PM} , C_{RM} , respectively) with respect to the four control quantities being used ($\theta_{.75}$, A_{1s} , B_{1s} , and $(\sin \alpha_s)$, or v_o , v_{1c} , v_{1s} , and $(\sin \alpha_s)$), for each respective column. The elements of this matrix are formulated using numerical differentiation of the Sample Page 22 performance results and are calculated for either set of control quantities, as appropriate. The ERROR VECTOR consists of the differences between the four requested trim quantities and those achieved in the preceding time-history. The two lines depicted give the error vector in dimensional (lb and lb-ft) and nondimensional forms, respectively. The CORRECTION VECTOR consists of those changes to the control quantities which should null the above described error vector. The correction vector is obtained from the premultiplication of the inverse of the G matrix with the error vector, but the corrections are scaled, if necessary, to prevent control changes of more than 2 degrees within any one iteration. The control parameters whose increments are depicted in this output page are, in respective order: $\theta_{.75}$, A_{1s} , B_{1s} , $(\sin \alpha_s)$, λ , C_T , v_o , v_{1c} , and v_{1s} ; the first three have units of degrees and the remainder are dimensionless or nondimensionalized.

TRIM ITERATION.	QW10 = X.XXKX-VV	QW11 = X.XXKX-VV	QW12 = X.XXKX-VV	QW13 = X.XXKX-VV	QW14 = X.XXKX-VV	QW15 = X.XXKX-VV	QW16 = X.XXKX-VV	QW17 = X.XXKX-VV	QW18 = X.XXKX-VV
(G) MATRIX									
X.XXKX-VV	X.XXKX-VV	X.XXKX-VV	X.XXKX-VV	0.000	0.000	0.000	0.000	0.000	0.000
X.XXKX-VV	X.XXKX-VV	X.XXKX-VV	X.XXKX-VV	0.000	0.000	0.000	0.000	0.000	0.000
X.XXKX-VV	X.XXKX-VV	X.XXKX-VV	X.XXKX-VV	0.000	0.000	0.000	0.000	0.000	0.000
X.XXKX-VV	X.XXKX-VV	X.XXKX-VV	X.XXKX-VV	0.000	0.000	0.000	0.000	0.000	0.000
LOADING VECTOR									
X.XXKX-VV	X.XXKX-VV	X.XXKX-VV	X.XXKX-VV	0.000	0.000	0.000	0.000	0.000	0.000
X.XXKX-VV	X.XXKX-VV	X.XXKX-VV	X.XXKX-VV	0.000	0.000	0.000	0.000	0.000	0.000
CONNECTION VECTOR									
X.XXKX-VV	X.XXKX-VV	X.XXKX-VV	X.XXKX-VV	X.XXKX-VV	X.XXKX-VV	X.XXKX-VV	X.XXKX-VV	X.XXKX-VV	X.XXKX-VV

Impedance Matrices

When the analysis is optionally used to calculate impedance matrices (as controlled by input items (S)41 through (S)50) these matrices are output as shown in Sample Pages 27 and 28. Sample Page 27 presents the blade passage harmonic characteristics of conventionally defined hub loads and their respective impedances due to vibratory hub acceleration. The column denoted HUB LOADS presents the N/rev harmonic content of the hub loads as determined by summing contributions from all blades, where N is indicated in the first line of this sample page. Thus, the values in this column are equal to the Nth harmonic values shown in Sample Page 24 but multiplied by the number of blades. Note that, as shown in Sample Page 27, the results would be appropriate for the 4th harmonic hub loads for a four-bladed rotor. The columns denoted LDXC, LDYC, LDZC, LDXS, LDYS and LDZS present the derivatives of the respective HUB LOADS values with respect to N/rev vibratory displacements in the x, y and z directions, cosine and sine components each. The columns denoted RDXC, RDYC, ..., RDZS present similar derivatives of the hub loads with respect to vibratory rotations about the x, y and z axes, cosine and sine components each. Note that the units of the loads and perturbational quantities are defined in the second line of this sample page. The positive directions of the loads are also defined and are consistent with those of Sample Page 24.

Sample Page 28 presents elements of an "augmented" impedance matrix representing the partial derivatives of the HUB LOADS components, but with respect to the six components of higher harmonic (pitch) control angle (HHC) appropriate to N/rev vibratory hub loads. Normally these components consist of the cosine and sine components each of the N-1, N and N+1 harmonics. Note that Sample Page 28 indicates harmonic components of HHC appropriate to 4/rev vibrations. As indicated in the first line of this sample page the pitch angle perturbations have the units of degrees.

SUMMARY OF ROTOR HUB 4/REV LOADS AND HUB IMPEDANCE MATRIX CALCULATIONS FOR 4/REV VIBRATORY HUB DISPLACEMENTS

UNITS... U(SHEAR) = LBS, U(MOMENT) = FT-LBS, U(LINEAR DISPLACEMENT) = FT, U(ROTATIONAL DISPLACEMENT) = RAD

CONVENTIONAL FOURIER SERIES REPRESENTATIONS

			HUB LOADS	LDXC	LDYC	LDZC	RDXC	RDYC	RDZC
LONG.	SHR (+, AFT)	COS	X.XXXE-YY	X.XXXE-YY	X.XXXE-YY	X.XXXE-YY	X.XXXE-YY	X.XXXE-YY	X.XXXE-YY
LAT.	SHR (+, STRBD)	COS	X.XXXE-YY	X.XXXE-YY	X.XXXE-YY	X.XXXE-YY	X.XXXE-YY	X.XXXE-YY	X.XXXE-YY
VERT.	SHR (+, UP)	COS	X.XXXE-YY	X.XXXE-YY	X.XXXE-YY	X.XXXE-YY	X.XXXE-YY	X.XXXE-YY	X.XXXE-YY
ROLL	MOMT (+, STRBD UP)	COS	X.XXXE-YY	X.XXXE-YY	X.XXXE-YY	X.XXXE-YY	X.XXXE-YY	X.XXXE-YY	X.XXXE-YY
PITCH	MOMT (+, NOSE UP)	COS	X.XXXE-YY	X.XXXE-YY	X.XXXE-YY	X.XXXE-YY	X.XXXE-YY	X.XXXE-YY	X.XXXE-YY
YAW	MOMT (+, OMEGA DIR.)	COS	X.XXXE-YY	X.XXXE-YY	X.XXXE-YY	X.XXXE-YY	X.XXXE-YY	X.XXXE-YY	X.XXXE-YY
LONG.	SHR (+, AFT)	SIN	X.XXXE-YY	X.XXXE-YY	X.XXXE-YY	X.XXXE-YY	X.XXXE-YY	X.XXXE-YY	X.XXXE-YY
LAT.	SHR (+, STRBD)	SIN	X.XXXE-YY	X.XXXE-YY	X.XXXE-YY	X.XXXE-YY	X.XXXE-YY	X.XXXE-YY	X.XXXE-YY
VERT.	SHR (+, UP)	SIN	X.XXXE-YY	X.XXXE-YY	X.XXXE-YY	X.XXXE-YY	X.XXXE-YY	X.XXXE-YY	X.XXXE-YY
ROLL	MOMT (+, STRBD UP)	SIN	X.XXXE-YY	X.XXXE-YY	X.XXXE-YY	X.XXXE-YY	X.XXXE-YY	X.XXXE-YY	X.XXXE-YY
PITCH	MOMT (+, NOSE UP)	SIN	X.XXXE-YY	X.XXXE-YY	X.XXXE-YY	X.XXXE-YY	X.XXXE-YY	X.XXXE-YY	X.XXXE-YY
YAW	MOMT (+, OMEGA DIR.)	SIN	X.XXXE-YY	X.XXXE-YY	X.XXXE-YY	X.XXXE-YY	X.XXXE-YY	X.XXXE-YY	X.XXXE-YY
			LDXS	LDYS	LDZS	RDXS	RDYS	RDZS	
LONG.	SHR (+, AFT)	COS	X.XXXE-YY	X.XXXE-YY	X.XXXE-YY	X.XXXE-YY	X.XXXE-YY	X.XXXE-YY	X.XXXE-YY
LAT.	SHR (+, STRBD)	COS	X.XXXE-YY	X.XXXE-YY	X.XXXE-YY	X.XXXE-YY	X.XXXE-YY	X.XXXE-YY	X.XXXE-YY
VERT.	SHR (+, UP)	COS	X.XXXE-YY	X.XXXE-YY	X.XXXE-YY	X.XXXE-YY	X.XXXE-YY	X.XXXE-YY	X.XXXE-YY
ROLL	MOMT (+, STRBD UP)	COS	X.XXXE-YY	X.XXXE-YY	X.XXXE-YY	X.XXXE-YY	X.XXXE-YY	X.XXXE-YY	X.XXXE-YY
PITCH	MOMT (+, NOSE UP)	COS	X.XXXE-YY	X.XXXE-YY	X.XXXE-YY	X.XXXE-YY	X.XXXE-YY	X.XXXE-YY	X.XXXE-YY
YAW	MOMT (+, OMEGA DIR.)	COS	X.XXXE-YY	X.XXXE-YY	X.XXXE-YY	X.XXXE-YY	X.XXXE-YY	X.XXXE-YY	X.XXXE-YY
LONG.	SHR (+, AFT)	SIN	X.XXXE-YY	X.XXXE-YY	X.XXXE-YY	X.XXXE-YY	X.XXXE-YY	X.XXXE-YY	X.XXXE-YY
LAT.	SHR (+, STRBD)	SIN	X.XXXE-YY	X.XXXE-YY	X.XXXE-YY	X.XXXE-YY	X.XXXE-YY	X.XXXE-YY	X.XXXE-YY
VERT.	SHR (+, UP)	SIN	X.XXXE-YY	X.XXXE-YY	X.XXXE-YY	X.XXXE-YY	X.XXXE-YY	X.XXXE-YY	X.XXXE-YY
ROLL	MOMT (+, STRBD UP)	SIN	X.XXXE-YY	X.XXXE-YY	X.XXXE-YY	X.XXXE-YY	X.XXXE-YY	X.XXXE-YY	X.XXXE-YY
PITCH	MOMT (+, NOSE UP)	SIN	X.XXXE-YY	X.XXXE-YY	X.XXXE-YY	X.XXXE-YY	X.XXXE-YY	X.XXXE-YY	X.XXXE-YY
YAW	MOMT (+, OMEGA DIR.)	SIN	X.XXXE-YY	X.XXXE-YY	X.XXXE-YY	X.XXXE-YY	X.XXXE-YY	X.XXXE-YY	X.XXXE-YY

HUB IMPEDANCE MATRIX FOR HHC PITCH ANGLES (UNITS = DEG)

			A3S	A4S	A5S	B3S	B4S	B5S
LONG.	SHR (+, AFT)	COS	X.XXXE-YY	X.XXXE-YY	X.XXXE-YY	X.XXXE-YY	X.XXXE-YY	X.XXXE-YY
LAT.	SHR (+, STRBD)	COS	X.XXXE-YY	X.XXXE-YY	X.XXXE-YY	X.XXXE-YY	X.XXXE-YY	X.XXXE-YY
VERT.	SHR (+, UP)	COS	X.XXXE-YY	X.XXXE-YY	X.XXXE-YY	X.XXXE-YY	X.XXXE-YY	X.XXXE-YY
ROLL	MOHT (+, STRBD UP)	COS	X.XXXE-YY	X.XXXE-YY	X.XXXE-YY	X.XXXE-YY	X.XXXE-YY	X.XXXE-YY
PITCH	MOHT (+, NOSE UP)	COS	X.XXXE-YY	X.XXXE-YY	X.XXXE-YY	X.XXXE-YY	X.XXXE-YY	X.XXXE-YY
YAW	MOHT (+, OMEGA DIR.)	COS	X.XXXE-YY	X.XXXE-YY	X.XXXE-YY	X.XXXE-YY	X.XXXE-YY	X.XXXE-YY
LONG.	SHR (+, AFT)	SIN	X.XXXE-YY	X.XXXE-YY	X.XXXE-YY	X.XXXE-YY	X.XXXE-YY	X.XXXE-YY
LAT.	SHR (+, STRBD)	SIN	X.XXXE-YY	X.XXXE-YY	X.XXXE-YY	X.XXXE-YY	X.XXXE-YY	X.XXXE-YY
VERT.	SHR (+, UP)	SIN	X.XXXE-YY	X.XXXE-YY	X.XXXE-YY	X.XXXE-YY	X.XXXE-YY	X.XXXE-YY
ROLL	MOHT (+, STRBD UP)	SIN	X.XXXE-YY	X.XXXE-YY	X.XXXE-YY	X.XXXE-YY	X.XXXE-YY	X.XXXE-YY
PITCH	MOHT (+, NOSE UP)	SIN	X.XXXE-YY	X.XXXE-YY	X.XXXE-YY	X.XXXE-YY	X.XXXE-YY	X.XXXE-YY
YAW	MOHT (+, OMEGA DIR.)	SIN	X.XXXE-YY	X.XXXE-YY	X.XXXE-YY	X.XXXE-YY	X.XXXE-YY	X.XXXE-YY

Results of Solution Part III - Transient Spectral Stability Analysis

Transient time-history solutions are often difficult to interpret for quantitative stability information. This is due to the fact that the total responses consist of several component modes simultaneously and transiently approaching (or departing from) multi-harmonic periodicity, and with a wide range of natural frequencies and inherent damping levels. The extraction of the component responses at discrete frequencies, in order to examine their individual attenuation characteristics, is the purpose of the Transient Spectral Stability Analysis (TSSA) portion of the program. The details of this analysis, which utilizes Fourier Transform techniques, are treated in reference 17.

Essentially, the TSSA first performs Fourier transformations of selected time-history data strings, which have been previously generated in the time-history solution portion of the analysis (Solution Part II) and saved. The purpose of the Fourier Transform is to identify, within these time-histories, those frequencies whose amplitudes are relatively largest and are denoted as "resonances". Then, the TSSA calculates the transient behavior of the extracted amplitudes of these resonances over the time-history time interval and estimates equivalent linear stability indices (characteristic exponent, critical damping ratio, and time to half-amplitude).

Sample Pages 29 and 30 depict the output typically generated by the TSSA. This sequence of output is duplicated for each of the transient response channels selected. Sample Page 29 shows the output generated by the Fourier Transform frequency identification portion of the TSSA. Shown at the top of the page is the transient response channel being analyzed and the frequency range wherein resonance identification is desired (input locations (S)46 and (S)47). The series of five output items to follow consist of parameters defining the numerical Fourier transform; note that the results of the TSSA incorporate a time nondimensionalization based on rotor speed, Ω . The tabulation of the Fourier Transform (not shown for clarity) follows wherein, for each frequency (harmonic of the fundamental as determined by the total nondimensional time interval), the real and imaginary parts, the square of the amplitude and the logarithm to the base 10 of the amplitude are output. Generally, this tabulation will consume more than the one page. After this listing is completed, those frequencies and their respective square amplitudes which are found to be resonances, are listed under the last heading on sample page 29.

Aside from their several nonlinearities, the dynamic equations of motion for rotor blades implicitly contain several linear aerodynamic terms which, under helicopter forward flight conditions, can become periodic. Therefore, the aeroelastic time-history responses generated by these equations should manifest

PART III. TRANSIENT SPECTRAL STABILITY ANALYSES OF SELECTED AEROELASTIC TRANSIENT RESPONSES

TRANSIENT RESPONSE CHANNEL NO. XX - FOURIER TRANSFORM AND RESONANT FREQUENCY IDENTIFICATION

DESIRED FREQUENCY RANGE = X.XX TO X.XX (/REV)

NUMBER OF POINTS IN TIME SERIES = XXX
(ND) TIME INCREMENT = X.XXXXX RAD
LENGTH OF INTERVAL = XX.XXXXX RAD
FUNDAMENTAL FREQUENCY = X.XXXXX /REV
HIGHEST FREQUENCY = XX.XXXXX /REV

RESONANCE FREQUENCIES FOUND BY SEARCH ROUTINE

1	.XXXXXXXX+YYY	.XXXXXXXX+YYY
2	.XXXXXXXX+YYY	.XXXXXXXX+YYY
3	.XXXXXXXX+YYY	.XXXXXXXX+YYY
4	.XXXXXXXX+YYY	.XXXXXXXX+YYY
5	.XXXXXXXX+YYY	.XXXXXXXX+YYY
6	.XXXXXXXX+YYY	.XXXXXXXX+YYY
7	.XXXXXXXX+YYY	.XXXXXXXX+YYY
8	.XXXXXXXX+YYY	.XXXXXXXX+YYY
9	.XXXXXXXX+YYY	.XXXXXXXX+YYY

RESONANT FREQUENCIES DETERMINED TO BE FUNDAMENTALS

1	.XXXXXXXX+YYY
2	.XXXXXXXX+YYY
3	.XXXXXXXX+YYY
4	.XXXXXXXX+YYY

Floquet Theory characteristics (see reference). In particular, the Fourier Transform is capable of identifying "multiple resonances" which are separated by (plus or minus) multiples of the rotor frequency and which would be found to have approximately the same damping level as measured by characteristic exponent. Hence, the resonant frequencies are further screened to extract only those which have distinct noninteger values and which, within the set having the same non-integer values, have the largest transform magnitudes. These extracted frequencies are denoted "fundamental resonances" and are the only ones examined further for stability in the TSSA.

Sample Page 30 depicts the results of frequency fine tuning and response stability estimation for each of the fundamental resonances extracted in the TSSA. The top horizontal blocks of output represent the frequency fine-tuning results. The values labeled OPTIMIZED FREQUENCY are, in nondimensional (per rotor rev) form, the best estimates of the frequency of the fundamental resonant frequencies. The remainder of the output on this sample page (for each fundamental resonance) consists of three horizontal blocks representing three alternate estimates of the effective damping characteristics. These three types of blocks are explained by considering, for each of the fundamental responses indicated in Sample Page 30, the (nondimensional) time variation in the natural logarithm of the resonant frequency content. If these amplitude logarithms attenuate with time, then the response with that frequency content (mode) is stable. Conversely, if the amplitude logarithms increase with time, then the response with that frequency content is unstable. The slope of the attenuation with time is thus a measure of the effective linear damping, and is obtained by a sample least-square fit. If the variation of amplitude logarithms with time is neither monotonic increasing nor decreasing, a condition of maximum or minimum amplitude is defined. By weighting the least-square fit either uniformly or with an appropriate function accentuating the initial or terminal ends of the amplitude logarithms data string, the three latter horizontal blocks of output depicted in Sample Page 30 are generated. Within each of these blocks, the first quantity is the nondimensional CHARACTERISTIC EXPONENT, which is analogous to and interpreted in the same way as the real part of the eigenvalue discussed in the output for Solution Part I. The REVS to (MAX/MIN) AMPL is an indication of the asymptotic behavior of the component response. STANDARD DEVIATION is the root-mean-squared error achieved in the least-square curve-fit and is an indication of the regularity of the amplitude logarithm function and of the accuracy of the stability estimation. Based upon the OPTIMIZED FREQUENCY the equivalent CRITICAL DAMPING RATIO is calculated from the characteristic exponent using standard formulas. Finally, the output item labeled REVS TO HALF AMPLITUDE is the third alternate way in which the equivalent linear damping result is presented.

TRANSIENT RESPONSE CHANNEL NO. XX - RESONANT FREQUENCY FINE TUNING AND CRITICAL DAMPING RATIO CALCULATIONS

INITIAL PERCENTAGE	XX.XX			
INITIAL NO. OF DATA PTS.	XXX			
NO. FOURIER COEF. CALCS.	XXX			
FINAL NO. OF DATA PTS.	XXX	XXX	XXX	XXX
INITIAL FREQUENCY ESTIMATE (/REV)	X.XXXXX	X.XXXXX	X.XXXXX	X.XXXXX
OPTIMIZED FREQUENCY (/REV)	X.XXXXX	X.XXXXX	X.XXXXX	X.XXXXX
HARMONIC	XX	XX	XX	XX
UNIFORMLY WEIGHTED CHARACTERISTICS				
CHARACTERISTIC EXPONENT	X.XXXXX	X.XXXXX	X.XXXXX	X.XXXXX
REVS TO (MAX/MIN) AMPL.	XX.XXXXX	XX.XXXXX	XX.XXXXX	XX.XXXXX
STANDARD DEVIATION	X.XXXXX	X.XXXXX	X.XXXXX	X.XXXXX
CRITICAL DAMPING RATIO	X.XXXXX	X.XXXXX	X.XXXXX	X.XXXXX
REVS TO HALF AMPLITUDE	XXXXX.XXXXX	XXXXX.XXXXX	XXXXX.XXXXX	XXXXX.XXXXX
INITIAL END WEIGHTED CHARACTERISTICS				
CHARACTERISTIC EXPONENT	X.XXXXX	X.XXXXX	X.XXXXX	X.XXXXX
REVS TO (MAX/MIN) AMPL.	XX.XXXXX	XX.XXXXX	XX.XXXXX	XX.XXXXX
STANDARD DEVIATION	X.XXXXX	X.XXXXX	X.XXXXX	X.XXXXX
CRITICAL DAMPING RATIO	X.XXXXX	X.XXXXX	X.XXXXX	X.XXXXX
REVS TO HALF AMPLITUDE	XXXXX.XXXXX	XXXXX.XXXXX	XXXXX.XXXXX	XXXXX.XXXXX
TERMINAL END WEIGHTED CHARACTERISTICS				
CHARACTERISTIC EXPONENT	X.XXXXX	X.XXXXX	X.XXXXX	X.XXXXX
REVS TO (MAX/MIN) AMPL.	XX.XXXXX	XX.XXXXX	XX.XXXXX	XX.XXXXX
STANDARD DEVIATION	X.XXXXX	X.XXXXX	X.XXXXX	X.XXXXX
CRITICAL DAMPING RATIO	X.XXXXX	X.XXXXX	X.XXXXX	X.XXXXX
REVS TO HALF AMPLITUDE	XXXXX.XXXXX	XXXXX.XXXXX	XXXXX.XXXXX	XXXXX.XXXXX

Subsequent Cases

Sample Page 31 is generated at the beginning of every case following the first case of a multiple case run. The two columns are the location numbers and data values for the next case run.

PROGRAM G400XXXX - CASE 2 OF A MULTI-CASE RUN. INPUT DATA REPRESENTING CHANGES TO THE PREVIOUS CASE ARE AS FOLLOWS:

XXXX
XXXX
XXXX
XXXX
XXXX
XXXX
XXXX
XXXX
XXXX
XXXX
XXXX
XXXX
XXXX
XXXX
XXXX
XXXX
XXXX
XXXX
XXXX
XXXX
XXXX

.XXXXXXXXE+YY
.XXXXXXXXE+YY
.XXXXXXXXE+YY
.XXXXXXXXE+YY
.XXXXXXXXE+YY
.XXXXXXXXE+YY
.XXXXXXXXE+YY
.XXXXXXXXE+YY
.XXXXXXXXE+YY
.XXXXXXXXE+YY
.XXXXXXXXE+YY
.XXXXXXXXE+YY
.XXXXXXXXE+YY
.XXXXXXXXE+YY
.XXXXXXXXE+YY
.XXXXXXXXE+YY
.XXXXXXXXE+YY
.XXXXXXXXE+YY
.XXXXXXXXE+YY
.XXXXXXXXE+YY

REFERENCES

1. Bielawa, R. L.: Aeroelastic Analysis for Helicopter Rotor Blades with Time-Variable, Nonlinear Structural Twist and Multiple Structural Redundancy-Mathematical Derivation and Program User's Manual. NASA Contractor Report CR-2638, October 1976.
2. Bielawa, R. L.: Aeroelastic Analysis for Helicopter Rotors with Blade Appended Pendulum Vibration Absorbers - Mathematical Derivations and Program User's Manual. NASA Contractor Report CR-165896, June 1982.
3. Egolf, T. A. and A. J. Landgrebe: A Prescribed Wake Rotor Inflow and Flow Field Prediction Analysis - User's Manual and Technical Approach. NASA CR-165894, June 1982.
4. Bisplinghoff, R. L., H. Ashley and R. L. Halfman: Aeroelasticity. Addison-Wesley Publishing Co., Inc., Reading, MA, 1955.
5. Halfman, R. L.: Dynamics, Vol. I, Particles, Rigid Bodies, and Systems. Addison-Wesley Publishing Co., Inc., Reading, MA, 1962.
6. Bielawa, R. L.: Blade Stress Calculations - Mode Deflections vs. Force Integration. Journal of the American Helicopter Society, Vol. 24, No. 3, July 1970.
7. Bielawa, R. L., R. M. Chi, S. A. Johnson and S. T. Gangwani: Aeroelastic Analysis for Propellers - Mathematical Formulations and Program User's Manual. NASA CR-3729, June 1983.
8. Gangwani, S. T.: Synthesized Airfoil Data Method for Prediction of Dynamic Stall and Unsteady Airloads. NASA CR-3672, February 1983.
9. Bielawa, R. L.: Synthesized Unsteady Airfoil Data with Applications to Stall Flutter Calculations. American Helicopter Society, 31st Annual Forum Proceeding No. 935, May 1975.
10. St. Hilaire, F. O. Carta, M. R. Fink and W. D. Jepson: The Influence of Sweep on the Aerodynamic Loading on an Oscillating NACA 0012 Airfoil, Vol. I - Technical Report. NASA CR-3092, 1979.
11. McCroskey, W. J., K. W. McAllister, L. W. Carr, S. L. Pucci, O. Lambert and R. F. Indergand: Dynamic Stall on Advanced Airfoil Sections. Preprint No. 80-1, American Helicopter Society, 36th Annual National Forum, Washington, DC, May 1980.

REFERENCES (Cont'd)

12. Gray, L. and J. Liiva: Two-Dimensional Tests of Airfoils Oscillating Near Stall, Vol. II, Data Report. USAAULABS TR-68-13B, USAAMRDL, Ft. Eustis, VA, April 1968.
13. Beddoes, T. S.: A Synthesis of Unsteady Aerodynamic Effects Including Stall Hysteresis. Vertica, Vol. 1, pp. 113-123, 1976.
14. Heyson, H. H.: Linearized Theory of Wind-Tunnel Jet-Boundary Corrections and Ground Effect for VTOL-STOL Aircraft. NASA TR-124, 1962.
15. Hildebrand, F. B.: Introduction to Numerical Analysis. McGraw-Hill Book Co., Inc., New York, NY, 1956, pp. 429-434.
16. Gessow, A. and G. C. Myers: Aerodynamics of the Helicopter. Frederick Ungar Publishing Co., New York, 1967.
17. Kuczynsky, W. A.: Inflight Rotor Stability Monitor. NASA Symposium on Flutter Testing Techniques, NASA Flight Research Center, Edwards AFB, California, October 1975.
18. Houbolt, J. C. and G. W. Brooks: Differential Equations of Motion for Combined Flapwise Bending, Chordwise Bending, and Torsion of Twisted Nonuniform Rotor Blades. NACA Report 1346, 1958.

APPENDIX I

UPDATES TO DOCUMENTATION OF BASIC G400 ANALYSIS

Since the publication of Reference 1 the original G400 analysis has undergone continual development. In this process many of the original formulations and derivations have been reassessed, rechecked, and, where appropriate, reformulated. This appendix presents some of these reformulations and are, in fact, an errata update sheet to both References 1 and 2.

1. The first update relates to the criterion used for evaluating the integration constants arising in the calculation of the structural twist related deflection correction functions. In particular, while the integration constants are properly zero for hingeless rotor blade configurations, care must be taken with regard to articulated rotor blades. As formulated in Reference 1, the deflection correction functions are formed from double integrations of the blade curvatures. The evaluation criterion presently used for articulated rotor configurations is that the blade elastic motions, including those from the deflection correction terms, must be orthogonal with the rigid body flapping and lead-lag motions. Thus, the first order terms occurring in Eqs. (7) and (8), respectively, of Reference 1 should be written as:

$$\Delta v_i = \Delta \hat{v}_i + C_{1i} \bar{r} \quad (\text{I.1a})$$

$$\Delta w_k = \Delta \hat{w}_k + C_{2k} \bar{r} \quad (\text{I.1b})$$

$$\Delta v_i^{(2)'} = \Delta \hat{v}_i^{(2)'} + C_{1i} \quad (\text{I.2a})$$

$$\Delta w_k^{(2)'} = \Delta \hat{w}_k^{(2)'} + C_{2k} \quad (\text{I.2b})$$

Similarly, those second order terms occurring in Eqs. (9) and (10), respectively, should be written as:

$$\Delta v_k = \Delta \hat{v}_k + C_{3k} \quad (\text{I.3a})$$

$$\Delta W_i = \hat{\Delta W}_i + C_{4_i} \quad (I.3b)$$

$$\Delta V_k^{(2)'} = \hat{\Delta V}_k^{(2)'} + C_{3_k} \quad (I.4a)$$

$$\Delta W_i^{(2)'} = \hat{\Delta W}_i^{(2)'} + C_{4_i} \quad (I.4b)$$

where the () denoted quantities are the deflection correction functions evaluated with zero valued constants of integration. The constants C , C , C , C are all evaluated internally (element DEFCOR) to assure orthogonality with the rigid body degrees of freedom. Finally, as developed in Reference 7, various new deflection correction terms have been defined relating to elastic torsion deflections combined with elastic axis offset. These terms are modified in the same manner.

2. The second update pertains to the formulation of the elements of the inertia coupling matrix, [A], (Eq. (45) of Reference 1). This matrix should be completely symmetric; the offending terms coupling with torsion should equal their respective transposed elements and include the effects of the nonlinear excitation functions given in Eqs. (39a-d):

$$A_{w_i \theta_j} = A_{\theta_j w_i} = \int_0^l m \left[y_{10CG} \gamma_{\theta_j} (\gamma_{w_i} - \Delta W_i) + \Gamma_{z \theta_j} (\gamma_{w_i} - \Delta W_i) - \Gamma_{y \theta_j} \Delta v_i \right] d\bar{r} \quad (I.5)$$

$$A_{v_k \theta_j} = A_{\theta_j v_k} = - \int_0^l m \left[y_{10CG} \gamma_{\theta_j} \Delta w_k + \Gamma_{y \theta_j} (\gamma_{v_k} - \Delta v_k) + \Gamma_{z \theta_j} \Delta w_k \right] d\bar{r} \quad (I.6)$$

$$A_{\beta \theta_j} = A_{\theta_j \beta} = \int_0^l \bar{m} (r - \beta_B h_{usl}) \left[(\gamma_{\theta_j} y_{10CG} + \Gamma_{z \theta_j}) \cos \Theta - \Gamma_{y \theta_j} \sin \Theta \right] d\bar{r} \quad (I.7)$$

$$A_{\delta\theta_j} = A_{\theta_j} \delta = \int_0^l \bar{m} r \left[(\gamma_{\theta_j} y_{10CG} + \Gamma_{z\theta_j}) \sin \Theta + \Gamma_{y\theta} \cos \Theta \right] d\bar{r} \quad (I.8)$$

$$A_{\theta_j \theta_m} = \int_0^l \bar{m} \left[(k_{y_{10}}^2 + k_{z_{10}}^2) + \Gamma_{y\theta_j} \Gamma_{y\theta_m} - \gamma_{\theta_j} \gamma_{\theta_m} \gamma_{10CG}^2 + (\Gamma_{z\theta_j} + \gamma_{\theta_j} y_{10CG})(\Gamma_{z\theta_m} + \gamma_{\theta_m} y_{10CG}) \right] d\bar{r} \quad (I.9)$$

3. The third and fourth updates pertain to the implementation of the redundant analysis of flexbeam-torque tube assemblies. The first of these two relates to the torsional stiffness characteristics of the flexbeams. A more correct statement of the boundary conditions for the flexbeam torsion equation (Eq. (115) of Reference 1) includes relating the flexbeam outboard twist rate, $\theta'(r_j)$, to the twist rate of the outer blade:

$$\theta'(r_j) = \Theta'_J \quad (I.10)$$

where the twist rate of the outer blade comes from built-in and response contributions:

$$\Theta'_J = \Theta'_B(r_J) + \sum_{j=1}^{NTM} \gamma_{\theta_j}'(r_J) q_{\theta_j} \quad (I.11)$$

The inclusion of this generally nonzero value of twist rate has the effect of modifying the resulting expression for the elastic torsion deflection of the flexbeam at the juncture (Eq. (129a)):

$$\Delta \Theta_J = \frac{1}{(e_{11} e_{23} - e_{21} e_{13})} \sum_{i=1}^4 \tau_i \left[e_{13} (f_{2, i+1} + e_{22} \Theta'_J) - e_{23} (f_{1, i+1} + e_{12} \Theta'_J) \right] \quad (I.12)$$

and the symbolic expression for this deflection (Eq. (130b)) then becomes:

$$\begin{aligned} \Delta \Theta = & \theta_{sx} S_{x5FB} + \theta_{Mx} M_{x5FB} + \theta_{sy} S_{y5FB} \\ & + \theta_{sz} S_{z5FB} + \theta_{My} M_{y5FB} + \theta_{Mz} M_{z5FB} \\ & + \theta_{\Theta'} \cdot \Theta'_J \end{aligned} \quad (I.13)$$

4. The fourth update pertains to the calculation of internal blade shears and moments in the blade adjacent to the juncture. As outlined in Reference 1 a force integration approach was implemented which necessitated extrapolations to estimate the modal accelerations. This calculation was found to be best performed using a mode deflection method instead. Thus, Eqs. (132b) and 132f) of Reference 1 are, respectively, replaced by the following expressions:

$$S_{y5B} = -s_{\Theta}_J \sum_{i=1}^{NFM} DS1_i q_{w_i} + c_{\Theta}_J \sum_{k=1}^{NEM} DS3_k q_{v_k} \quad (I.14a)$$

$$S_{z5B} = c_{\Theta}_J \sum_{i=1}^{NFM} DS1_i q_{w_i} + s_{\Theta}_J \sum_{k=1}^{NEM} DS3_k q_{v_k} \quad (I.14b)$$

$$M_{x5B} = \sum_{j=1}^{NTM} DS5_j q_{\theta_j} \quad (I.14c)$$

$$M_{y5B} = c_{\Theta}_J \sum_{i=1}^{NFM} DS2_i q_{w_i} - s_{\Theta}_J \sum_{k=1}^{NEM} DS4_k q_{v_k} \quad (I.14d)$$

$$M_{z5B} = s_{\Theta}_J \sum_{i=1}^{NFM} DS2_i q_{w_i} + c_{\Theta}_J \sum_{k=1}^{NEM} DS4_k q_{v_k} \quad (I.14e)$$

where:

$$DS1_i = \omega_{w_i}^2 \int_{\bar{r}_J}^1 m \gamma_{w_i} d\bar{r} \quad (I.15a)$$

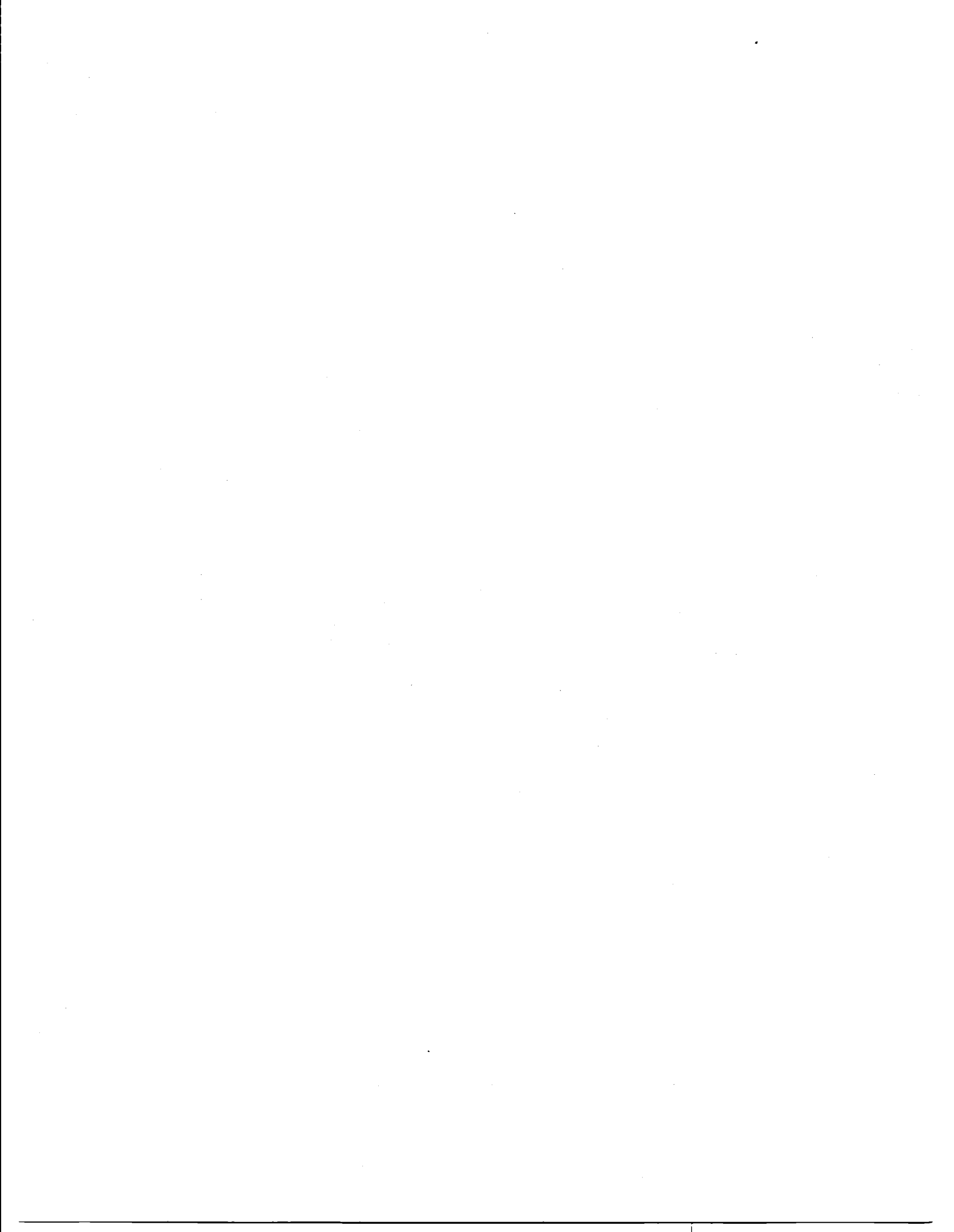
$$DS2_i = \int_{\bar{r}_J}^I m \left[(\bar{r} - \bar{r}_J) \omega_{w_i}^2 \gamma_{w_i} - \bar{r} (\gamma_{w_i}(\bar{r}) - \gamma_{w_i}(\bar{r}_J)) \right] d\bar{r} \quad (I.15b)$$

$$DS3_k = (\omega_{v_k}^2 + 1) \int_{\bar{r}_J}^I m \gamma_{v_k} d\bar{r} \quad (I.15c)$$

$$DS4_k = \int_{\bar{r}_J}^I m \left[(\bar{r} - \bar{r}_J) (\omega_{v_k}^2 + 1) - \bar{r} (\gamma_{v_k}(\bar{r}) - \gamma_{v_k}(\bar{r}_J)) \right] d\bar{r} \quad (I.15d)$$

$$DS5_j = \int_{\bar{r}_J}^I m \gamma_{\theta_j} \left[\omega_{\theta_j}^2 (k_{z_{10}}^{-2} + k_{y_{10}}^{-2}) + \bar{k}_{y_{10}}^2 - \bar{k}_{z_{10}}^2 \right] d\bar{r} \quad (I.15e)$$





1. Report No. NASA CR-172455		2. Government Accession No.		3. Recipient's Catalog No.	
4. Title and Subtitle Extended Aeroelastic Analysis for Helicopter Rotors with Prescribed Hub Motion and Blade Appended Pendulum Vibration Absorbers				5. Report Date December 1984	
				6. Performing Organization Code	
7. Author(s) Richard L. Bielawa				8. Performing Organization Report No. UTRC81-45	
9. Performing Organization Name and Address United Technologies Research Center East Hartford, Connecticut 06108				10. Work Unit No.	
				11. Contract or Grant No. NAS1-16803	
				13. Type of Report and Period Covered Contractor Report	
12. Sponsoring Agency Name and Address National Aeronautics and Space Administration Washington, DC 20546				14. Sponsoring Agency Code 505-42-39-89	
15. Supplementary Notes Langley technical monitor: Lynn Bowman Final Report Richard L. Bielawa is currently at Rensselaer Polytechnic Institute, Troy, NY 12181.					
16. Abstract Mathematical development is presented for the expanded capabilities of the United Technologies Research Center (UTRC) G400 Rotor Aeroelastic Analysis. The G400PA expanded analysis simulates the dynamics of all conventional rotors, blade pendulum vibration absorbers, and the higher harmonic excitations resulting from prescribed vibratory hub motions and higher harmonic blade pitch control. The analysis includes the methodology for modeling the unsteady stalled airloads of two-dimensional airfoils. Formulations are also presented for calculating the rotor impedance matrix appropriate to the higher harmonic blade excitations. This impedance matrix, and the associated vibratory hub loads, are the rotor dynamic characteristic elements for use in the Simplified Coupled Rotor/Fuselage Vibration Analysis (SIMVIB). Updates to the development of the original G400 theory, program documentation, user instructions and information are presented.					
17. Key Words (Suggested by Author(s)) Rotor Aeroelasticity Vibration Higher Harmonic Control Vibration Absorber Teetered Rotors			18. Distribution Statement Unclassified - Unlimited Subject Category 02		
19. Security Classif. (of this report) Unclassified		20. Security Classif. (of this page) Unclassified		21. No. of Pages	22. Price*

